Graduate Theses and Dissertations

Graduate School

3-25-2009

# Advanced Transceiver Algorithms for OFDM(A) Systems

Hisham A. Mahmoud
*University of South Florida*

Advanced Transceiver Algorithms for OFDM(A) Systems

by

Hisham A. Mahmoud

A dissertation submitted in partial fulfillment
of the requirements for the degree of
Doctor of Philosophy
Department of Electrical Engineering
College of Engineering
University of South Florida

Major Professor: Hüseyin Arslan, Ph.D.
Ken Christensen, Ph.D.
Richard D. Gitlin, Sc.D.
Joseph Mitola III, Ph.D.
Ravi Sankar, Ph.D.

Date of Approval:
March 25, 2009

**DEDICATION**

To my parents.

# ACKNOWLEDGEMENTS

First, I would like to thank Dr. Huseyin Arslan for his support and advice throughout the duration of my study at USF. Without the lengthy discussions we had and without his guidance, this dissertation would not be the same. I wish to thank Dr. Ken Christensen, Dr. Richard D. Gitlin, Dr. Joseph Mitola III, and Dr. Ravi Sankar for agreeing to serve in my committee; and for their valuable time, feedback, and suggestions. I am also thankful to Dr. Nagarajan Ranganathan for chairing my defense. I would like to acknowledge Dr. Paris Wiley, Gayla Montgomery, Irene Wiley, Becky Brenner, and Norma Paz from the Electrical Engineering Department at USF who have been always helpful and understanding. To all of you, I am very thankful.

I owe much to Dr. Kemal Ozdemir and Francis Retnasothie at Logus Broadband Wireless Solutions Inc. who supported my research financially for the majority of my Ph.D. duration and continuously offered their advice and help. I am also grateful to my colleagues at USF and my friends at the Wireless Communications and Signal Processing (WCSP) group. I would like to especially mention Dr. Tevfik Yucek, Dr. Ismail Guvenc, Dr. Hasari Celebi, Ali Gorcin, Serhan Yarkan, and Mustafa Emin Sahin.

Last but by no means least, I thank my parents, my grandparents, my sister, my two brothers, and my wife. I would like to express my deepest gratitude to my parents whom this work is dedicated to. Without your unconditional support, your kind words, and your sound advice, I would not be the person I am today.

**TABLE OF CONTENTS**

# LIST OF TABLES

# LIST OF FIGURES

# LIST OF ACRONYMS

| | |
|---|---|
| 3GPP | 3rd Generation Partnership Project |
| AAS | adaptive antenna systems |
| ACI | adjacent channel interference |
| ADC | analog to digital converter |
| ADSL | asymmetric digital subscriber line |
| AMS | adaptive MIMO switching |
| AP | access point |
| AST | adaptive symbol transition |
| AWGN | additive white Gaussian noise |
| BEM | basis expansion model |
| BER | bit error rate |
| BPSK | binary phase shift keying |
| BS | base station |
| BSC | binary symmetric channel |
| CC | cancellation carrier |
| CCI | co-channel interference |
| CDF | cumulative distribution function |
| CDMA | code division multiple access |
| CFR | channel frequency response |
| CINR | carrier-to-interference-plus-noise ratio |
| CIR | channel impulse response |
| CP | cyclic prefix |
| CR | cognitive radio |

| | |
|---|---|
| CRC | cyclic redundancy check |
| CSMA | carrier sense multiple accessing |
| DAB | digital audio broadcasting |
| DAC | digital to analog converter |
| DFS | dynamic frequency selection |
| DL | downlink |
| DS-CDMA | direct spread code division multiple access |
| DVB | digital video broadcasting |
| DVB-T | terrestrial digital video broadcasting |
| EVM | error vector magnitude |
| FDMA | frequency division multiple accessing |
| FEC | forward error correction |
| FER | frame error rate |
| FFT | fast Fourier transform |
| FHDC | frequency hopping diversity combining |
| I | inphase |
| ICI | inter-carrier interference |
| IEEE | Institute of Electrical and Electronics Engineers |
| IF | intermediate frequency |
| IFFT | inverse fast Fourier transform |
| i.i.d. | independent and identically distributed |
| ISI | inter-symbol interference |
| IST | Information society technologies |
| ITU | International Telecommunication Union |
| LNA | low noise amplifier |
| LO | local oscillator |
| LOS | line-of-sight |

| | |
|---|---|
| LS | least squares |
| LTE | long term evolution |
| LU | licensed user |
| MAC | medium access control |
| MB-OFDM | multi-band OFDM |
| MC-CDMA | multi-carrier code division multiple access |
| MIMO | multiple-input multiple-Output |
| ML | maximum likelihood |
| MMSE | minimum mean-square error |
| MSE | mean-squared-error |
| MUI | multiuser interference |
| NBI | narrow-band interference |
| NLOS | non-line-of-sight |
| OFDM | orthogonal frequency division multiplexing |
| OFDMA | orthogonal frequency division multiple access |
| PA | power amplifier |
| PAM | pulse amplitude modulation |
| PAPR | peak-to-average-power ratio |
| PDF | probability density function |
| PHY | physical layer |
| PSAM | pilot-symbol-aided modulation |
| PSD | power spectral density |
| Q | quadrature |
| QAM | quadrature amplitude modulation |
| QPSK | quadrature phase shift keying |
| RC | raised cosine |
| RF | radio frequency |

| | |
|---|---|
| RMS | root-mean-squared |
| RSSI | received signal strength indicator |
| RTD | round trip delay |
| RU | rental user |
| SB-OFDM | single-band OFDM |
| SDR | software defined radio |
| SER | symbol error rate |
| SINR | signal-to-interference-plus-noise ratio |
| SM | spatial multiplexing |
| SNR | signal-to-noise ratio |
| SS | subscriber station |
| STC | space time coding |
| SVD | singular value decomposition |
| TDMA | time division multiple access |
| TOA | time of arrival |
| TPC | transmit power control |
| UCD | uplink channel descriptor |
| UL | uplink |
| UWB | ultra wide band |
| VSA | vector signal analyzer |
| WiFi | wireless fidelity |
| WiMAX | worldwide interoperability for microwave access |
| WINNER | wireless world initiative new radio |
| WLAN | wireless local area network |
| WMAN | wireless metropolitan area network |
| WPAN | wireless personal area network |
| WRAN | wireless regional area network |

WSS  wide-sense stationary

ZF   zero-forcing

# ADVANCED TRANSCEIVER ALGORITHMS FOR OFDM(A) SYSTEMS

## Hisham A. Mahmoud

## ABSTRACT

With the increasing advancements in the digital technology, future wireless systems are promising to support higher data rates, higher mobile speeds, and wider coverage areas, among other features. While further technological developments allow systems to support higher computational complexity, lower power consumption, and employ larger memory units, other resources remain limited. One such resource, which is of great importance to wireless systems, is the available spectrum for radio communications. To be able to support high data rate wireless applications, there is a need for larger bandwidths in the spectrum. Since the spectrum cannot be expanded, studies have been concerned with fully utilizing the available spectrum. One approach to achieve this goal is to reuse the available spectrum through space, time, frequency, and code multiplexing techniques. Another approach is to optimize the transceiver design as to achieve the highest throughput over the used spectrum.

From the physical layer perspective, there is a need for a highly flexible and efficient modulation technique to carry the communication signal. A multicarrier modulation technique known as orthogonal frequency division multiplexing (OFDM) is one example of such a technique. OFDM has been used in a number of current wireless standards such as wireless fidelity (WiFi) and worldwide interoperability for microwave access (WiMAX) standards by the Institute of Electrical and Electronics Engineers (IEEE), and has been proposed for future 4G technologies such as the long term evolution (LTE) and LTE-advanced standards by the 3rd Generation Partnership Project (3GPP), and the wireless world initiative new radio (WINNER) standard by the Information society technologies (IST). This is due to OFDM's high spectral efficiency, resistance to narrow band interference, support for high data rates, adaptivity, and scalability.

In this dissertation, OFDM and multiuser OFDM , also known as orthogonal frequency division multiple access (OFDMA), techniques are investigated as a candidate for advanced wireless systems. Features and requirements of future applications are discussed in detail, and OFDM's ability to satisfy these requirements is investigated. We identify a number of challenges that when addressed can improve the performance and throughput of OFDM-based systems. The challenges are investigated over three stages. In the first stage, minimizing, or avoiding, the interference between multiple OFDMA users as well as adjacent systems is addressed. An efficient algorithm for OFDMA uplink synchronization that maintains the orthogonality between multiple users is proposed. For adjacent channel interference, a new spectrum shaping method is proposed that can reduce the out-of-band radiation of OFDM signals. Both methods increase the utilization of available spectrum and reduce interference between different users.

In the second stage, the goal is to maximize the system throughput for a given available bandwidth. The OFDM system performance is considered under practical channel conditions, and the corresponding bit error rate (BER) expressions are derived. Based on these results, the optimum pilot insertion rate is investigated. In addition, a new pilot pattern that improves the system ability to estimate and equalize various radio frequency (RF) impairments is proposed.

In the last stage, acquiring reliable measurements regarding the received signal is addressed. Error vector magnitude (EVM) is a common performance metric that is being used in many of today's standards and measurement devices. Inferring the signal-to-noise ratio (SNR) from EVM measurements has been investigated for either high SNR values or data-aided systems. We show that using current methods does not yield reliable estimates of the SNR under other conditions. Thus, we consider the relation between EVM and SNR for nondata-aided systems. We provide expressions that allow for accurate SNR estimation under various practical channel conditions.

# CHAPTER 1

## INTRODUCTION

With the increasing demand for more applications to become wireless, wireless systems are challenged to meet higher data rate requirements. Considering the frequency spectrum as being a limited and valuable resource, wireless devices are faced with the necessity to utilize the available opportunities of the spectrum and coexist with other legacy or otherwise future systems.

Studies to increase the system throughput have been concerned with improving signal detection algorithms and reducing the impact of various practical impairments to wireless signals. Timing and frequency offsets, radio channel propagation effects, and baseband modulator gain and phase imbalances are examples of signal degradation sources that need to be estimated and equalized. Minimizing the effects of these impairments increase the effective signal-to-noise ratio (SNR) at the receiver and allow the system to support higher modulation orders and consequently higher data rates. This approach can be considered as maximizing the system spectral efficiency for a given allocated spectrum or bandwidth.

Recently, a new direction for utilizing the available spectrum has been suggested. This approach calls for allowing non-licensed users, also called rental or secondary users, to operate within licensed bands that are not heavily occupied by their intended users, also called licensed or primary users. The secondary users, however, can only operate within licensed band given they do not interfere or block the primary users. Recent measurements show that wide ranges of the licensed spectrum are rarely used most of the time, while other bands are heavily occupied [1]. This indicates that the above approach can significantly improve the spectrum utilization. This opportunistic use of the spectrum has been proposed by the use of cognitive radio (CR) [2–4]. The formal definition of CR has not been agreed upon at the moment, but CR can be defined as an intelligent wireless system that is aware of its surrounding environment through sensing and measurements; a system that uses its gained experience to plan future actions and adapt to improve the overall communication quality

and meet user's needs. It is noteworthy to mention that systems based on the above approach has also been referred to as spectrum sharing systems and overlay systems.

Considering the above two approaches to designing future wireless systems, it can be inferred that there is a need for a physical layer (PHY) which is highly flexible, adaptable, and spectrum efficient. On one hand, detected spectrum opportunities should be exploited by shaping the transmitted signal accordingly. On the other hand, the system should be able to utilize available measurements regarding the operational environment to maximize the spectral efficiency on used bands. The ability to support multiple users is also an important aspect of wireless systems. Orthogonal frequency division multiplexing (OFDM) technology is a special case of multicarrier systems that, we believe, has the potential of fulfilling the aforementioned requirements.

In this chapter, a brief introduction to OFDM technology is given followed by an outline of the remainder of this dissertation.

## 1.1   OFDM Technology

OFDM is one of the most widely used technologies in current communication systems. The use of OFDM can be found in the PHY of legacy standards such as the wireless local area network (WLAN) [5–7], wireless metropolitan area network (WMAN) standards [8, 9], and asymmetric digital subscriber line (ADSL) [10]. In Europe, OFDM is used by the digital audio broadcasting (DAB) [11] and terrestrial digital video broadcasting (DVB-T) [12] standards. OFDM is also a strong candidate for future technologies such as the wireless personal area network (WPAN) standard [13] by the Institute of Electrical and Electronics Engineers (IEEE), the long term evolution (LTE) and LTE-Advanced [14] standards proposed by the 3rd Generation Partnership Project (3GPP), the wireless world initiative new radio (WINNER) [15] standard proposed by the Information society technologies (IST), and finally wireless regional area network (WRAN) standard which is known as the first cognitive radio standard [16].

One of the main reasons for choosing OFDM as a multicarrier modulation method is due to its robustness and high spectral efficiency specially for high data rate systems. OFDM divides the allocated spectrum into subbands that are modulated with orthogonal subcarriers. Over frequency-selective channels, the subcarrier bandwidth becomes smaller than the channel coherence bandwidth. This effect allows the system to use single-tap channel equalizers, instead of the complex equalizers that are usually needed for high bandwidth single carrier signals. Another result of this subcarrier

division is that every symbol is modulated over a longer time duration which reduces the inter-symbol interference (ISI) effects caused by multipath propagation. Other advantages of OFDM include its scalability and easy implementation using fast Fourier transform (FFT) methods.

A special case of OFDM that is of interest to this study is the multiple user OFDM technology, known as orthogonal frequency division multiple access (OFDMA). By assigning subcarriers within the same symbol and over different symbols to multiple users, OFDMA enables multiple user access over frequency and time domains, respectively. In addition, by maintaining the orthogonality between subcarriers belonging to different users, OFDMA is able to achieve higher spectral efficiency when compared to other multiple access technologies.

## 1.2 Dissertation Outline

For the remainder of this dissertation, advantages and challenges to OFDM technology when applied to future communication systems are identified. Further, a number of these challenges that improves the performance and increases the throughput of OFDM-based communication systems are addressed. In this section, the studies presented in the remainder of this dissertation are motivated and the following chapters are outlined.

To identify challenges to OFDM-based systems, the block diagram of a generic digital communication system is considered in Fig. 1.1. The figures shows the basic elements of the PHY. At the transmitter side, the raw bits, usually passed to the PHY by the medium access control (MAC) layer, are encoded by introducing some redundancy to the information sequence. The encoding process allows for forward error correction (FEC) at the receiver and improves the reliability of the received data through error detection techniques. Encoded data are then modulated to any one of possible waveforms to allow the signal to be transmitted over the communication channel. In OFDM-based systems, this step also involves loading modulated symbols to orthogonal subcarriers. At the receiver, demodulated symbols are compared to originally transmitted symbols to obtain channel measurements such as error vector magnitude (EVM). The measurements could be obtained either using known transmitted symbols or blindly by remodulating detected symbols.

Part of transmitted symbols are reserved for pilots or preambles. This step allows the receiver to estimate and equalize the channel effect, mostly modeled as a filter response, imposed on the transmitted signal. The channel effect is usually considered as the combined effects of the propagation channel and other radio frequency (RF) impairments (e.g. timing and frequency offsets, filters
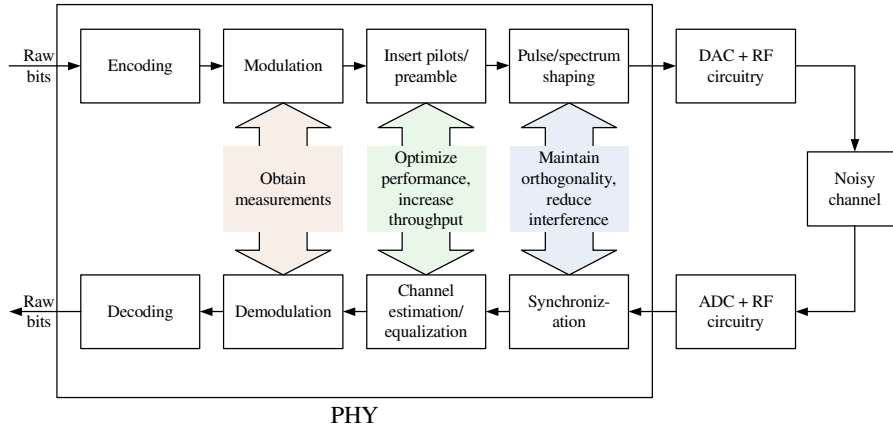
Figure 1.1 Basic elements of the PHY in digital communication systems.

response). The ratio of the energy or number of symbols dedicated for pilots to the energy or number of symbols dedicated for data is one of the factors that determine the overall system efficiency and throughput.

The last step in the PHY is to pass the signal through a pulse shaping filter. In conventional communication systems, this process improves the spectrum characteristics of the modulated signal and limits or negates the ISI between consecutive symbols. In CR systems, the process may also involve shaping the signal spectrum adaptively to fit into a desired spectrum profile which allows for multiple rental user (RU) access or minimize interference to licensed users (LU) currently operating within the used band.

A detailed study of OFDM advantages and challenges when used in CR systems is presented in Chapter 2. Examining the elements discussed above, the issues to address for future wireless systems when OFDM is employed can be divided intro three main issues:

- Maintain orthogonality and reduce interference.

- Optimize performance and increase throughput.

- Obtain signal measurements.

Fig. 1.1 shows these three issues and their relations to the PHY components.

The first issue to consider is maintaining orthogonality and reducing interference. OFDM is able to achieve high spectrum efficiency because of the orthogonality between its subcarriers. Fig 1.2 shows a multiple user OFDM, or an OFDMA, system operating within licensed band. If the orthogonality between subcarriers is lost due to synchronization errors, then adjacent subcarriers will

4
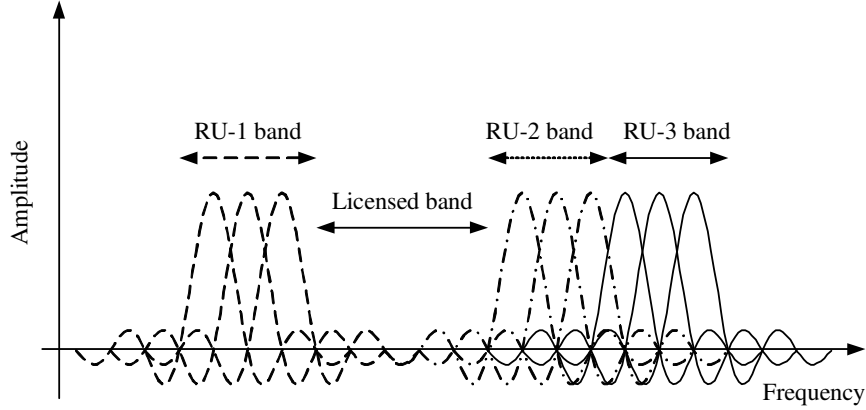
Figure 1.2  OFDM subcarrier assignment within used available bands in CR systems.

interfere with each other causing inter-carrier interference (ICI). Operating under such conditions can degrade the performance of the OFDM system significantly. This is actually one of the drawbacks of OFDM systems; its sensitivity to timing and frequency offsets. For single user OFDM systems, all subcarriers are modulated by the same user. In this case, the receiver only needs to synchronize to the signal of that user to avoid synchronization errors and maintains orthogonality between subcarriers. However, this does not apply to the uplink (UL) signal of OFDMA systems, where different subcarriers are assigned to different users. In this case, the orthogonality is maintained only if all users' signals reach the receiver synchronously. The synchronization in OFDMA UL systems is discussed in detail in Chapter 3.

Considering CR systems, there are possibly one or more LU operating within the used band. In this case, the OFDM system needs to avoid interfering with these LU bands through spectrum shaping techniques. Although disabling the set of subcarriers that lay within the licensed band as shown in Fig. 1.2 can reduce the radiation leaked to the licensed band, there is still a significant amount of interference to the LU. The reason for this high adjacent channel interference (ACI) is due to the high sidelobes of OFDM subcarriers. To further minimize OFDM out-of-band radiation to neighboring bands, it is conventional to disable subcarriers that operate at the edge of used bands, also known as guard subcarriers. This process leads to lower spectrum efficiency as the vacant bands are not fully utilized. In Chapter 4, some of the advanced methods used to shape the spectrum of OFDM signals are discussed. We also introduce a novel method for OFDM spectrum shaping that can outperform current methods.

In the first issue discussed above, the concern is to utilize the available spectrum opportunities while minimizing or avoiding the interference between multiple users of the same system as well as between RUs and LUs sharing the same band. Based on the vacant bands of the spectrum and the used spectrum shaping method, the number of usable OFDM subcarriers are determined. Part of used subcarriers are then dedicated to pilots or preambles to aid in the channel estimation and equalization process at the receiver. Increasing the number of pilot subcarriers improves the channel estimation which reduces the bit error rate (BER) at the receiver. However, using too many subcarriers for pilots reduces the overall throughput of the system. On the other hand, an insufficient number of pilot subcarriers leads to worse channel estimation and increases the BER which in turns decreases the system throughput. Thus, there is usually an optimum number of pilots that maximize the system throughput depending on the channel statistics and the used channel estimation method. The optimum pilot insertion rate for OFDM systems has been presented in the literature. Methods that were developed for OFDM systems assumed all available pilots could be used for channel estimation and equalization since they belong to a single user. In addition, optimum channel estimation techniques were assumed. When considering OFDMA-UL systems, the problem is more complicated since multiple user access means the received signal is actually a sum of multiple signals received over different channels. Moreover, since pilots are divided among users, the number of pilots per channel are not sufficient for optimum channel estimation techniques. Recently, some studies investigated possible channel estimation techniques for OFDMA-UL systems. However, these studies did not provide neither the BER performance of the system under channel estimation errors nor the optimum pilot insertion rate. In Chapter 5, the performance of OFDMA-UL systems over time-varying frequency-selective channels is considered. We provide BER expressions for the received signal under channel estimation errors. Based on the derived expressions, an optimum pilot insertion rate, in both time and frequency directions, that maximizes the system throughput is identified.

A direct conversion receiver, also known as zero-IF receiver, is an attractive architecture for OFDM systems since it avoids costly intermediate frequency (IF) filters, reduces power consumption, and allows for easier integration than super-heterodyne structure [17]. However, direct conversion receivers cause more distortions to the baseband signal due to the imbalance between the inphase (I) and quadrature (Q) branches. The IQ imbalance results in a degradation in the system performance. This drawback of direct conversion receivers becomes more significant with OFDM systems as they

are known to be sensitive to receiver front-end non-idealities [18]. As mentioned earlier, channel estimation and equalization process takes into account not only the channel propagation effects but also other impairments to the signal. In Chapter 6, the effects of IQ imbalance on OFDMA-UL systems are considered. Methods to estimate and equalized both the multiuser channels and IQ distortions are investigated. A novel pilot pattern is designed which is then used by two proposed methods to efficiently mitigate signal distortions caused by the combined effects of the wireless communication channels and IQ imbalances of multiple users. Compared to Chapter 5 where we investigate optimum pilot insertion rate, in Chapter 6, we investigate optimum pilot patterns.

Finally, the third issue to consider is obtaining reliable measurements of the received signal quality. BER and EVM are two primary specifications that determine the performance of the wireless system in terms of transmitted and received symbols. While BER is useful as a conceptual figure of merit, it suffers from a number of practical drawbacks such as the complexity and delay required for calculation. In addition, it has limited diagnostic value. If the BER value measured exceeds accepted limits, it offers no clue regarding the probable cause or source of signal degradation. Hence, EVM has been considered as a viable alternative test method when looking for a figure of merit in wireless channels. EVM is calculated by comparing originally modulated symbols (at the output of the modulator) to received symbols (at the input to the demodulator) in data aided cases. In nondata aided cases, detected symbols at the output of the demodulator are remodulated and used as a reference instead. EVM can offer insightful information on the various transmitter imperfections, including carrier leakage, IQ mismatch, nonlinearity, local oscillator (LO) phase noise and frequency error [19]. Requirements on EVM are already part of most wireless communications standards such as the IEEE 802.11a-1999 standard [6] and the IEEE 802.16e-2005 standard [9]. Relating EVM to other performance metrics such as SNR and BER is an important research topic as these relations allow the reuse of already available EVM measurements to infer more information regarding the communication system. Moreover, using EVM measurements could reduce the system complexity by getting rid of the need to have separate modules to estimate or measure other metrics. In Chapter 7, we consider the relation between EVM and SNR for nondata-aided receivers. The signal degradation sources are modeled as additive white Gaussian noise (AWGN), Rayleigh fading channels, and IQ imbalances. The exact value of EVM for nondata-aided symbol detection is derived and expressed in terms of the SNR. The results show that SNR can be accurately estimated using measured EVM even when symbol sequences are unknown, and the SNR level is low.

In the remainder of this chapter, a more detailed outline of the following chapters in this dissertation are introduced.

### 1.2.1 Chapter 2: OFDM for Cognitive Radio, Merits and Challenges

CR is a novel concept that allows wireless systems to sense the environment, adapt, and learn from previous experience to improve the communication quality. However, CR needs a flexible and adaptive PHY in order to perform the required tasks efficiently. In this chapter, CR systems and their requirements of the PHY are discussed and OFDM technique is investigated as a candidate transmission technology for CR. The challenges that arise from employing OFDM in CR systems are identified. The cognitive properties of some OFDM-based wireless standards are also discussed in order to indicate the technical trend toward a more CR.[1]

### 1.2.2 Chapter 3: Synchronization in OFDMA Uplink Systems

Synchronization is one of the most important processes in the OFDMA-based systems such as the mobile worldwide interoperability for microwave access (WiMAX) standard. Synchronization between a base station (BS) and all users within a cell are done through what is known as the ranging process. In this chapter, the details of the ranging process are presented. Some of the proposed algorithms, as well as a novel algorithm to carry out a successful ranging process are discussed. Performance curves and computational complexity comparisons between proposed algorithm and current algorithms are presented. The system performance is evaluated for both AWGN channels and practical frequency-selective fading channels with multiuser interference (MUI). It is shown that the proposed algorithm offers a reduced complexity ranging method that can be employed in practical OFDMA-based BSs.[2]

### 1.2.3 Chapter 4: Spectrum Shaping of OFDM-based Cognitive Radio Signals

In this chapter, OFDM spectrum shaping using various techniques to reduce ACI is investigated. The trade-offs between interference level and spectral efficiency, power consumption, and computational complexity are discussed. Simulation results along with detailed analysis showing the advantages and disadvantages of considered technique are presented. In addition, we introduce a new method for OFDM sidelobe suppression. An extension is added to OFDM symbols that is

---

[1]Contents of this chapter were published in parts in [20, 21].
[2]Contents of this chapter were published in parts in [22, 23].

8

calculated using optimization methods to minimize ACI while keeping the extension power at an acceptable level. Using this technique, interference to adjacent signals is reduced significantly at the cost of a small decrease in the useful symbol energy. The proposed method can be used by CR systems to shape the spectrum of OFDM signals and to minimize interference to LUs, or to reduce the size of guard bands used in conventional OFDM systems.[3]

### 1.2.4 Chapter 5: Analysis and Optimization of OFDMA Uplink Systems Over Time-Varying Frequency-Selective Rayleigh Fading Channels

Channel estimation and equalization is one the processes that significantly impacts the overall performance of OFDMA systems. In this chapter, the performance of OFDMA-UL systems over time-varying frequency-selective Rayleigh fading channels is investigated. Expressions for the BER performance for quadrature phase shift keying (QPSK) and quadrature amplitude modulation (QAM) signals under channel estimation errors are derived. Based on BER performance, the optimum pilot insertion rates for a tile-based OFDMA system to maximize the overall system throughput are investigated.

### 1.2.5 Chapter 6: IQ Imbalance Correction for OFDMA Uplink Systems

Direct conversion receivers are attractive for low cost systems as they avoid IF filters. However, the direct conversion from RF to complex I and Q baseband signals in one mixing step introduces additional front-end distortions. These IQ distortions lead to a degradation in the system performance. The problem becomes more significant in OFDMA systems where multiple user signals with different IQ impairments are combined in the UL signal. In this chapter, detection methods for OFDMA-UL signals corrupted by IQ distortions are investigated. The received signal as a function of transmitted signals, IQ parameters, and communication channels is mathematically formulated. We designed a novel pilot pattern that is used by two proposed estimation and compensation methods for the IQ impairments in the signal. Through simulations, proposed methods were shown to significantly improve the system performance.[4]

---

[3]Contents of this chapter were published in parts in [24, 25].
[4]Contents of this chapter were published in parts in [26].

### 1.2.6 Chapter 7: Error Vector Magnitude Based SNR Estimation in Blind Receivers

EVM is one of the widely accepted figure of merits used to evaluate the quality of communication systems. In the literature, EVM has been related to SNR for data-aided receivers, where preamble sequences or pilots are used to measure the EVM, or under the assumption of high SNR values. In this chapter, this relation is examined for nondata-aided receivers and is shown to perform poorly, especially for low SNR values or high modulation orders. The EVM for nondata-aided receivers is then evaluated and its value is related to the SNR for QAM and pulse amplitude modulation (PAM) signals over AWGN channels and Rayleigh fading channels, and for systems with IQ imbalances. The results show that derived equations can be used to reliably estimate SNR values using EVM measurements that are made based on detected data symbols. Thus, presented work can be quite useful for measurement devices such as vector signal analyzers (VSA) or other wireless standards, where EVM measurements are readily available.[5]

---

[5]Contents of this chapter were published in parts in [27].

# CHAPTER 2

# OFDM FOR COGNITIVE RADIO: MERITS AND CHALLENGES

## 2.1  Introduction

With emerging technologies and with the increasing number of wireless devices, the radio spectrum is becoming increasingly congested everyday. On the other hand, measurements show that wide ranges of the spectrum are rarely used most of the time, while other bands are heavily used. Depending on the location, time of the day, and frequency bands, the spectrum is actually found to be underutilized. However, those unused portions of the spectrum are licensed and thus cannot be used by systems other than the license owners. Hence, there is a need for a novel technology that can benefit from these opportunities. cognitive radio (CR) arises to be a tempting solution to spectral crowding problem by introducing the opportunistic usage of frequency bands that are not heavily occupied by licensed users (LU) [2, 4]. CR can be defined as an intelligent wireless system that is aware of its surrounding environment through sensing and measurements; a system that uses its gained experience to plan future actions and adapt to improve the overall communication quality and meet user's needs.

A main aspect of CR is to autonomously exploit locally unused spectrum to improve spectrum utilization. Other aspects include interoperability across several networks, devices, and protocols; roaming across borders while being able to stay in compliance with local regulations; adapting the system, transmission, and reception parameters without user intervention; and having the ability to understand and follow actions and choices taken by their users to learn and become more responsive over time. The focus of this chapter is the first aspect, i.e. CR's ability to sense and be aware of its operational environment, and dynamically adjust its radio operating parameters accordingly. For CR to achieve this objective, the physical layer (PHY) needs to be highly flexible and adaptable. A special case of multicarrier transmission known as orthogonal frequency division multiplexing (OFDM) is one of the most widely used technologies in current wireless communications systems.

OFDM has the potential of fulfilling the aforementioned requirements of CR inherently or with minor modifications. Because of its attractive features, OFDM has been successfully used in numerous wireless standards and technologies. We believe that OFDM will play an important role in realizing CR concept as well by providing a proven, scalable, and adaptive technology for air interface.

In this chapter, OFDM technique is investigated as a candidate for CR systems. CR features and requirements are discussed in detail, and OFDM's ability to satisfy these requirements is explained. In addition, we go through the challenges that arise from employing OFDM technology in CR.

This chapter is organized as follows. The basic system model of OFDM systems is introduced in Section 2.2. In Section 2.3, the structure of an OFDM-based CR is presented. Section 2.4 discusses the merits of OFDM technology and its advantages when employed by CR systems. Challenges to a practical OFDM-based CR system and possible solutions are addressed in Section 2.5. Section 2.6 looks into present and future technologies that use OFDM with Cognitive features. Section 2.7 concludes the chapter.

## 2.2 A Basic OFDM System Model

A simplified block diagram of a basic OFDM system is given in Fig. 2.1. In a multipath fading channel, due to the frequency selectivity, each subcarrier can have different attenuation. The power on some subcarriers may be significantly less than the average power because of deep fades. As a result, the overall bit error rate (BER) may be largely dominated by a few subcarriers with the lowest power level. To reduce the degradation of system performance due to this problem, channel coding can be used prior to the modulation of the bits. Channel coding can reduce the BER significantly depending on the code rate, decoder complexity, signal-to-noise ratio (SNR) level among other factors. Interleaving is also applied to randomize the occurrence of bit errors and introduce system immunity to burst errors. Coded and interleaved data bits are then mapped to the constellation points to obtain data symbols. This step is represented by the modulation block of Fig. 2.1. The serial data symbols are then converted to parallel data symbols which are fed to the inverse fast Fourier transform (IFFT) block to obtain the time domain OFDM symbols. Time domain samples
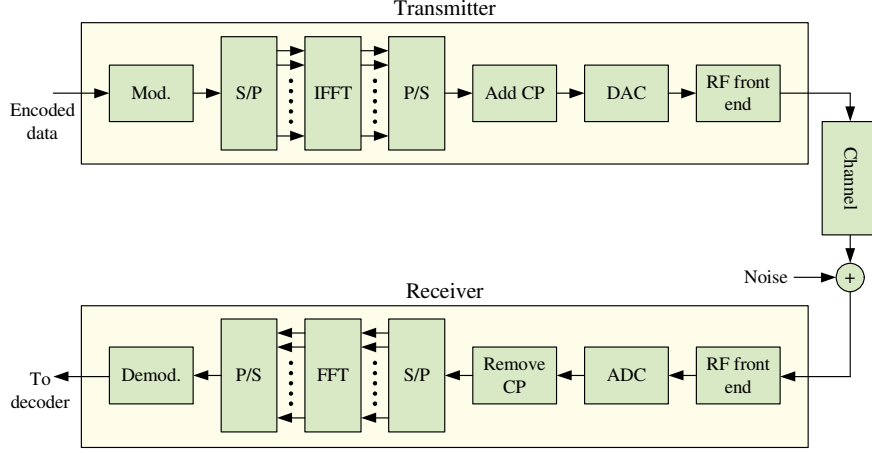
Figure 2.1 Block diagram of a generic OFDM transceiver.

is represented as

$$
\begin{aligned}
x(n) &= \text{IFFT}\left\{X(k)\right\} \\
&= \sum_{k=0}^{N-1} X(k)\exp\left(\frac{j2\pi nk}{N}\right), \qquad 0 \le n \le N-1
\end{aligned}
\tag{2.1}
$$

where $X(k)$ is the transmitted symbol on the $k$th subcarrier and $N$ is the number of subcarriers. Time domain signal is cyclically extended to avoid residual inter-symbol interference (ISI) from the previous OFDM symbols. A simplified baseband digital signal is converted to analog signal through the digital to analog converter (DAC) block. Then, the signal is fed to the radio frequency (RF) front end. The RF front end up-converts the signal to the RF frequencies using mixers, amplifies it using power amplifiers (PA), and transmits it through antennas.

In the receiver side, the received signal is passed through a band-pass noise rejection filter and down-converted to baseband by the RF front end. The analog to digital converter (ADC) digitizes the analog signal and re-samples it. After frequency and time synchronization (which are not shown in the figure for simplicity), cyclic prefix (CP) is removed and the signal is transformed to the frequency domain using the fast Fourier transform (FFT) block. A simplified baseband model of the received symbols in the frequency domain can be written as

$$
Y(k) = H(k)X(k) + W(k)
\tag{2.2}
$$
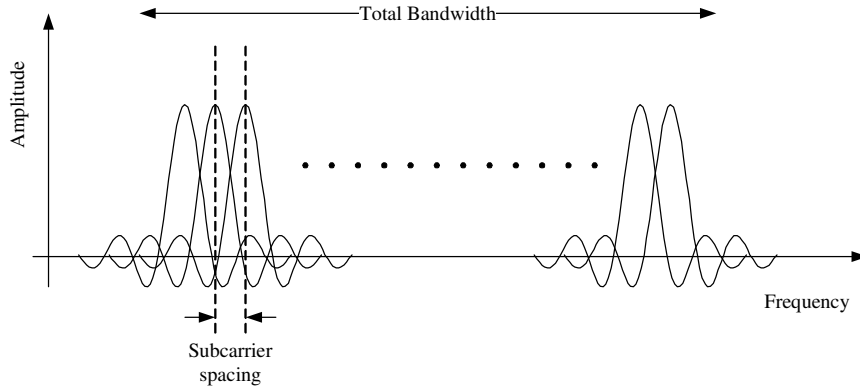
Figure 2.2  OFDM waveform.

where $Y(k)$ is the received symbol on the $k$th subcarrier, $H(k)$ is the frequency response of the channel on the same subcarrier, and $W(k)$ is the additive noise plus interference sample which is usually assumed to be a Gaussian variable with zero mean and variance of $N_0/2$. Note that OFDM converts the convolution in time domain into multiplication in frequency domain, and hence simple one-tap frequency domain equalizers can be used to recover the transmitted symbols. After FFT, the symbols are demodulated, deinterleaved and decoded to obtain the transmitted information bits.

Fig. 2.2 shows a typical OFDM waveform in frequency domain. The figure shows the orthogonal subcarriers to modulate the transmitted data. For a given bandwidth, the communication channel affects some of the design parameters of the OFDM system. The main parameter of an OFDM system are the symbol time, the subcarrier spacing (or consequently the number of subcarriers), the CP length. In order to design an OFDM system properly, one should first understand the impact of wireless communication channels on an OFDM signal.

The transmitted signal usually arrives at the intended receiver either directly in a straight line, also called line-of-sight (LOS) communication, or after being reflected on surfaces of buildings, cars, and other surroundings in the environment, also called as non-line-of-sight (NLOS). The NLOS communication is more common for long range wireless systems. As a result of the signal being reflected on multiple surfaces, the received signal becomes a sum of the transmitted signal with different delays and gains corresponding to the multiple paths the signal traveled through. Such a channel is usually referred to as multipath channel (see Fig. 2.3).

The main effects of multipath channel on the received signal are frequency-selective fading and ISI. Frequency selective fading means that the channel does not affect all frequency components of

14
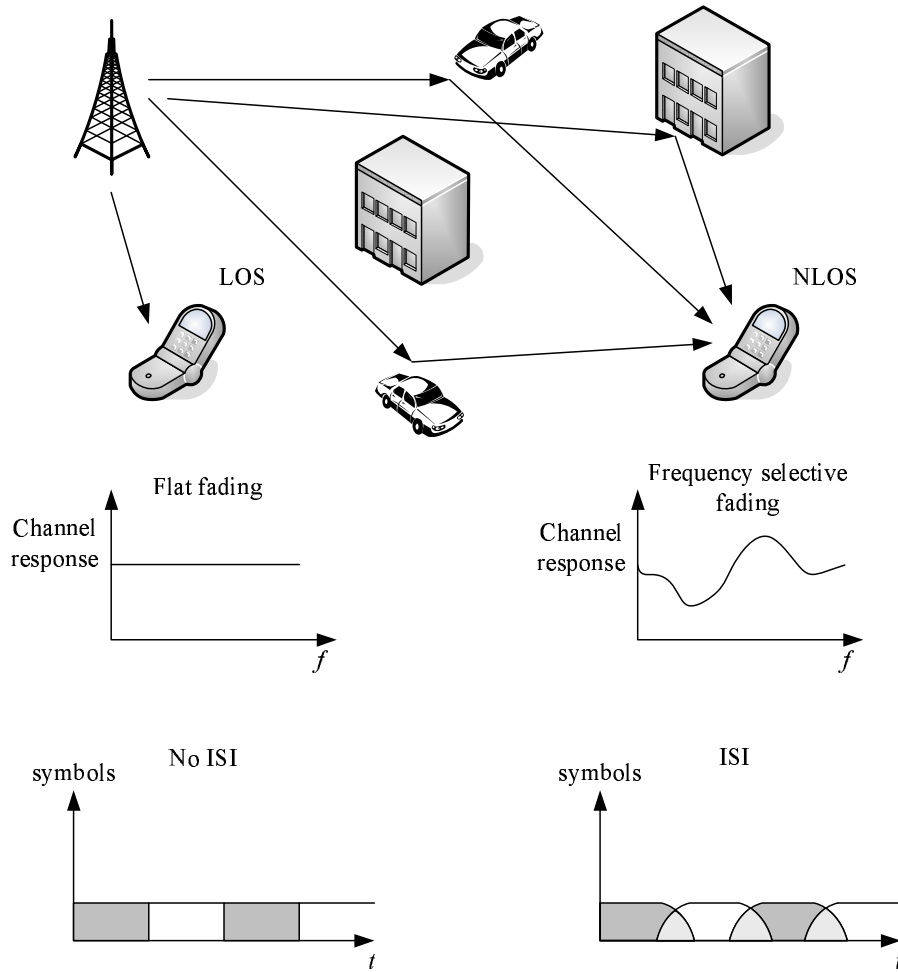
Figure 2.3  Multipath channels.

the signal equally which results in high distortion of the received signal. On the other hand, ISI is the interference between consequent symbols of the same signal. Due to receiving multiple copies of the signal with different delays, a symbol can leak a part of its energy into the following symbol. If not dealt with, both frequency-selective fading and ISI can result in a significant degradation to the system performance.

Channel Equalizers are usually used to compensate multipath effects. Equalizers can considerably increase the system complexity as their complexity increases depending on the number of channel paths. In OFDM system, however, the need for equalizers can be avoided by careful system design. To avoid ISI, symbols duration are extended by adding a guard band to the beginning of each symbol in what is known as CP. If we define the delay spread, or multipath spread, of the channel as the delay

between the first and last received paths over the channel, the CP should be equal to or longer than that delay. On the other hand, the frequency-selective fading is avoided by decreasing the subcarrier spacing or consequently increasing the number of subcarriers. We define the channel coherence bandwidth as the bandwidth over which the channel could be considered flat. Since ODFM signal can be considered as group of narrow band signals, by increasing the number of subcarriers, the bandwidth of each subcarrier, also known as the subcarrier spacing, becomes narrower. By choosing the subcarrier spacing to be less than the coherence bandwidth of the channel, each subcarrier is going to be affected by a flat channel and thus complex channel equalization is not needed.

Another channel effect that should be considered in the OFDM systems design is the mobility. For fixed communication systems, the channel can be considered constant over time. However, if either of the transmitter or the receiver is mobile, the channel is going to vary over time resulting in fast fading of the received signal. Coherence time of the channel is defined as the time over which the channel is considered constant. To avoid fast fading effect, OFDM symbol time is chosen to be equal to or shorter than the coherence time of the channel. In the frequency domain, mobility results in a frequency spread of the signal which is dependent on the operating frequency and the relative speed between the transmitter and receiver, also know as Doppler spread [28]. Doppler spread of OFDM signals results in inter-carrier interference (ICI) which can be reduced by increasing the subcarrier spacing.

In conclusion, while increasing the symbol time reduces ISI effect, shorter symbol time is desirable to avoid fast fading of the signal. And while decreasing subcarrier spacing reduces ICI, narrower subcarrier spacing helps avoiding frequency selectivity. As a matter of fact, there exist an optimum value of these parameters that should be used to improve the system performance [29].

In the aforementioned, a single user system model is represented, where the available channel is used by a single user. Note that OFDM by itself is not a multiple access technique. However, it can be combined with existing multiple accessing methods to allow multiple users to access to the available channel. Some of the most common multiple access techniques that can be employed by OFDM systems are time division multiple access (TDMA), carrier sense multiple accessing (CSMA) [6], frequency division multiple accessing (FDMA), and code division multiple access (CDMA) based schemes [30]. In addition, a mix of TDMA and FDMA known as orthogonal frequency division multiple access (OFDMA) [31] is also possible. Note that in the above system model, the interference from other users and other technologies, such as co-channel interference (CCI), adjacent channel

interference (ACI), narrow-band interference (NBI), etc.; are all folded into the noise term for the sake of simplicity. However, in reality, when the received signal is impaired by a dominant interferer, a more accurate model needs to be used.

## 2.3  OFDM-Based CR

In this chapter, we assume a CR system operating as a rental user (RU) in a licensed band. The CR system identifies available or unused parts of the spectrum and exploit them. The goal is to achieve maximum throughput while keeping interference to LUs to a minimum. An example of such a CR system could be the IEEE 802.22 standard-based system where the spectrum allocated for TV channels is reused. In this case, the TV channels are the LU and the standard-based systems are the RUs (see section 2.6.2 for more details). A block diagram of the CR-OFDM system considered in this chapter is shown in Fig. 2.4[1]. Note that all of the layers can interact with the Cognitive engine. The cognitive engine is responsible for making intelligent decisions and configuring the radio and PHY parameters. The transmission opportunities are identified by the decision unit based on the information from policy engine as well as local and network spectrum sensing data. As far as the PHY layer is concerned, CR can communicate with various radio access technologies in the environment, or it can improve the communication quality depending on the environmental characteristics, by simply changing the configuration parameters of the OFDM system (see Table 2.1 for some example parameters) and the RF interface. Note that coding type, coding rate, interleaver pattern, and other medium access control (MAC) and higher layer functionalities, etc., should also be changed accordingly.

## 2.4  Why OFDM is a Good Fit for CR

OFDM's underlying sensing and spectrum shaping capabilities together with its flexibility and adaptivity make it probably the best transmission technology for CR systems. In the following, we present some of the requirements for CR and explain how OFDM can fulfill these requirements. A summary of these requirements and strength of OFDM in meeting them are presented in Table 2.2.

---

[1]Some OFDM functions are skipped or simplified in order to keep the figure simple.
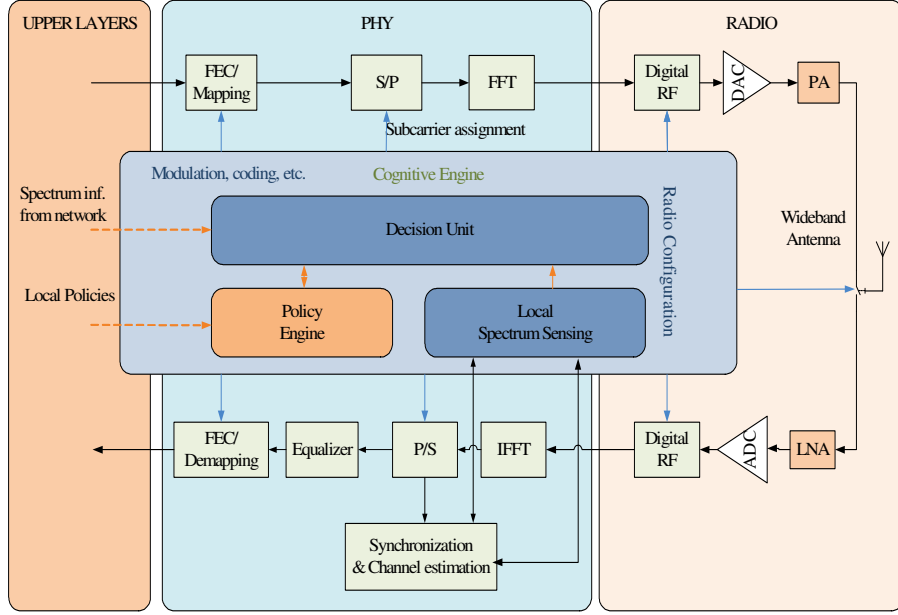
Figure 2.4  OFDM-based CR system block diagram.

Table 2.1  OFDM-based wireless standards.

| Standard | IEEE 802.11(a/g) | IEEE 802.16(d/e) | IEEE 802.22 | DVB-T |
|---|---|---|---|---|
| FFT size | 64 | 128, 256, 512, 1024, 2048 | 1024, 2048, 4096 | 2048, 8192 |
| CP size/FFT size | 1/4 | 1/4, 1/8, 1/16, 1/32 | variable | 1/4, 1/8, 1/16, 1/32 |
| Bit per symbol | 1, 2, 4, 6 | 1, 2, 4, 6 | 2, 4, 6 | 2, 4, 6 |
| Pilots | 4 | variable | 96, 192, 384 | 62, 245 |
| Bandwidth (MHz) | 20 | 1.75 to 20 | 6, 7, 8 | 8 |
| Multiple accessing | CSMA | OFDMA, TDMA | OFDMA, TDMA | N/A |

### 2.4.1   Spectrum Sensing and Awareness

One of the most important elements of CR concept is the ability to measure, sense, learn, and be aware of important operating conditions [32]. This includes parameters related to the radio channel characteristics, availability of spectrum, interference temperature, and radio's operational environments. In addition, the system should be aware of user requirements and applications, available networks infrastructures and nodes, local policies and other operating restrictions. CR

Table 2.2  OFDM properties vs. CR requirements.

| CR Requirements | OFDM Strengths |
| --- | --- |
| Spectrum sensing | Inherent FFT operation of OFDM eases spectrum sensing in frequency domain. |
| Efficient spectrum utilization | Waveform can easily be shaped by simply turning off some subcarriers where LUs exist. |
| Adaptation/scalability | OFDM systems can be adapted to different transmission environments and available resources. Some adaptable parameters are FFT size, subcarrier spacing, CP size, modulation, coding, subcarrier powers. |
| Advanced antenna techniques | Techniques such as multiple-input multiple-Output (MIMO) are commonly used with OFDM mainly because of the reduced equalizer complexity. OFDM also supports smart antennas. |
| Interoperability | With wireless local area network (WLAN) (IEEE 802.11), wireless metropolitan area network (WMAN) (IEEE 802.16). wireless regional area network (WRAN) (IEEE 802.22), WPAN (IEEE 802.15.3a) all using OFDM as their PHY techniques, interoperability becomes easier compared to other technologies. |
| Multiple accessing and spectral allocation | Support for multiuser access is already inherited in the system design by assigning groups of subcarriers to different users (i.e. OFDMA). |
| NBI Immunity | NBI affects only some subcarriers in OFDM systems. These subcarriers can be simply turned off. |

should be able to identify and exploit the unused parts of the spectrum in a fast and efficient way. In OFDM systems, conversion from time domain to frequency domain is achieved by using FFT. Hence, all the points in the time-frequency grid of the OFDM system's operating band can be scanned without any extra hardware or computation thanks to the hardware reuse of FFT cores. Using the time-frequency grid, the selection of bins that are available for exploitation (spectrum holes) can be carried out using simple hypothesis testing. In [33, 34], FFT is applied to the received signal. By using the output of FFT, the receiver tries to detect the existence of a LU in the band. In [34], more than one FFT output (averaging in time) is used. However, averaging in time increases the delay or temporal overhead. In [35], the averaging size (number of FFTs) is adapted in order to increase the efficiency in a cooperative sensing environment. The LU signal is usually spread over a group of FFT output samples as the bandwidth of LU is expected to be larger than the considered bandwidth divided by the FFT size. Using this fact, the FFT output is filtered for noise averaging in order to obtain a better performance [36]. In these sensing algorithms, the availability of FFT circuitry in OFDM systems eases the requirements on the hardware. Moreover, the computational
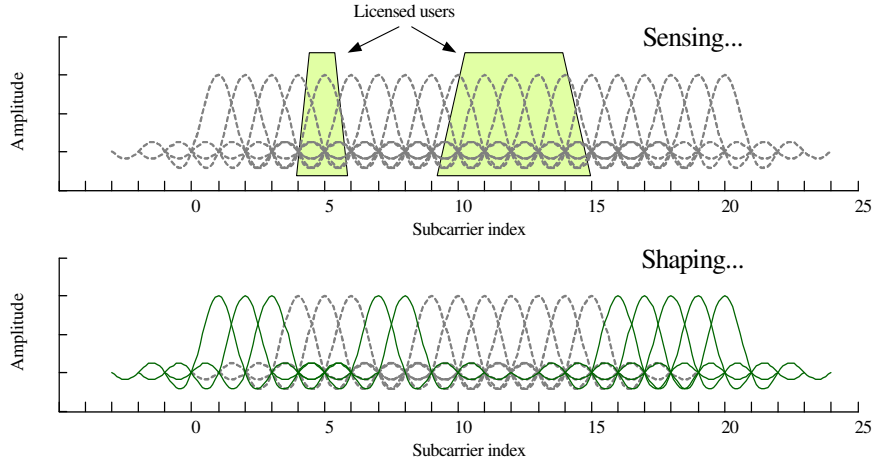
Figure 2.5  Spectrum sensing and shaping using OFDM.

requirements of the spectrum sensing algorithm is reduced as the receiver already applies FFT to the received signal in order to transform the received signal into frequency domain for data detection.

### 2.4.2  Spectrum Shaping

After a CR system scans the spectrum and identifies active LUs, other RUs, and available opportunities; comes the next step: spectrum shaping. Ideally, it is desired to allow RUs to freely use available bands in the spectrum. It is desired to have a flexible spectrum mask and have control over waveform parameters such as signal bandwidth, power level, and center frequency. OFDM systems can provide such flexibility thanks to the unique nature of OFDM signaling. By disabling a set of subcarriers, the spectrum of OFDM signals can be adaptively shaped to fit into the required spectrum mask[2]. Assuming the spectrum mask is already known to the CR system, choosing the disabled subcarriers is a relatively simple process.

An example of spectrum sensing and shaping procedures in OFDM-based CR systems is illustrated in Fig. 2.5. The two LUs are detected using the output of the FFT block, and subcarriers that can cause interference to these LUs are turned off. The transmitter then uses the unoccupied part of the spectrum for signal transmission.

---

[2]See Section 2.5.5 for more details and for more advanced algorithms.

### 2.4.3 Adapting to the Environment

Adaptivity is one of the key requirements of CR. By combining gathered information (awareness) with knowledge of current system capabilities and limitations, CR can perform various tasks. CR can adapt its waveform to interoperate with other friendly communication devices, choose the most appropriate communication channel or network for transmission, and allocate best frequency to transmit in a free band of the spectrum. The system waveform can also be adapted to compensate for channel fading, and nullify any interfering signal. OFDM offers a great flexibility in this regard as the number of parameters for adaptation is quite large [37]. An OFDM-based system can adaptively change the modulation order, coding, and transmit power of each individual subcarrier based on user needs or the channel quality [38]. This adaptive allocation can be optimized to achieve various goals such as increasing the system throughput, reducing BER, limiting interference to LUs, increasing coverage, or to prolong unit battery life. In multiuser OFDM systems, subcarriers allocation to users can be done adaptively as well to achieve the same goals [39].

One of the attractive features of OFDM for broadband communications is its ability to operate using simple one tap equalizers, in the frequency domain. To maintain this feature, the subcarrier spacing in set to be less than the channel coherence bandwidth. In addition, to avoid ISI, the system appends a CP to each symbol with a duration longer than the channel maximum delay spread. Based on estimated channel parameters, an OFDM-based CR system can adaptively change the length of the CP to maintain an ISI-free signal while maximizing the system throughput [29]. Similarly, OFDM system can adaptively change the subcarrier spacing to reduce ICI or peak-to-average-power ratio (PAPR) [29], the data subcarrier interleaving to reduce BER [40], or even the used pilot patterns [41].

The adaptivity in OFDM systems can be performed either at algorithm level or at parameter level. In classical wireless systems, usually algorithm parameters, e.g. coding rate, have been adapted in order to optimize the transmission. However, in cognitive OFDM systems, algorithm type, e.g. channel coding type, can also be adapted in order to achieve interoperability with other systems and/or to further optimize system performance. To achieve such adaptivity, a fully configurable hardware platform would be needed.

### 2.4.4 Advanced Antenna Techniques

Advanced antenna techniques are not necessarily required for CRs. However, they are desirable as they provide better spectral efficiency which is the primary motivation for CR. Smart antennas and multiple-input multiple-Output (MIMO) systems can be used to exploit the spatial dimension of spectrum space, e.g. through beam forming, to improve the efficiency. In essence, multi-antenna systems can help to find spectral opportunities in the spatial domain and can help to exploit these opportunities in full. The use of MIMO techniques offers several important advantages including spatial degree of freedom, increased spectral efficiency and diversity [42]. These advantages can be used to increase the spectrum utilization of the overall system. Furthermore, beamforming, diversity combining, and space-time equalization can also be applied to cognitive OFDM systems. Another application of adaptive antenna techniques is the reduction of the interference in OFDM systems [43].

MIMO systems commonly employ OFDM as their transmission technique because of simple diversity combination and equalization, particularly at high data rates. In MIMO-OFDM, the channel response becomes a matrix. Since each tone can be equalized independently, the complexity of space-time equalizers is avoided and signals can be processed using relatively straightforward matrix algebra. Moreover, the advantages of OFDM in multipath are preserved in MIMO-OFDM system as frequency selectivity caused by multipath increases the capacity.

### 2.4.5 Multiple Accessing and Spectral Allocation

The resources available to a CR have to be shared among users. Several techniques can be used to achieve such a task. OFDM supports well-known multiple accessing techniques such as TDMA, FDMA and CSMA. Moreover, CDMA can be used together with OFDM, in which case the transmission is known as multi-carrier code division multiple access (MC-CDMA) or multicarrier direct spread code division multiple access (DS-CDMA).

OFDMA, a special case of OFDM, has gained significant attention recently with its usage in fixed and mobile worldwide interoperability for microwave access (WiMAX) standard [9]. In OFDMA, subcarriers are grouped into sets each of which is assigned to a different user. Interleaved, randomized, or clustered subcarrier assignment schemes can be used. Therefore, OFDMA offers very flexible multiple accessing and spectral allocation capability for CR without any extra hardware complexity. The allocation of subcarriers can be tailored according to the spectrum availability. The flexibility

PAN

IEEE 802.15.3a
(MB-OFDM)*

LAN

IEEE 802.11a/g
Wi-Fi
HIPERLAN

MAN

IEEE 802.16
WiMAX
HIPERMAN

WAN

IEEE 802.22
3GPP*

* Proposed
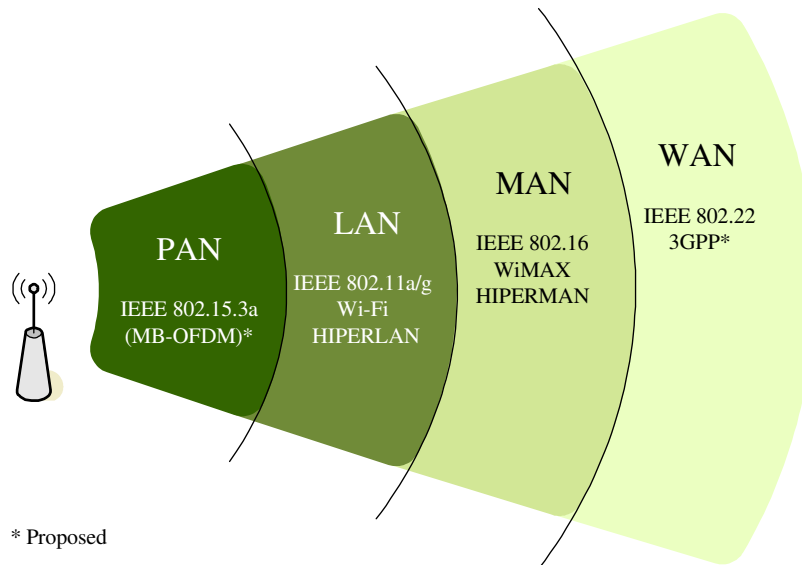
Figure 2.6  OFDM-based wireless technologies.

and support of OFDM systems for various multiple accessing techniques enable interoperability and accelerate the adaptation of CR in future wireless systems.

### 2.4.6  Interoperability

Interoperability is defined as the ability of two or more systems or components to exchange information and to use the information that has been exchanged [44]. Since CR systems may have to deal with LUs as well as other RUs, the ability to detect and encode the existing signals within the used band can improve the performance of CR systems. Furthermore, some recent unfortunate disasters manifested the importance of interoperability in terms of wireless communications for the first responders.  CR has the potential to improve the disaster relief operations by developing the coordination among first responders [45].

To achieve interoperability, OFDM is one of the best signaling candidates.  OFDM signaling has been successfully used in various technologies including the IEEE 802.11a [6] and IEEE 802.11g [46] wireless local area network (WLAN) standards, the IEEE 802.16e-2005 [9] wireless metropolitan area network (WMAN) standard, and the European digital audio broadcasting (DAB) and digital video broadcasting (DVB)standards. Fig. 2.6 shows some of the OFDM-based wireless technologies according to communication range.  As shown in this figure, OFDM has been used in both short range and long range communication systems.  Hence, a CR system employing OFDM can communicate

OFDM Challenges

• ICI
• PAPR
• Synchron-
  ization
• ...

Cognitive
radio-OFDM
Specific
Challenges

Cognitive Radio Challenges

• Spectrum
  sensing
• Cross layer
  adaptation
• Interference
  avoidance
• ...
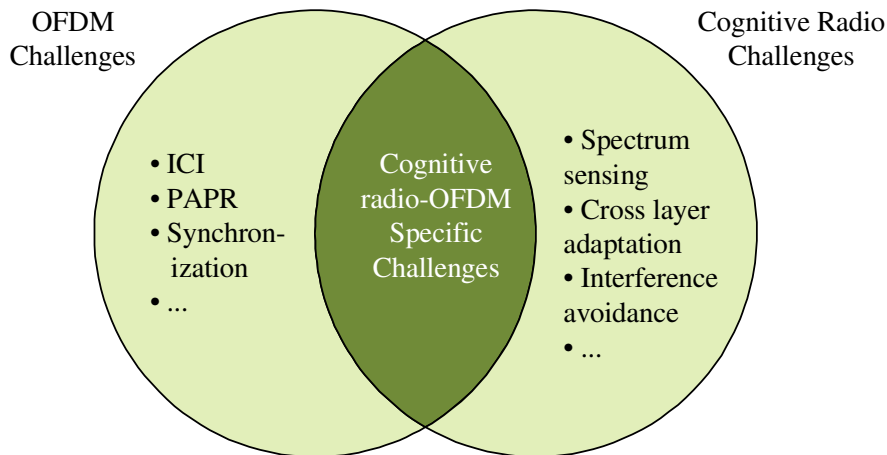
Figure 2.7  Research challenges in CR and OFDM.

with systems using other OFDM-based technologies with much ease. Only the knowledge of signal parameters of intended users is needed (see Table 2.1). However, for such task to be successful, the system needs to know all standard-related information required to decode the signal, such as the data and pilot mapping to the frequency subcarriers, frame structure, and the coding type and rate. More importantly, the RF circuitry of the CR system needs to be flexible enough to accommodate different signal bandwidths and center frequencies. As a result, CR should be built around a software defined radio (SDR) architecture to provide required flexibility to the system.

## 2.5  Challenges to Cognitive OFDM Systems

As an intelligent system with features such as awareness, adaptivity and learning, CR represents the future of wireless systems with the promise of offering solutions to various communication problems. However, with this new technology, new challenges appear, raising interesting research topics. Considering an OFDM-base CR system, the challenges can be grouped into three categories as illustrated in Fig. 2.7. The first category includes the challenges that are unique to classical OFDM systems such as PAPR, and sensitivity to frequency offset and phase noise. The second category includes problems faced by all CRs such as spectrum sensing, cross layer adaptation, and interference avoidance. Our main focus in this article is on the third category: challenges that arise when OFDM technique is employed by CR systems. In the following, we discuss major challenges

to a practical system implementation as well as some of the proposed approaches for solving these challenges.

### 2.5.1 Multiband OFDM System Design

So far we have considered the more conventional single-band OFDM (SB-OFDM) systems. In SB-OFDM systems, the available portion of the spectrum is occupied by a single OFDM signal. If LU exist within the used band, the CR system shapes the OFDM signal as to avoid interference to those users as shown in Fig. 2.5. For systems utilizing wide bands of the spectrum, multi-band signaling approach, where the total bandwidth is divided into smaller bands, can prove to be more advantageous over using single band signaling. This appears to be more significant if the detected free parts of the spectrum are scattered over a relatively wide band. While using a single band simplifies the system design, processing a wide band signal requires building highly complex RF circuitry for signal transmission/reception. High speed ADCs are required to sample and digitize the wideband signal. In addition, higher complexity channel equalizers are also needed to capture sufficient multipath signal energy for further processing. On the other hand, multi-band signaling relaxes the requirements on system hardware as smaller portions of the spectrum are processed separately. Dividing the spectrum into smaller bands allows for better spectrum allocation as well.

For OFDM-based CR, the question becomes when to use multi-band and when to use single band. Given a certain scanned spectrum shape, choosing the number of bands depends on various parameters. Required throughput, hardware limitations, computational complexity, number of spectrum holes and their bandwidth, and interference level are examples of what could affect a CR choice. We further illustrate the importance of multi-band signaling with the next example.

Consider the scenario where a CR senses the spectrum and finds the results shown in Fig. 2.8. Two main spectrum holes are detected with 10 MHz and 15 MHz bandwidth. One of the spectrum holes contains NBI. The detected vacancies in the spectrum are 1 GHz apart. In such scenario, if the system chooses to use SB-OFDM, then the bandwidth of the OFDM signal is going to be 1.025 GHz. A signal with such bandwidth requires ADCs with a sampling rate of at least 1.025 GHz according to Nyquist rate. In addition, a large number of subcarriers is required to guarantee that subcarriers can better fit into the spectrum holes as well as keep the subcarrier's channel relatively flat. Unfortunately, large number of subcarriers results in a more complex FFT operation. Moreover, in order to avoid the NBI in the 15 MHz band, the system drops two out of three subcarriers that are

(a) Sensing spectrum and detecting spectrum holes.

(b) Exploiting spectrum holes using SB-OFDM approach.

(c) Exploiting spectrum holes using MB-OFDM approach.
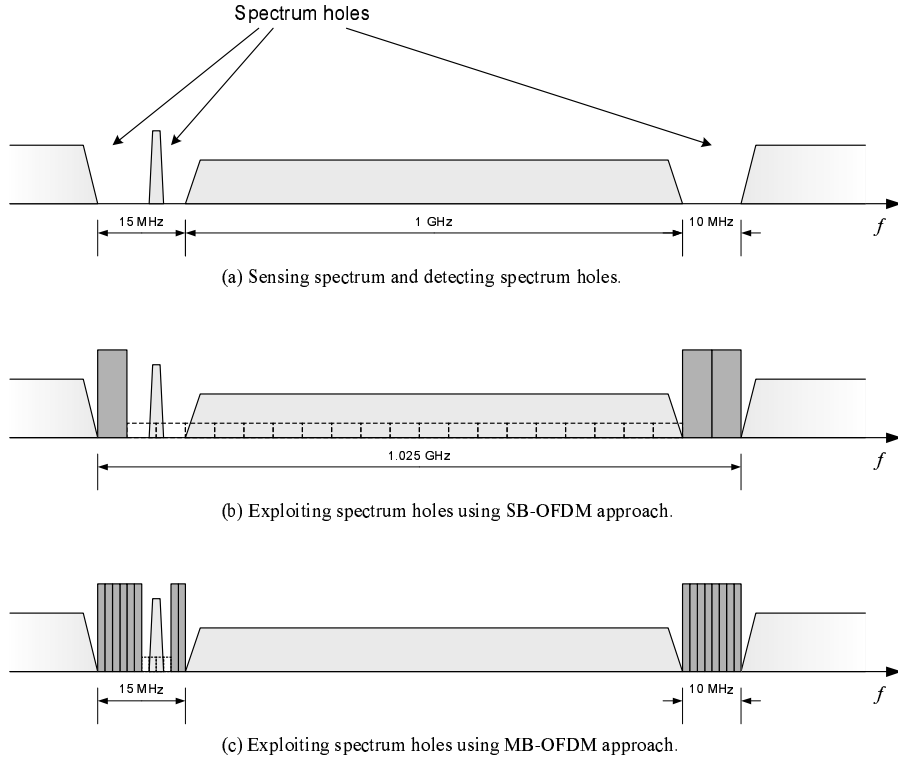
Figure 2.8  Filling spectrum holes using SB-OFDM or MB-OFDM signals.

used to fill the spectrum hole, resulting in a low spectrum efficiency. Now, let's consider multi-band OFDM (MB-OFDM).

By using MB-OFDM, the spectrum holes can be filled with two OFDM signals with 15 and 10 MHz bandwidths. ADCs with a sampling rate of 25 MHz is the minimum requirement for the system. A large number of subcarriers is not necessary for either OFDM signals in that case. In addition, the system has more control over the signal spectrum in each band due to the small subcarrier spacing. Hence, avoiding NBI is achieved while maintaining a higher spectral efficiency. However, the system is now processing two OFDM signals. While sampling frequency is reduced in this MB-OFDM case, the system is performing receiver algorithms (e.g. synchronization, channel estimation and equalization) separately for each band. Another example is shown in Fig. 2.9. In this example a SB-OFDM could be a better choice for the system rather than using five bands in a MB-OFDM scheme. The improvement of spectrum efficiency introduced by using MB-OFDM may not be as significant as the increase in system complexity.

1.025 GHz

(a) Sensing spectrum and detecting spectrum holes.

(b) Exploiting spectrum holes using SB-OFDM approach.

Band 1 Band 2 Band 3 Band 4 Band 5

(c) Exploiting spectrum holes using MB-OFDM approach.
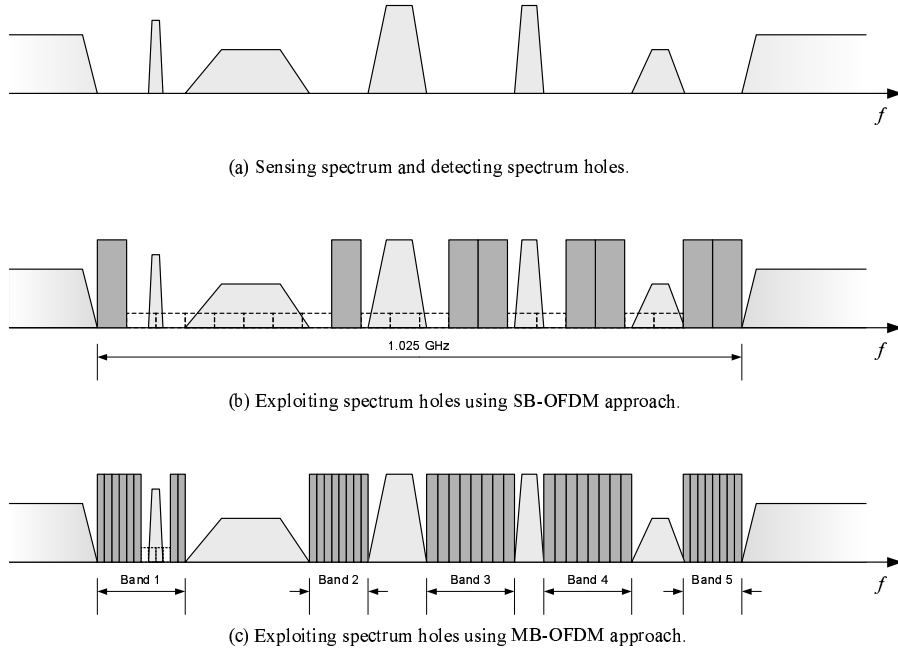
Figure 2.9  Filling spectrum holes using SB-OFDM or MB-OFDM signals.

It is worth mentioning that MB-OFDM is employed in some ultra wide band (UWB) systems. Instead of using a single band UWB signal, the spectrum is divided into sub-bands (with approximately 500 MHz bandwidth each) and OFDM signals are used to transmit data over each band [47, 48]. Fig. 2.10 shows an illustration of the UWB signal in frequency domain. However, while UWB is one of the applications of MB-OFDM, it is only limited to a specific scenario where all sub-bands have almost equal size, and OFDM signals used in sub-bands are identical in other parameters such as CP size and subcarrier spacing.

From a practical point of view, designing a cost effective multi-band transceiver with high performance has been studied in the literature [49–53]. On most proposed transceivers, direct conversion architecture is used to eliminate the need for image rejection filters, and relax the bandwidth requirements for the baseband filters and converters [49, 50]. The challenges that face the implementation of a broadband multi-band OFDM system includes the need for wide range frequency synthesizers, broadband circuits and matching, gain switch in the low noise amplifier (LNA) without degrading the input match, broadband transmit/receive switch at the antenna, desensitization due to adjacent LU interference, and fast band hopping to avoid interference to occupied bands [51]. Frequency synthesizers that can operate in seven bands [52, 53], nine bands [50], and even 12 bands [51] have been presented recently.
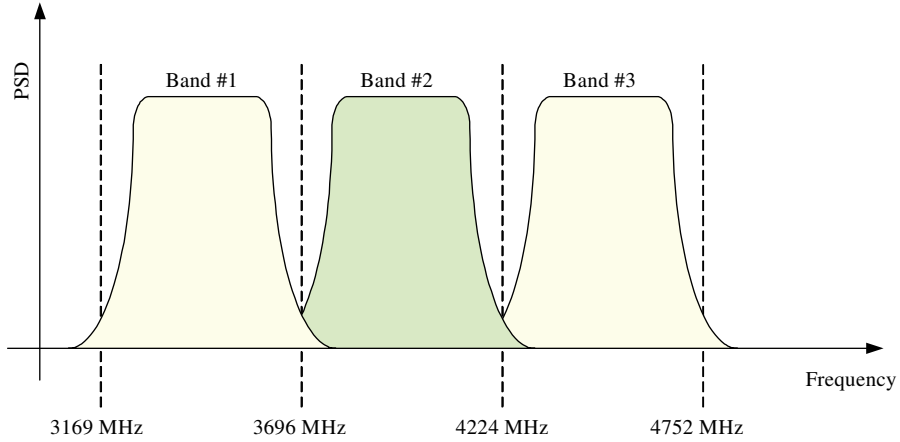
Figure 2.10  Sub-bands of MB-OFDM-based UWB systems in frequency domain.

If single-band transmission is employed, there might be many subcarriers that are deactivated. In such a case, the efficiency of FFT algorithms can be increased and the execution time can be decreased by removing operations on input values which are zero; a process known as pruning. Designing effective pruning algorithms specific to CR-OFDM as to achieve higher performance is an important study subject  [54].

### 2.5.2  Location Awareness

Geolocation information can be used to enable location-based services, optimize the network traffic, and adapt the transceiver to the environment. Applications utilizing location information can be grouped into four categories; location-based services, network optimization, transceiver algorithm development and optimization, and environment characterization. Although some of the existing wireless networks have a miniature utilization of location information, CR is expected to have a more comprehensive location information utilization [55–57].

OFDM signaling can be used to obtain the geolocation information in CRs without the need for any external positioning systems [58]. Pilot sequences, or preambles, which are commonly used in OFDM systems for synchronization, can be used for acquisition and tracking of units' locations. In the literature, both time and frequency domain techniques are proposed to estimate the time of arrival (TOA) using received OFDM signal. Existing WLAN systems are being studied for indoor positioning applications while MB-OFDM-based UWB is proposed for high precision applications. Such positioning capabilities help OFDM to fulfill another requirement of CR.

### 2.5.3 Signaling the Transmission Parameters

In a CR system, communication units sense the surrounding environment and gather up information that can be used to improve the communication link. Based on gathered information, the system selects transmission parameters such as LU bands, spectral mask, operating frequency, coding, and modulation. While some of these parameters can be detected blindly by intended receivers, other parameters need to be known prior to establishing a communication link. Distributing information among communication units rather than using local sensing reduces the complexity and improves the performance of the system. Thus, it is crucial for the success of CR to successfully distribute such information to operational RUs.

One approach to this problem is to dedicate a communication channel for the exchange of measured information and transmission parameters among RUs. However, this requires that a channel be predefined, or licensed, for that purpose. As a result, the ability of RUs to adaptively operate within any given unlicensed band becomes dependent on the availability of such a channel. Moreover, as the number of operating units in the same cell increases, the amount of information that needs to be distributed increases as well. This can result in a huge overhead that the dedicated channel may not be able handle.

Other approaches solve the distribution problem by either reducing the information overhead or by improving the performance of blind detectors. For example, in OFDM systems, based on the scanned channel, waveform is adjusted by turning off some subcarriers in order to exploit the available spectrum holes similar to what is shown in Fig. 2.5. The receivers, however, should be informed about detected spectrum holes, or which subcarriers are deactivated. The overhead is reduced by broadcasting the vector containing disabled subcarriers rather than exchanging the spectrum sensing results. One method to further reduce the overhead is proposed in [59], where the activation/deactivation of subcarriers is performed over a block of subcarriers instead of individual subcarriers. Hence, the signaling overhead can be reduced by a factor of the block size. On the other hand, instead of sharing the spectrum sensing information, tone-boosting can be used to RU of which subcarriers are disabled [60]. Once a RU detects a LU signal within the band, it sends a tone with maximum power but with a very short time duration over the detected signal band. The purpose is to inform other RUs that a LU is operating within this band. As a result, the probability of interference to LUs is reduced, which is one of the main purposes of spectrum sensing. Meanwhile, the short duration of these tones causes no significant interference to LUs.
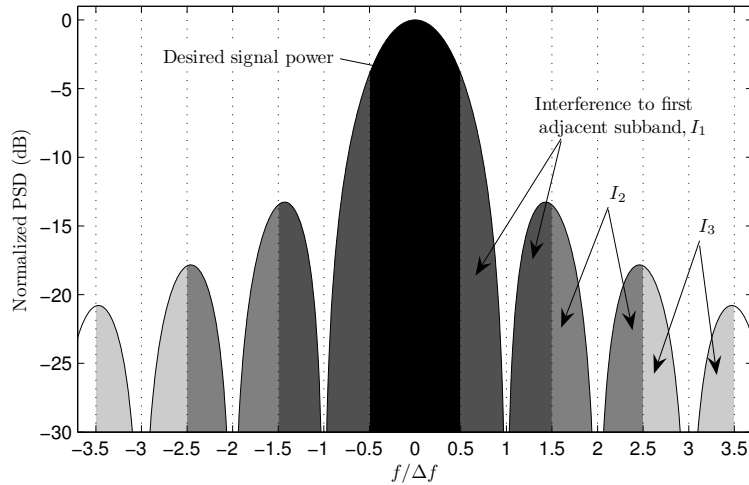
Figure 2.11 Power spectrum density of a single OFDM subcarrier.

### 2.5.4 Synchronization

Synchronization is an important issue that needs to be addressed in OFDM system design. With the introduction of CR, conventional synchronization methods become insufficient. For example, the NBI can distort the preamble that is used for synchronization [61]. The incomplete set of active subcarriers is expected to impact the preamble. Pilots as well may fall into deactivated subcarriers. Moreover, if multiple accessing is employed, subcarriers are assigned to different users. Thus, to keep the orthogonality between subcarriers and to avoid interference, all users should be synchronized to the receiver prior to transmission. In [61], it is shown that longer preambles are required in CR-OFDM systems as compared to conventional OFDM systems. In addition, new preamble structures are introduced and their performances for the time and frequency synchronization are investigated.

### 2.5.5 Mutual Interference

The sidelobes of modulated OFDM subcarriers are known to be large as shown in Fig. 2.11. As a result, there is power leakage from OFDM signals to adjacent channels. In addition, used subcarriers' power leaks to nulled subcarriers which causes mutual interference to LUs. Various techniques are proposed in the literature to reduce this leakage and to enable co-existence of CR-OFDM systems with LUs. One technique is to window the time domain OFDM symbols [62, 63]. In [64], a raised cosine (RC) window is applied. By changing the roll-off factor of the RC window, interference reduction of up to 6 dB can be achieved. Fig. 2.12 and Fig. 2.13 show the RC window shape for
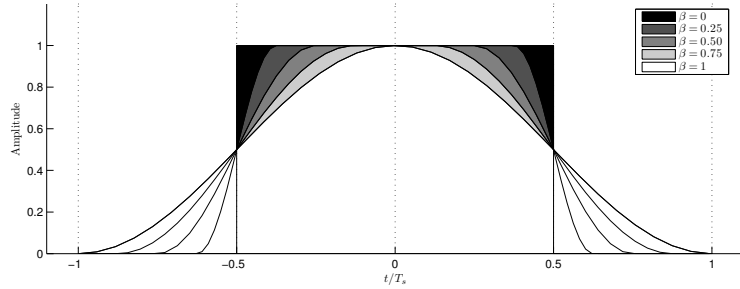
Figure 2.12 RC windowing with different rolloff ($\beta$) values.
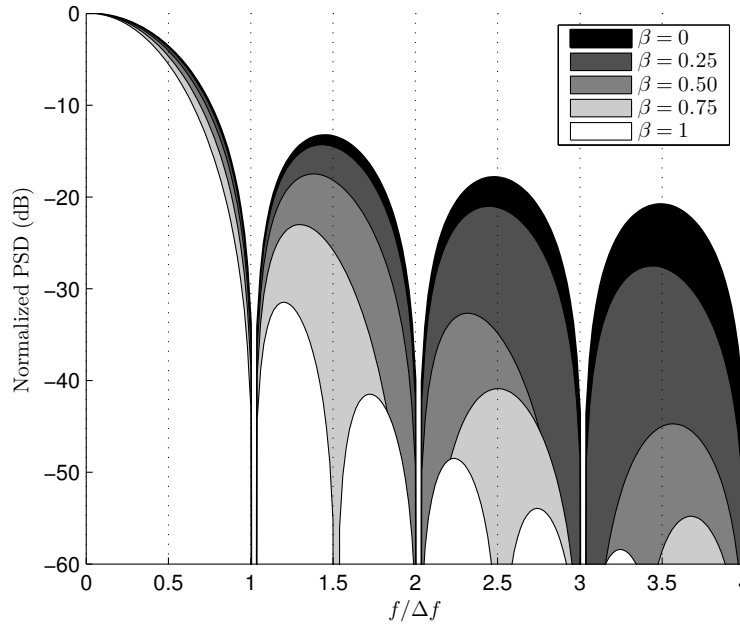


Figure 2.13 Rolloff effect on the PSD of a single OFDM subcarrier.

different roll-off values and the corresponding power spectral densities, respectively. However, the spectrum shape improvement, in this case, comes at the cost of longer OFDM symbol duration and thus a reduction in the spectrum efficiency of the system. Another approach is to increase the number of nulled subcarriers to achieve lower interference levels to LU bands as most of the interference is caused by neighboring subcarriers. However, the obvious disadvantage of this method is again the reduction of spectral efficiency.

A method that reduces interference to spectrum holes while keeping high spectrum efficiency is proposed in [65] and in [66, 67] and is referred to as active interference cancellation and cancellation

carriers, respectively. Instead of disabling subcarriers adjacent to spectrum holes, a much smaller number of those adjacent subcarriers is used to reduce the interference leaked to spectrum holes. The cancellation subcarriers are pre-calculated to reduce subcarrier sidelobes inside spectrum holes. This technique achieves significant reduction of ACI. The disadvantage of this technique is the increase in overall system complexity due to the calculation of cancellation carrier values for each symbol. In addition, for larger spectrum holes, more cancellation carriers are needed to maintain the desired interference level. Analog or digital filters can also be used to filter-out the unwanted spectral components of the OFDM signal prior to transmission. However, since the spectrum mask of a CR signal needs to be adaptive, the use of analog filters is not practical. On the other hand, digital filters introduce an increase in the system computational complexity and processing delay. Other methods to reduce OFDM interference to adjacent channels are presented in [24, 68]. A detailed discussion on this topic is presented in Chapter 4.

## 2.6 A Step Toward Cognitive-OFDM: Standards and Technologies

As CR concept is attracting more interest everyday, recently developed standards are considering more cognitive features. Dynamic frequency selection (DFS), transmit power control (TPC), and spectrum sensing are just a few examples of features that are included in some of the current standards. These standards can be considered as a step toward the future implementation of a CR. In this section, some of the OFDM-based standards which utilize cognitive features are introduced.

### 2.6.1 IEEE 802.16

The first WiMAX standard, IEEE 802.16a [69], operates in the 10 to 66 GHz range. In this frequency range, only LOS communications are possible. The standard later evolved in 2004 to the IEEE 802.16-2004 [8]; also know as IEEE 802.16d. The IEEE 802.16-2004 standard supports the operation in the 2 to 11 GHz range allowing for a NLOS communications. It provides point-to-multipoint access for fixed subscribers. The IEEE 802.16e-2005 [9] standard updates and extends this standard to allow for mobile subscriber stations (SS) traveling at vehicular speeds. A scalable version of OFDMA is introduced improving the overall system performance. While IEEE's role is to develop standards for the PHY and MAC layers, WiMAX forum ensures compatibility and interoperability between vendors' equipments through its certification process.

OFDMA PHY mode is probably the most interesting mode supported by WiMAX. In this mode, a WiMAX base station (BS) is able to support multiple fixed or mobile users at the same time. A BS system can utilize the available channel by dividing the available subcarriers into subchannels. A number of subchannel grouped with a number of OFDMA symbols constitutes a tile. A tile is defined as the minimum data allocation unit [8]. The tile definition shows that the system resources are being shared between users in two domains. The first dimension is frequency which is represented by the number of subcarriers in each tile. The second dimension is time which is represented by number of OFDMA symbols. Fig. 2.14 shows the OFDMA signal structure used for a WiMAX-based system. Note that this figure is only for illustration purposes and thus the number of subcarriers or the tile size does not necessarily reflect the actual numbers used by the standard.

A WiMAX BS can assign users different bandwidths, time durations, transmit power levels, and modulation orders based on various parameters (see Table 2.1) such as the user carrier-to-interference-plus-noise ratio (CINR), received signal strength indicator (RSSI) or the available bandwidth. Moreover, OFDMA PHY offers multiple FFT sizes, CP sizes, and pilot allocation schemes. The FFT size can be selected as 128, 256, 512, 1024 or 2048 depending on the transmission bandwidth[3]. Similarly, the CP length can be set to 1/4, 1/8, 1/16 and 1/32 times the OFDM symbol length. The CP size can be changed depending on the environment characteristics. With all these adaptive features, WiMAX has the ability to adapt to various channel conditions and communication scenarios.

WiMAX standard is also rich in terms of advanced antenna techniques as well. Table 2.3 shows MIMO features available in the IEEE 802.16E-2005 standard [9]. The standard use of these techniques is not directly related to CR, but rather to increase the spectral efficiency and increase the overall throughput of the system. However, advanced antenna techniques could be used to achieve some of the CR goals as well. For example, the CR transmitter can exploit location awareness to focus its radiation only in the direction of intended receivers using adaptive beamforming [4, 70]. On the other hand, the CR receiver can use the same technique to adaptively cancel the interference caused by unintended transmitters [71]. The goal in both cases would be to achieve coexistence of WiMAX devices in unlicensed bands.

---

[3]This is known as scalable OFDMA. Various FFT sizes are used to keep the subcarrier spacing constant for different transmission bandwidths

Table 2.3  Advanced antenna features of WiMAX.

| Techniques | Details | Advantages |
|---|---|---|
| Adaptive antenna systems (AAS) - beamforming | The BS uses multiple antennas to form the beams in the direction of a subcarrier. | Extended range and increased capacity thanks to lower interference. |
| Space time coding (STC) | Transmit diversity such as Alamouti code is used. | Increase in system gain through spatial diversity and reduced fade margin. |
| Spatial multiplexing (SM) | Independent and separately encoded data signals are transmitted over multiple antennas. | Increase in capacity. |
| Collaborative SM | Two users can transmit collaboratively in the same tile as if two streams are spatially multiplexed from two antennas of the same user. | Increase in capacity. |
| Antenna selection | Any combination of antennas are selected (on-off type of selection of group of antennas from the available antennas) based on the channel feedback. | Efficient use of available power. |
| Antenna grouping | The BS can group multiple antennas for different carriers in different ways based on the feedback from the BS. For example, if we have three transmit antennas, the BS can group the first two antennas in some carriers, and the last two antennas in some other carriers. | Maximize diversity and increase capacity. |
| MIMO precoding | The antenna elements are weighted with a matrix before mapping them to transmit antennas based on the feedback from SSs. This scheme is similar to a water-pouring algorithm. | Increase in capacity. |
| STC sub-packet combining | In the initial transmission, the packets are transmitted in a full MIMO spatial multiplexing mode, with no diversity. If the data can not be decoded correctly, i.e. cyclic redundancy check (CRC) check failed, then the packets are sent in full STC mode, or full transmit diversity mode. The receiver combines the initial data and the later data for better detection. | Provides incremental redundancy. |
| Frequency hopping diversity combining (FHDC) | This scheme, as for STC, transmits two complex symbols using the multiple input single output channel. | |
| Adaptive MIMO switching (AMS) | STC or SM is selected adaptively to adapt to channel conditions. | Optimize spectral efficiency is achieved. |
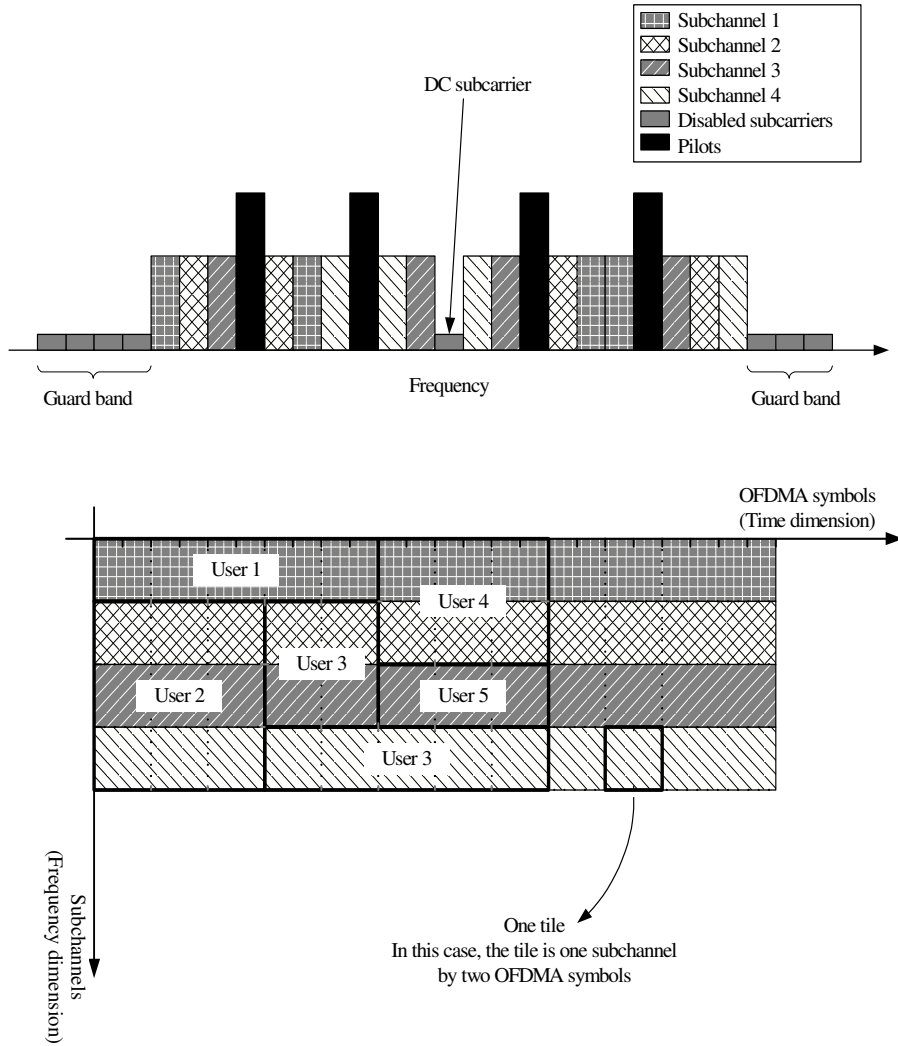
Figure 2.14  Illustration of OFDMA signal structure used in WiMAX.

## 2.6.2  IEEE 802.22

IEEE 802.22 standard is also known as the first CR standard because of the amount of cognitive features that are employed by it. These cognitive features include channel sensing, LUs detection, DFS, and TPC. Even though IEEE 802.22 standard is not finalized yet, the current draft proposal is based on OFDM transmission and it is anticipated that the final version will be the same. The IEEE 802.22 standard is designed for a fixed point-to-multipoint communication topology where the BS acts as the master mandating all the operation parameters of users within the cell. And while the users can share sensing information with the BS through distributed sensing, it is up to the BS to change a user transmit power, modulation, coding or operating frequency.

35

One of the most distinctive features of IEEE 802.22 standard is its sensing requirements which is based on two stages: fast sensing and fine sensing. In the fast sensing stage, a coarse algorithm is employed, e.g. energy detector. The fine sensing stage is initiated based on the previous stage results. However, a more detailed and powerful sensing methods are used in the second stage. The results are returned to the BS which uses these results for managing transmissions.

One challenge in designing the IEEE 802.22 standard is the initialization of new users who desire to communicate with the BS. Unlike current wireless technologies, frequency and time duration of the initialization channel are not predefined. Therefore, initial users have to scan parts, if not all, of the TV bands to find the BS operating frequency and time. In addition, users should be able to differentiate between incumbent signals and the BS signal. This could prove to be very challenging especially if the BS is operating over a combination of multiple frequency bands.

### 2.6.3 IEEE 802.11

The WLAN standard, IEEE 802.11a/g, is probably the most commonly known OFDM-based standard. The main standard is upgraded to have cognitive features with the IEEE 802.11h and the IEEE 802.11k standards. The IEEE 802.11h standard is designed to allow estimation of channel characteristics and DFS. In addition, TPC is incorporated as well, providing the system with more control over signal range and interference level. The purpose of the IEEE 802.11h standard is to allow WLAN systems to share the 5 GHz spectrum with LUs (e.g. military radar systems).

Note that the DFS proposed for the aforementioned standards can be considered as channel switching or frequency hopping technique. Thus, it can be applied to any transmission technology and is not exclusive to OFDM. However, it is also noteworthy to mention that many recent published articles have proposed new methods to facilitate DFS use for OFDM systems. OFDM subcarriers are split into subchannels that can be disabled, enabled, or assigned to multiple users, according to sensing measurements. These recent studies can be divided into two categories: addressing the reduction of interference between different subchannels [24, 65–68, 72–75], and addressing the optimization of the subcahnnel allocation process [76, 77]. In following amendments to wireless standards, we expect that the above advanced OFDM-based techniques will be considered for DFS.

On the other hand, the IEEE 802.11k standard is proposed for radio resource management. It defines several types of measurements such as channel load report, noise histogram report, and station statistics report. The noise histogram report provides methods to measure interference levels

WLAN

WMAN

WRAN

IEEE 802.11

802.11h & 802.11k
DFS, TPC
Site report
RF channel measurements
Hidden nodes sensing
Shared statistics

IEEE 802.16

802.16-2004 & 802.16e-2005
Adaptive FFT size, CP, pilots,
bandwidth allocation

IEEE 802.22

Reuse TV bands
(spectrum sensing)
DFS, TPC
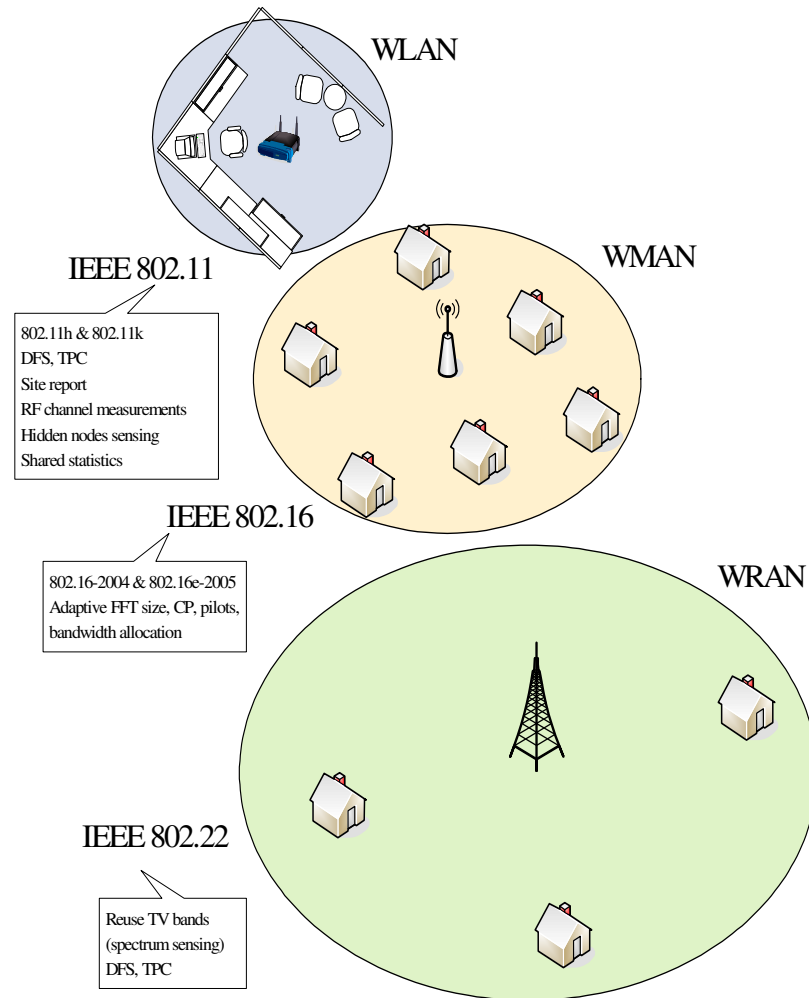
Figure 2.15  Standards and technologies developments.

that display all non-IEEE 802.11 energy on a channel as received by the SSs. The access point (AP) collects channel information from each unit and makes its own measurements. This data is then used by the AP to regulate access to a given channel.

Other features such as tracking of hidden nodes and sharing clients statistics are included in the standard. By applying both the IEEE 802.11h and the IEEE 802.11k standards to current IEEE 802.11-based WLAN systems, the performance and efficiency of wireless networking can be improved significantly. Adding cognitive features such as channel sensing and estimation, statistics distribution, DFS, TPC to WLAN devices will soon be possible. Fig. 2.15 shows an illustration of the discussed current and future technologies and standards.

## 2.7    Conclusion

CR is an exciting and promising technology that offers a solution to the spectrum crowding problem. On the other hand, OFDM technique is used in many wireless systems and proven as a reliable and effective transmission method. OFDM can be used for realizing CR concept because of its inherent capabilities that are discussed in detail in this chapter. By employing OFDM transmission in CR systems; adaptive, aware and flexible systems capable of interoperating with current technologies can be realized. However, the challenges identified in this chapter need to be researched further in order to address the open issues. Practical CR systems can be developed using two approaches: current wireless technologies can evolve to support more cognitive features over time, or new systems that support full cognitive features can be developed. In either case, we foresee that OFDM will be one of the dominant PHY technologies for CR.

# CHAPTER 3

# SYNCHRONIZATION IN OFDMA UPLINK SYSTEMS

## 3.1  Introduction

Worldwide interoperability for microwave access (WiMAX), as a relatively new technology, has received the attention of researchers and wireless companies. This new wireless technology promises to deliver both high data rates and long-range coverage. With the approval of the mobile WiMAX standard (IEEE 802.16e-2005) at the beginning of the year 2006, this technology became even more exciting. Unlike WiFi [78, 79], which is designed for indoor applications and wireless local area network (WLAN), WiMAX is optimized for outdoor applications and wireless metropolitan area network (WMAN).

One of the exciting aspects of WiMAX is that its medium access control (MAC) layer supports more than one physical layer (PHY) mode [9]. This feature not only enables companies to differentiate their products from each other, but also makes WiMAX an adaptive technology that can satisfy different needs depending on the application. One of the most promising PHY modes supported by WiMAX standard is orthogonal frequency division multiple access (OFDMA) PHY mode. OFDMA PHY mode enables a WiMAX base station (BS) to support multiple user access, fixed or mobile, over both time and frequency domains. In this mode, a BS system utilizes the channel by dividing available subcarriers into subchannels that can be assigned to multiple users in a sophisticated and adaptive way. As a matter of fact, users can be assigned to different bandwidths, different time durations, and different modulation orders based on various parameters such as the user carrier-to-interference-plus-noise ratio (CINR) and the available bandwidth.

One of the problems that faces WiMAX systems, and OFDMA systems in general, is synchronization between the BS and subscriber stations (SS) within the cell. While other orthogonal frequency division multiplexing (OFDM) receivers can easily synchronize to the received signal [80, 81], this is not the case for OFDMA receivers. At an OFDMA receiver, where multiple users arrive at the

same time, if users are not synchronized with the receiver, they will interfere with each other, and therefore the BS will not be able to recover individual signals of each user. Hence, for OFDMA PHY mode to work properly, all users should arrive at the BS at the same time with a considerably high timing accuracy. This can be achieved if all users are synchronized with the BS before the communication link is established. The standard states that for a user to join the channel, first, the round trip delay (RTD) between the user and the BS must be known to the user [9]. This delay estimation is used by the user to synchronize its signal such that it arrives at the BS in its allocated time. The process in which this delay is estimated is called initial ranging, and this is mandated for all SSs that desire to synchronize to the channel initially.

As stated in the IEEE 802.16e-2005 standard [9], the MAC layer at the BS defines a ranging channel as a group of six (or more) subchannels, where a subchannel is a group of subcarriers that are chosen according to a randomization formula. In addition, users are allowed to collide in this ranging channel. Any SS that attempts to establish a communication link is required to carry out a successful initial ranging process with the BS over the ranging channel. Once a SS senses a BS, for network entry, it first scans for a downlink (DL) channel and synchronizes itself with the BS. Then, the SS shall acquire transmit parameters, which are included in the uplink channel descriptor (UCD), uplink (UL)-MAP, and DL-MAP. Using acquired parameters, the SS initiates the initial ranging process by sending a ranging code over the UL frame. At the receiver side, the BS is required to detect different received ranging codes and estimate the timing offset and the power for each user that bears an initial ranging code. The BS then broadcasts the detected ranging codes with adjustment instructions for the timing and power level. The status notifications of either a successful ranging process or retransmission are also broadcasted.

In initial ranging, the SS chooses one of the available ranging codes randomly and transmits it twice over two consecutive OFDMA symbols with binary phase shift keying (BPSK) modulation. The SS should transmit the ranging code during the UL frame as long as there is a ranging opportunity. UL-MAP shows if a ranging opportunity is available through the next UL frame. Another option is to send two consecutive ranging codes over four OFDMA symbols to increase the probability of code detection [9]. In this study, ranging over two symbols is considered since the same concept can be applied to the four symbols case.

Synchronization for multiuser OFDM systems has been discussed in the literature. The use of filters matched to the intended user's subcarriers (in our case, the ranging channel subcarriers) and

then use of cyclic prefix (CP) redundancy to estimate the timing offset is proposed in [81]. However, in OFDMA systems with interleaved subcarrier assignment such as WiMAX, the ranging subcarriers are not necessarily adjacent, which makes the filtering process inapplicable. In [82], it is proposed to synchronize users to the BS one at a time, with the assumption that other users are already synchronized. This method cannot be used for OFDMA with multiple users colliding in the ranging channel. In addition, this approach requires the users who are not yet synchronized to the system to be aware of other users attempt to synchronize. Finally, in [83, 84] it is proposed to use a bank of correlators (corresponding to number of ranging codes) in time or in frequency domain to detect received ranging codes. The disadvantage of this approach is that the computational complexity increases as the number of available ranging codes increases.

In this chapter, a new algorithm for OFDMA-UL synchronization or initial ranging is proposed. System parameters are chosen based on the WiMAX standard, since it represents the most recent standard that employs OFDMA. The proposed algorithm is examined using theoretical analysis and computer simulations over additive white Gaussian noise (AWGN) and dispersive channels in the presence of multiuser interference. A performance and complexity comparison between the proposed algorithm and prior algorithms in practical system conditions are presented. It is demonstrated that the proposed algorithm offers a significant reduction in computational complexity while carrying out a successful initial ranging process. The reduction in complexity makes the proposed algorithm more attractive to practical implementations of OFDMA systems. For example, the proposed algorithm can be applied to low-cost OFDMA-based femtocell BS implementations where the number of users per BS is limited.

The remainder of this chapter is organized as follows. The system model is introduced in Section 3.2. Current and proposed ranging algorithms are discussed in detail in Sections 3.3 and 3.4, respectively. In Section 3.5, the computational complexity of the proposed algorithm is calculated and compared to current ranging algorithms. Simulation results and discussions demonstrating the performance of the proposed ranging algorithm compared to other algorithms are presented in Section 3.6. Finally, the conclusions are outlined in Section 3.7.

## 3.2   System Model

The system model is based on the IEEE 802.16e-2005 standard [9]. The UL of an OFDMA system with $N$ subcarriers is considered. After assigning DC and guard subcarriers, the remaining subcar-

riers, $N_d$, are grouped into $Q$ subchannels. Each subchannel has $N_Q = N_d/Q$ subcarriers, where $Q$ is chosen such that $N_d$ is an integer multiple of $Q$. Each user in the UL is assigned one or more subchannels. The BS defines a group of six subchannels (or more) for ranging. Note that the subcarriers assigned to each subchannel are chosen randomly and thus they are not necessarily adjacent. The BS broadcasts all the ranging information (i.e. ranging opportunities, ranging channels, ranging codes and so on) in the UL-MAP. One ranging time slot spans two OFDMA symbol duration. The $k$th ranging user signal in frequency domain is denoted as $\mathbf{c}_p^{(k)} = [c_p^{(k)}(1), c_p^{(k)}(2), ..., c_p^{(k)}(L)]^T$, where $p$ is the index of the randomly chosen ranging code and $L$ is the size of the ranging code. The signal is then extended to $N$ by inserting $N - L$ zeros, which results in $\mathbf{X}_p^{(k)} = [X_p^{(k)}(1), X_p^{(k)}(2), ..., X_p^{(k)}(N)]^T$. Note that

$$X_p^{(k)}(m) = \begin{cases} c_p^{(k)}(n), & \text{if } m = i_r(n), \\ 0, & \text{otherwise} \end{cases} \tag{3.1}$$

where $i_r(n)$ is the index of the $n$th subcarrier within the ranging channel subcarriers set $\mathbf{i}_r = [i_r(1), i_r(2), ..., i_r(L)]^T$. The vector $\mathbf{X}_p^{(k)}$ is then fed to an $N$-point inverse fast Fourier transform (IFFT). The resulting signal in time domain is extended over two OFDMA symbols by repeating $\mathbf{x}_p^{(k)}$ twice and adding the cyclic prefix with no phase discontinuity, where $\mathbf{x}_p^{(k)}$ is the time representation of $\mathbf{X}_p^{(k)}$. Note that the BS receiver uses an observation window of $(N + N_g)$ to acquire OFDMA symbols, where $N_g$ is the size of the CP. Finally, the transmitted signal is denoted as $\mathbf{s}_p^{(k)} = [s_p^{(k)}(1), s_p^{(k)}(2), ..., s_p^{(k)}(2N + 2N_g)]^T$, where,

$$\mathbf{s}_p^{(k)} = \Big[ x_p^{(k)}(N - N_g + 1), \ldots, x_p^{(k)}(N), x_p^{(k)}(1), \ldots, x_p^{(k)}(N),$$
$$x_p^{(k)}(1), \ldots, x_p^{(k)}(N), x_p^{(k)}(1), \ldots, x_p^{(k)}(N_g) \Big]^T. \tag{3.2}$$

The transmitted signal $\mathbf{s}_p^{(k)}$ is then received by the BS after being corrupted by the communication channel. In the following analysis, we assume that the channel is nondispersive and that the received signals from multiple users are only affected by complex AWGN. However, we will evaluate the proposed ranging algorithm performance for both AWGN and dispersive channels. A similar approach has been used in [85] to analyze the proposed algorithm.

All users other than the users performing initial ranging are assumed to be already synchronized to the BS. This is a valid assumption as synchronizing to the BS is mandatory before a SS can

establish the communication link. Hence, it is guaranteed that there is no interference from synchronized user signals to the ranging channel. Note that this is not the case for ranging users as their unsynchronized signal can cause interference to synchronized users. As this situation is unavoidable, initial ranging SS is required by the standard to start the ranging process with minimum possible power level. Then, as long as the SS fails to get a response from the BS, the power is increased incrementally until a response is detected. If the maximum power level is reached and the SS still cannot get a response from the BS, the user starts from the minimum power level and the process is repeated. This shows how important it is for a BS to detect ranging users with the lowest signal levels possible.

## 3.3 Existing Ranging Algorithms

To detect ranging codes at the BS, one approach would be to cross-correlate the received signal with all possible ranging codes in time domain [83]. To reduce the high computational complexity of this process, one can instead auto-correlate the received signal with its delayed replica to exploit the repetition in the ranging code. However, for this approach to work properly, the system needs to extract other non-ranging user signals from the received signal as the ranging users are frequency-multiplexed with those synchronized users. Not only does such a process increase the complexity and delay of the algorithm, but it is also affected by the performance of non-ranging users signal estimator. In addition, the codes used for ranging are modulated in frequency domain and performing the correlation in time domain weakens the auto-correlation/cross-correlation properties of used codes.

Another approach to detect ranging codes is to perform the cross-correlation on the frequency-domain signal at the output of the fast Fourier transform (FFT) [84]. In this case, a complete OFDMA ranging symbol in the observation window results in a correct ranging code in the frequency domain even if a timing offset exists. The effect of the timing offset is translated into a linear phase shift, also called a phase rotation, in the frequency domain. To estimate the timing offset of the ranging code, the system applies all possible linear phase shifts, corresponding to possible timing offsets, to the signal. Then, the received signal is correlated with all ranging codes. A threshold is set to detect the existence of a ranging code in the current observation window and its timing offset. One advantage of performing the cross-correlation process in frequency domain is that there is no interference from non-ranging users to the ranging channel. Thus, the probability of a

missed detection or a false alarm, due to multiuser interference, is reduced. Another advantage of this approach is that operating in frequency domain utilizes the auto-correlation/cross-correlation properties of used ranging codes.

The main disadvantage of the previously mentioned algorithms is the high computational complexity. Consider the maximum RTD to be $\tau_{\max}T_S$, where $T_S$ is the sampling time. If the total number of codes is $K$, then $K\tau_{\max}$ cross-correlation operations are needed for every OFDMA symbol. In the WLAN IEEE 802.16a [69] and IEEE 802.16a/b [86] standards considered in [83] and in [84], respectively, the number of long ranging codes used for initial ranging is only 16. However, for IEEE 802.16e-2005 [9], the number of ranging codes is 256. These codes are divided into three categories: initial ranging codes, periodic ranging codes, and bandwidth-request codes. Initially, the BS is expected to assign more codes for initial ranging as users within the cell start entering the network. If we assume that 128 codes would be assigned for initial ranging, then for OFDMA systems based on IEEE 802.16e-2005, the computational complexity for the ranging process would be eight times as much as the complexity of IEEE 802.16a/b. Other ranging algorithms were proposed in the literature (e.g., [87] and [88]). However, those algorithms are not applicable to the considered standard. Hence, they are not considered in this study.

## 3.4  Proposed Algorithm

In the proposed algorithm, we concentrate more on the trade off between computational complexity and performance of the ranging process so that the algorithm can be realized in practical systems. We choose an observation window with one OFDMA symbol size and apply the algorithm in frequency domain for the advantages of this method that is mentioned earlier in Section 3.3. However, instead of directly cross-correlating with every possible code and every possible phase offset for every OFDMA symbol, we break the initial ranging process into three main tasks. Our first task is to find OFDMA symbols containing ranging codes. This step allows the system to find out which symbols it should process further and which ones the system should just drop so that no additional computations are performed on empty OFDMA symbols. Energy detectors, which are discussed in more detail in Section 3.4.1, are used to detect OFDMA symbols containing ranging codes in the ranging channel. Next, the algorithm finds how many codes there are within detected OFDMA symbols from step one and determine the timing offsets (or linear phase shifts) for each code. Again, in this step the system further reduces the computational complexity by first finding

44

the timing offset of the codes before performing the cross-correlation with all possible codes for every possible linear phase shift. Section 3.4.2 discusses the details of this step. The last step in the algorithm is identification of multiuser codes by cross-correlating detected codes with all possible ranging codes after removal of any timing offsets. This step is covered in Section 3.4.3. Using this approach, the computational complexity is greatly reduced while the performance is still acceptable as shown in Sections 3.5 and 3.6.

### 3.4.1   Energy Detector

If there is a ranging opportunity in the next UL frame, the ranging channel will be available through the entire UL subframe duration. The BS samples the received signal and groups it into $N + N_g$ samples. The CP is removed and the remaining $N$ samples are fed to the FFT unit. The ranging channel contains noise and energy from ranging users. The received unsynchronized signal of a ranging user consists of two ranging symbols with no phase discontinuity. The OFDMA symbols processed by the BS can be only one of three possible cases: $a$) empty symbols containing only noise, $b$) symbols containing incomplete parts of the ranging signal, which cause interference to subcarriers other than the ranging subcarriers and thus interfere with synchronized users, and $c$) symbols that are entirely filled with the ranging signal, referred to as symbols with complete ranging signal. We are interested in detecting the third kind, as it contains the required information to detect the user ranging code. For every ranging user signal, at least one symbol with complete ranging signal should be received by the BS since the ranging signal spans two OFDMA symbols. Empty symbols should be ignored since they contain no information. The information included in OFDMA symbols with incomplete ranging signal (i.e. the ranging code, its timing offset, and signal power) can be extracted from the symbols with complete ranging signal. Therefore, a missed detection of symbols with incomplete signal should not affect the performance of the algorithm. In order to detect symbols with a complete ranging signal we use a simple energy detector in frequency domain. The energy detector measures the energy within the ranging channel. This method has two advantages: $a$) since the energy is measured in the frequency domain and since the ranging subcarriers are not adjacent, the likelihood of a pulse of noise triggering the energy detector by mistake is low, $b$) the energy is already measured to obtain the noise variance of the channel and can also be used later to measure the signal power of ranging users. Therefore, no additional computational complexity is required for this step.

The measured energy in the ranging channel is,

$$\mathcal{E}_g = \sum_{n=0}^{L-1} |Y(m)|^2 \qquad (3.3)$$

where $m = i_r(n)$ and $\mathbf{Y}$ is the $N$ vector at the output of the FFT unit at the receiver side.

After measuring the energy within the ranging channel, a threshold $\eta_1$ is used to decide if the OFDMA symbol contains a ranging code or not. To find the best value for $\eta_1$, the probability of a false alarm $P_{fa}$ and the probability of missed detection $P_{md}$ are calculated. The probability of a false alarm is defined as the probability of noise energy in empty OFDMA symbols exceeding $\eta_1$. In the same manner, the probability of missed detection is defined as the probability of the energy of an OFDMA symbol not exceeding $\eta_1$ while containing a complete ranging signal. Note that the case of an OFDMA symbol containing incomplete ranging signal is ignored in the calculation of $P_{md}$ as missing this symbol does not affect the algorithm performance. In fact, detecting an incomplete ranging signal can additionally provide correct ranging information if the timing offset is relatively small. If the current OFDMA symbol contains no ranging code, then $Y(m) = W(m)$, where $\mathbf{W}$ is a vector of complex AWGN samples with zero mean and $N_0/2$ variance. From (3.3),

$$\mathcal{E}_g = \sum_{n=0}^{L-1} |W(m)|^2 ,$$
$$= \sum_{n=0}^{L-1} W_{\Re}^2(m) + \sum_{n=0}^{L-1} W_{\Im}^2(m) \qquad (3.4)$$

where $W_{\Re}(m)$ and $W_{\Im}(m)$ are the real and imaginary parts of $W(m)$, respectively. The energy in this case is the sum of $2L$ samples of the square of normally-distributed random variables with zero mean and $N_0/2$ variance. Hence, the measured energy can be described as a random variable with Chi-square distribution having a mean $\mu_1 = LN_0$ and variance $\sigma_1^2 = LN_0^2$. Using the central limit theorem, and assuming $2L$ is large enough, the energy distribution can be approximated as a normally-distributed random variable with the same mean and variance. Based on the standard [9], $L$ or the ranging code length is equal to 144 which is large enough to validate the above approximation. The probability of a false alarm then becomes [89],

$$P_{fa} = 0.5 \, \mathrm{erfc} \left( \frac{\eta_1 - \mu_1}{\sqrt{2\pi\sigma_1^2}} \right) \qquad (3.5)$$

where erfc is the complementary error function. For an OFDMA symbol containing a complete ranging signal, if a user $k$ signal has a timing offset of $\tau_k$ samples[1], then the OFDMA symbol with complete ranging signal contains a copy of the ranging code which is cyclically shifted by $\tau_k$ samples. The OFDMA symbol in the frequency domain has a linear phase shift of $2\pi n\tau_k/N$ where $n$ is the subcarrier index. In this case,

$$\mathcal{E}_g = \sum_{n=0}^{L-1} \left| c_p^{(k)}(m) \exp\left[ \jmath \phi_m(\tau_k) \right] + W(m) \right|^2 \tag{3.6}$$

where $\phi_m(\tau_k) = 2\pi m\tau_k/N$. Since BPSK modulation is used, $c_p^{(k)}(m) = \pm 1$. Thus,

$$\mathcal{E}_g = \sum_{n=0}^{L-1} \Bigg\{ 1 + W_{\Re}^2(m) + W_{\Im}^2(m) + $$

$$2c_p^{(k)}(m) \cos\left[ \phi_m(\tau_k) \right] W_{\Re}(m) + 2c_p^{(k)}(m) \sin\left[ \phi_m(\tau_k) \right] W_{\Im}(m) \Bigg\}. \tag{3.7}$$

Using the central limit theorem, the distribution of this energy can be approximated as a normally-distributed random variable with mean $\mu_2 = L + LN_0$ and variance $\sigma_2^2 = LN_0^2 + 2LN_0$ as shown in Appendix A. Hence, the probability of a missed detection becomes,

$$P_{md} = 1 - 0.5 \operatorname{erfc}\left( \frac{\eta_1 - \mu_2}{\sqrt{2\pi\sigma_2^2}} \right). \tag{3.8}$$

Fig. 3.1 shows $P_{fa}$ and $P_{md}$ against normalized $\eta_1$ (normalized by $L$ and $N_0$) for different signal-to-noise ratio (SNR) levels. Note that $P_{fa}$ does not change as the SNR changes since $\eta_1$ is normalized and since $P_{fa}$ depends only on $N_0$. In this study, $N_0$ is assumed to be available for choosing the best value of $\eta_1$. This is a valid assumption since the BS needs to estimate the noise level for calculations of different users SNR. An example of a received UL frame with ranging codes is shown in Fig. 3.2. The received symbols of ranging users are shown in time domain. Also, the figure shows the measured energy on the ranging channel for every OFDMA symbol and for an SNR of 10 dB. Note that in the above analysis, it is assumed that only one complete ranging signal exists in the received symbol. This assumption is based on worst case scenario, since $P_{md}$ gets even lower if more than one complete signal exists in the received symbol as shown in Fig. 3.2.

---

[1]We only consider timing offset that is integer multiple of the sampling time. The non-integer part of the delay is insignificant to the OFDMA system performance and is usually incorporated as part of the communication channel.
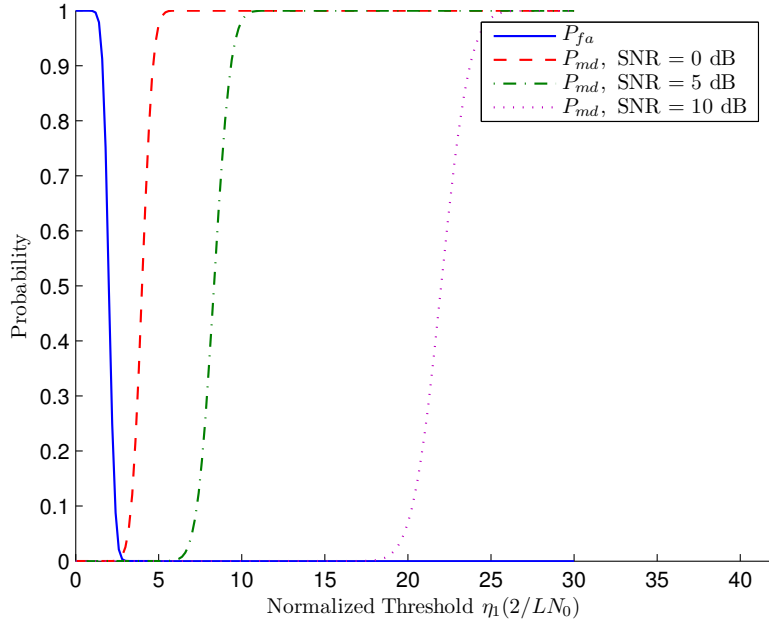
Figure 3.1  $P_{fa}$ and $P_{md}$ for different noise levels.

### 3.4.2  Timing Offset Estimation

In the previous step, the system detects OFDMA symbols containing one or more complete ranging signals. The next step is to identify how many codes are in each symbol and estimate the timing offset for each of these codes. Since the proposed algorithm is applied in frequency domain, timing offset would be directly translated into a linear phase shift. In this case, what is estimated is actually the linear phase shift for each code in the current OFDMA symbol. This can be done by cross-correlating the ranging channel of the current OFDMA symbol with all possible codes after applying all possible linear phase shifts to the symbol. The correlator output is followed by a threshold detector to detect different ranging codes and their phase shifts within the current symbol. However, this is computationally complex. We intended to reduce the complexity of this operation by exploiting the fact that timing offsets only affect the phase of the frequency domain signal. Since BPSK modulation is used, the signal should not have an imaginary part. If there are $K$ ranging users within the current OFDMA symbol, each user has a timing offset $\tau_k$ samples, where $0 < \tau_k < \tau_{\max}$ and $\tau_{\max}$ is the maximum RTD between the SS and the BS within the current cell.
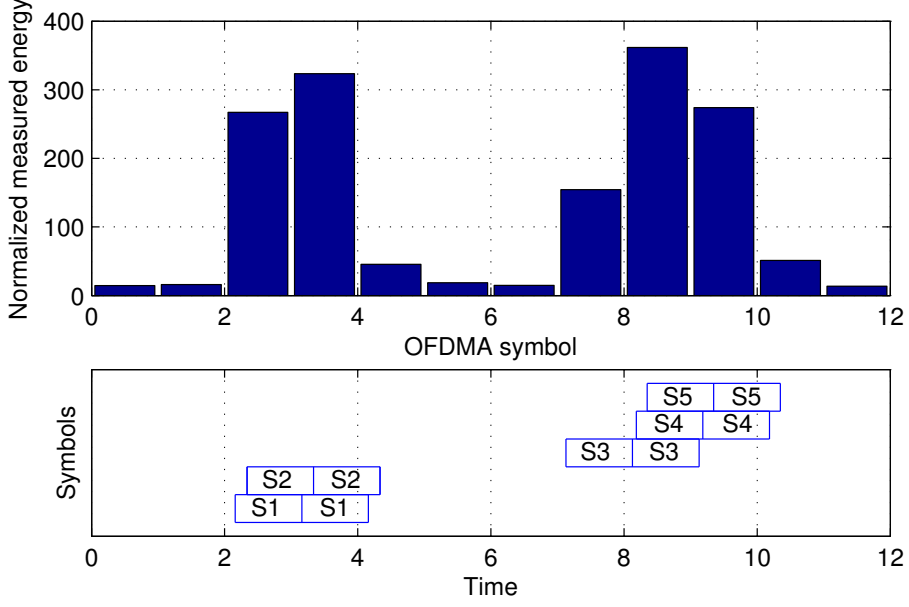
Figure 3.2 Normalized measured energy on the ranging channel at SNR = 10 dB.

Then,

$$Y(m) = \sum_{k=0}^{K-1} c_p^{(k)}(m) \exp\left[\jmath\phi_m(\tau_k)\right] + W(m) \tag{3.9}$$

where $m = i_r(0), i_r(1), ..., i_r(L-1)$. As can be seen in (3.9), if there were no timing offsets (i.e. $\tau_k = 0$ for $k = 0, 1, ..., K-1$), the whole energy of the ranging user will be only in the real part of the signal and the imaginary part will contain only noise. By applying all possible linear phase shifts and taking the energy of the real part of the signal, we have,

$$\mathcal{E}_r(u) = \sum_{n=0}^{L-1} \Re^2\left\{Y(m)\exp\left[\jmath\phi_m(u)\right]\right\}$$
$$= \sum_{n=0}^{L-1}\left[\sum_{k=0}^{K-1} c_p^{(k)}(m)\cos\left[\phi_m(\tau_k - u)\right] + \hat{W}_\Re(m)\right]^2 \tag{3.10}$$

where $u = 0, 1, ..., \tau_{\max}$, $\hat{W}(m) = W(m)\exp[\jmath\phi_m(u)]$ and $\hat{W}_\Re(m) = \Re\{\hat{W}(m)\}$. User timing offset $\tau_k$, is assumed to be a uniformly-distributed random variable between 0 and $\tau_{\max}$. Since $m$ is chosen randomly from the available subcarriers, the phase $[2\pi m(\tau_k - u)/N]$ can be approximated as a uniformly-distributed random variable between $-\pi$ and $\pi$. Note that $\hat{\mathbf{W}}$ and $\mathbf{W}$ have the same distribution, average and variance. For $\tau_k = u$, $\cos[\phi_m(\tau_k - u)] = 1$ resulting in a peak in the measured energy $\mathcal{E}_r(u)$. Therefore, a threshold $\eta_2$ is set to detect those peaks and obtain an estimate

49

of $\tau_k$ for all values of $k$. The measured real energy is normalized with respect to the average real energy of the symbol $\overline{\mathcal{E}}_r$ such that,

$$\tilde{\mathcal{E}}_r(u) = \left[\mathcal{E}_r(u) - \overline{\mathcal{E}}_r\right] / \overline{\mathcal{E}}_r \tag{3.11}$$

where,

$$\overline{\mathcal{E}}_r = \frac{1}{K} \sum_{u=0}^{K-1} \mathcal{E}_r(u). \tag{3.12}$$

As shown in Appendix B,

$$E\left\{\mathcal{E}_r(u)\right\} \approx \begin{cases} L\left(K + 1 + N_0\right)/2, & \text{for } u = \tau_k \\[2mm] L\left(K + N_0\right)/2, & \text{for } u \neq \tau_k. \end{cases} \tag{3.13}$$

From (3.12) and (3.13) we get,

$$\overline{\mathcal{E}}_r = \frac{KE\left\{\mathcal{E}_r(u)|u = \tau_k\right\} + (\tau_{\max} - K)E\left\{\mathcal{E}_r(u)|u \neq \tau_k\right\}}{\tau_{\max}}. \tag{3.14}$$

The above equation is valid given that $K < \tau_{\max}$, which is a reasonable assumption since, depending on the cell radius, $\tau_{\max}$ can go up to $N/2$, while the number of ranging users within the same OFDMA symbol is usually much lower than this value. Fig. 3.3 shows $E\{\tilde{\mathcal{E}}_r(u)|u = \tau_k\}$ and $E\{\tilde{\mathcal{E}}_r(u)|u \neq \tau_k\}$ for different values of $K$ and for SNR $=$ 10 dB. For simulated results, we use the system setup presented in Section 3.6.1. Assuming all ranging users are received with equal power, the signal-to-interference-plus-noise ratio (SINR) level for a given number of ranging users per OFDMA symbol and for an SNR level of 10 dB is calculated in Table 3.1, where SINR is defined as the ratio of the power of one user signal to the power of the remaining users signals plus noise power. The figure shows that as the number of ranging users increases, the probability of a missed detection increases since the difference between the two means decreases. In addition, the variance of the measured energy also increases with the number of ranging users, since they act as interference noise for $u \neq \tau_k$ as shown in (3.10). Note that since $K$ is usually very small compared to $\tau_{\max}$, then from (3.14), $\overline{\mathcal{E}}_r \approx E\left\{\mathcal{E}_r(u)|u \neq \tau_k\right\}$ and $E\left\{\tilde{\mathcal{E}}_r(u)|u \neq \tau_k\right\} \approx 0$, as shown in Fig. 3.3.
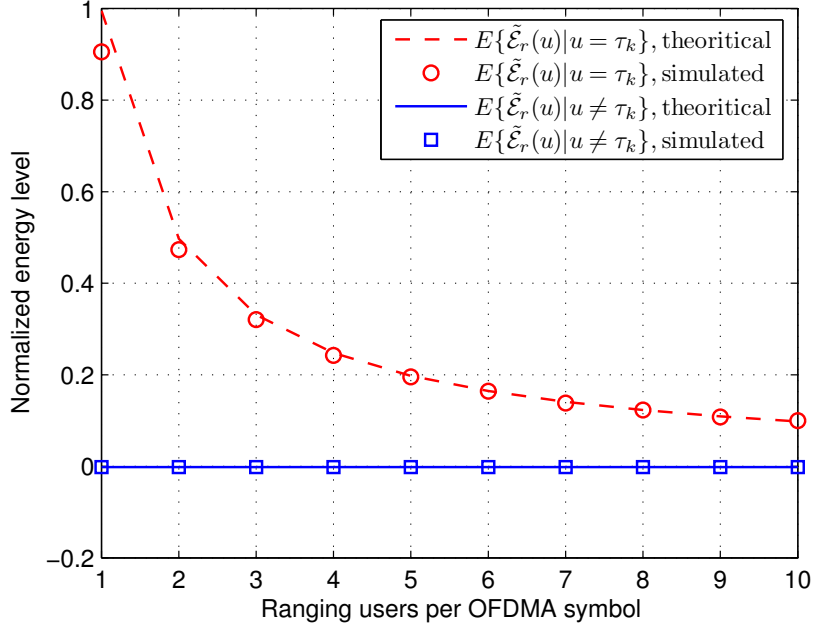
Figure 3.3 $E\{\tilde{\mathcal{E}}_r(u)|u = \tau_k\}$ and $E\{\tilde{\mathcal{E}}_r(u)|u \neq \tau_k\}$ for different numbers of ranging users.

Table 3.1 SINR vs. number of users per OFDMA symbol.

| Number of users | SINR (dB) | Number of users | SINR (dB) |
|---|---|---|---|
| 1 | 10.0 | 6 | −7.1 |
| 2 | −0.4 | 7 | −7.9 |
| 3 | −3.2 | 8 | −8.5 |
| 4 | −4.9 | 9 | −9.1 |
| 5 | −6.1 | 10 | −9.6 |

### 3.4.3   Code Detector

In the previous two steps of the algorithm, OFDMA symbols containing ranging codes were detected and their timing offsets were estimated. The last stage is to identify which codes were transmitted out of the available ranging codes, $P$, where $P$ is the number of codes assigned by the BS for initial ranging. In this step, the linear phase shift corresponding to each detected ranging code is removed and then a cross-correlation with all possible ranging codes is performed. The correlator output is,

$$\mathcal{E}_c^{(v)}(i) = \sum_{n=0}^{L-1} \Re\left\{Y(m) \exp\left[\jmath\phi_m(\hat{\tau}_v)\right]\right\} c_p^{(i)}(n) \tag{3.15}$$

51

where $i = 0, 1, ..., P - 1$, and $\hat{\tau}_v$ is the estimated timing offset of the $v$th user. The vector $\boldsymbol{\mathcal{E}}_c^{(v)}$ is calculated for every detected ranging code, $v$, where $v = 0, 1, ..., \hat{K} - 1$, and $\hat{K}$ is the total number of detected ranging codes in the second step. $\boldsymbol{\mathcal{E}}_c^{(v)}$ is then compared to a threshold, $\eta_3$, to identify which ranging code is within the current OFDMA symbol. Note that $\eta_3$ is normalized by the root mean square value of $\boldsymbol{\mathcal{E}}_c^{(v)}$. Since this step should not be reached unless at least one ranging code exists in the current OFDMA symbol, the code with maximum correlation could just be chosen for every value of $v$. However, a threshold is used so that the algorithm can detect multiple codes with the same timing offset which would be interpreted as a single code in the second step of the algorithm. In this case, $\hat{K}$ is updated to reflect the increase in the number of detected ranging codes. In addition, if two users happen to use the same ranging code and both their signals are received in the same symbol but with different timing offsets, the system declares a collision and both codes are dropped. The corresponding users then have to retry in the next available ranging opportunity.

## 3.5    Computational Complexity

For practical applications, the computational complexity of an algorithm is important. In this section, we evaluate the complexity of the proposed algorithm and compare it to other algorithms.

The proposed algorithm is compared with the two proposed algorithms in [83] and [84], which are referred to as algorithm 1 and algorithm 2, respectively. For algorithm 1, an observation window with the OFDMA symbol size is used. A bank of correlators, equal to the number of available ranging codes $P$, is used to separate ranging codes in the received signal. If the maximum possible delay is $\tau_{\max}$, then $(\tau_{\max} + 1)P$ cross-correlation operations are performed for every OFDMA symbol with ranging opportunity. Assuming the current UL consists of $N_{\mathrm{UL}}$ OFDMA symbols, where $N_{\mathrm{UL}}$ is required by the standard to be an integer multiple of 3, then the total number of correlation operations performed would be $N_{\mathrm{UL}}(\tau_{\max} + 1)P$. The same number applies for threshold comparison operations. Algorithm 2, on the other hand, performs the cross-correlation in frequency domain. Thus, to perform the cross-correlation at every possible timing offset, a linear phase shift of $\phi_m(u)$ where $u = 0, 1, ..., \tau_{\max}$, is applied to the frequency domain signal prior to the cross-correlators bank. As a result, algorithm 2 has an addition of $\tau_{\max} + 1$ linear phase shifts added to its computational complexity. However, since the correlation is performed in the frequency domain, and since BPSK modulation is used, the correlations are done on real-signals unlike algorithm 1 which has to perform complex-signal correlations.

In the proposed algorithm, the energy of the ranging channel for every OFDMA symbol is calculated. As a result, $N_{\mathrm{UL}}$ energy calculation operations and threshold comparisons are needed. The energy calculation is already performed for $N_0$ estimation. Assuming that every ranging symbol triggers the energy detector over two OFDMA symbols, then at most $2K$ OFDMA symbols will reach the next stage of the algorithm, where $K$ is the total number of ranging users within the current UL frame. Of course, if one or more codes collide, then less OFDMA symbols will reach the next stage. In the second stage, all possible linear phase shifts are applied to the OFDMA symbol (i.e. from 0 to $\tau_{\max}$). The energy of the real part of the signal is measured and compared to a threshold. Thus, $(1 + \tau_{\max})$ linear phase shifts, real energy calculation, and comparison operations are performed. A maximum of $K$ ranging codes, within $2K$ ranging OFDMA symbols, will reach the third and last stage. A cross-correlation with all possible codes is performed. As a result, $2KP$ correlations and comparison operations (CMPs) are performed at this stage.

Table 3.2 shows the number of additions (ADDs) and multiplications (MULs) needed for each operation. Using Table 3.2, the computational complexity of the algorithms under investigation is,

- Algorithm 1:

$$N_{\mathrm{UL}}P(\tau_{\max} + 1)(4L - 2) \text{ ADD} + 4LN_{\mathrm{UL}}P(\tau_{\max} + 1) \text{ MUL} + N_{\mathrm{UL}}P(\tau_{\max} + 1) \text{ CMP}$$

- Algorithm 2:

$$(\tau_{\max} + 1)(2L + N_{\mathrm{UL}}PL - N_{\mathrm{UL}}P) \text{ ADD}+$$
$$L(\tau_{\max} + 1)(4 + N_{\mathrm{UL}}P) \text{ MUL} + N_{\mathrm{UL}}P(\tau_{\max} + 1) \text{ CMP}$$

- Proposed Algorithm:

$$\left[N_{\mathrm{UL}}(4L - 2) + 2K(\tau_{\max} + 1)(3L - 1) + 2KP(L - 1)\right] \text{ ADD}+$$
$$\left[2L(KP + 2) + 10KL(\tau_{\max} + 1)\right] \text{ MUL} + \left[N_{\mathrm{UL}} + 2K(\tau_{\max} + P + 1)\right] \text{ CMP}$$

Finally, the complexity of all three algorithms is calculated for a practical system[2]. We assume $N_{\mathrm{UL}} = 12$ OFDMA symbols, $P = 256$ codes (maximum), $L = 144$ bits (standard-based [9]), and

---

[2]Using CPU cycle counts based on XilinX DSP48 slice.

Table 3.2  Proposed algorithm's computational complexity.

| Operation | ADD | MUL |
|---|---|---|
| Correlation, complex | $2(L-1)+2L$ | $4L$ |
| Correlation, real | $L-1$ | $L$ |
| Energy calc., complex | $2(L-1)+2L$ | $4L$ |
| Energy calc., real | $L-1$ | $L$ |
| Phase shift | $2L$ | $4L$ |

$\tau_{\max} = 512$ samples for $N = 1024$. The number of cycles needed by each algorithm is as follows,

$$\text{Algorithm 1: } 3.629 \times 10^9 \text{ cycles,}$$

$$\text{Algorithm 2: } 9.088 \times 10^8 \text{ cycles,}$$

$$\text{Proposed Algorithm : } 2.963 \times 10^6 \text{ cycles for } K = 1,$$

$$5.909 \times 10^7 \text{ cycles for } K = 20.$$

The difference in computational complexity is evident. The complexity of the proposed algorithm is a few orders of magnitude lower than the complexity of algorithms 1 and 2. While both of algorithm 1 and 2 maintain fixed complexity regardless of the number of ranging users $K$, the proposed algorithm can update to $K$, which gives it the lowest limit in computational complexity. Note that the above results are optimistic as we assume there are no false alarms in the first and second stages of the proposed algorithm. A complexity comparison for a typical WiMAX system operating in a practical wireless environment is presented in the following section.

## 3.6  Simulation Results

### 3.6.1  System Setup

An OFDMA system model based on [9, 90] is used with the following parameters: $N = 1024$, $N_g = 128$ samples, $N_{\text{UL}} = 12$ OFDMA symbols, $L = 144$ bits. The system is assumed to be operating at $2\,\text{GHz}$ center frequency with a bandwidth of $10\,\text{MHz}$ and a sampling frequency of $11.2\,\text{MHz}$. The maximum RTD considered is $45.71\,\mu\text{S}$ ($\tau_{\max} = 512$ samples) allowing for a cell radius of $6.86\,\text{Km}$. The total number of ranging codes is 256 codes. In the considered system, all codes are assigned to initial ranging, i.e. $P = 256$. The ranging channel is made up of six subchannels and spanning 144 subcarriers per OFDMA symbol. Ranging users choose two consecutive symbols randomly to

Table 3.3  Characteristics of the ITU Vehicular A channel environment.

| Tap | Relative delay (nS) | Average power (dB) |
|-----|---------------------|--------------------|
| 1 | 0 | 0.0 |
| 2 | 310 | −1.0 |
| 3 | 7104 | −9.0 |
| 4 | 1090 | −10.0 |
| 5 | 1730 | −15.0 |
| 6 | 2510 | −20.0 |

send their ranging code during the UL frame with equal probability. In each simulation, $10,000$ UL frames or $120,000$ OFDMA symbols are used to evaluate the system performance.

### 3.6.2  Channel Model

The performance of the proposed ranging algorithm is evaluated in both an AWGN channel and an outdoor dispersive channel. For the dispersive channel, we use one of the standard channel models defined by International Telecommunication Union (ITU) [90, 91]. The time-varying channel impulse response for these models can be described by

$$h(\tau, t) = \sum_{\ell} h_{\ell}(t) \delta(\tau - \tau_{\ell}). \tag{3.16}$$

This equation defines the impulse response of a tapped-delay channel with every tap $\ell$ having a delay of $\tau_{\ell}$ and gain of $\alpha_{\ell}(t)$. In this study, we consider the Vehicular A channel environment [91]. The taps' relative delays and average powers are shown in Table 3.3. The channel taps $\alpha_{\ell}(t)$ are complex Gaussian processes, and are independent for different paths. Different user channels are assumed independent and the channels are also independent between UL frames.

The multipath fading channel is expected to degrade the performance of the ranging algorithms under investigation. For the proposed algorithm, only the second and third steps are significantly affected by the multipath channel. The impact of channel models on the third step, where the signal is correlated with all possible codes, has already been discussed in [84] where algorithm 2 is presented. Therefore, we are mainly interested in examining the effect of a dispersive channel on the second step where we detect ranging codes within the OFDMA symbol and estimate their timing offsets.
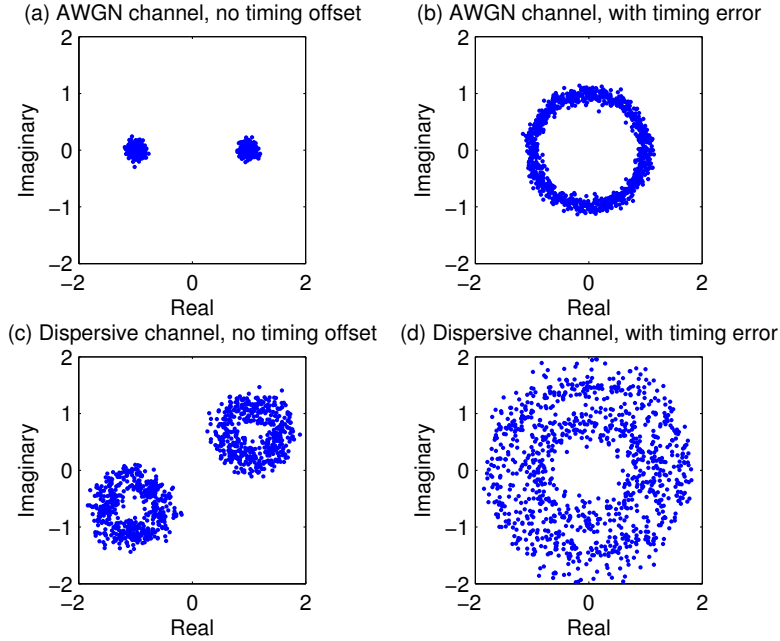
Figure 3.4   The effect of synchronization error on the constellation points of a typical BPSK-modulated OFDMA symbol received over AWGN and dispersive channels.

As discussed earlier, the subcarriers of an OFDMA symbol with a timing error exhibit a linear phase shift. Therefore, by applying the appropriate linear phase shift to the received symbols, this effect is compensated. Fig. 3.4 shows that effect on the constellation points of a typical BPSK-modulated OFDMA symbol received over AWGN channel with SNR $= 10\,\text{dB}$ and over the dispersive channel referred to earlier. As seen in the figure, the linear phase shift causes the symbol energy to be distributed equally between the real and imaginary parts of the signal. On the other hand, at the correct timing offset, the energy is more concentrated into a single axis. The effect of the dispersive channel is that at the correct timing offset, the signal is more noisy and there is also a random gain and phase shift. However, the correct timing offset is still detectable compared to the same signal with wrong timing offset. The real part of the signal contains 50% of the total symbol energy when a timing offset is present regardless of the wireless channel. In the above example and with no timing offset, the real part of the signal holds 99% and 69% of the total symbol energy over AWGN and multipath fading channels, respectively. To further illustrate this effect, computer simulations were used to calculate the probabilities $\Pr\{|\tilde{\mathcal{E}}_r(u)| > \eta_2|u = \tau_k\}$ and $\Pr\{|\tilde{\mathcal{E}}_r(u)| > \eta_2|u \neq \tau_k\}$ for different values of $\eta_2$ over nondispersive and dispersive channels. The
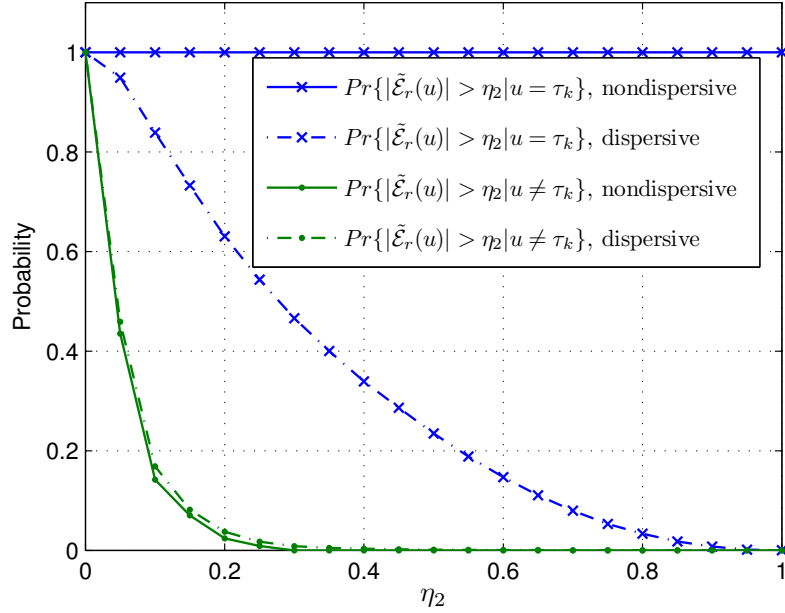
Figure 3.5  $\Pr\{|\tilde{\mathcal{E}}_r(u)| > \eta_2 | u = \tau_k\}$ and $\Pr\{|\tilde{\mathcal{E}}_r(u)| > \eta_2 | u \neq \tau_k\}$ for different values of $\eta_2$ over nondispersive and dispersive channels.

results are shown in Fig. 3.5. Note that we consider $|\tilde{\mathcal{E}}_r(u)|$ as to avoid negative values that can result from phase shifts introduced by the channel. As expected, the $\Pr\{|\tilde{\mathcal{E}}_r(u)| > \eta_2 | u = \tau_k\}$ is significantly higher than the $\Pr\{|\tilde{\mathcal{E}}_r(u)| > \eta_2 | u \neq \tau_k\}$ for a given threshold level $\eta_2$. The figure shows that for both channels, $\Pr\{|\tilde{\mathcal{E}}_r(u)| > \eta_2 | u \neq \tau_k\}$ exhibits the same behavior where it decays at a fast rate as $\eta_2$ increases. $\Pr\{|\tilde{\mathcal{E}}_r(u)| > \eta_2 | u = \tau_k\}$ on the other hand, decreases as $\eta_2$ increases only for dispersive channels.

### 3.6.3  Proposed Algorithm Performance

The system performance is evaluated at an SNR $= 10\,\mathrm{dB}$ over both AWGN and Vehicular A dispersive channels. The proposed algorithm performance is compared to that of algorithm 2. The performance is investigated for different numbers of ranging users per UL frame. To be able to fairly evaluate the system performance for different numbers of ranging users, it is assumed that all ranging signals are received with equal powers. However, both the proposed algorithm and algorithm 2 can operate when different users have different power levels. For the results presented in this chapter, the SINR corresponding to a given number of users per OFDMA symbol is shown in Table 3.1. Based on our analysis and the simulation results shown in Fig. 3.1 and Fig. 3.5, the
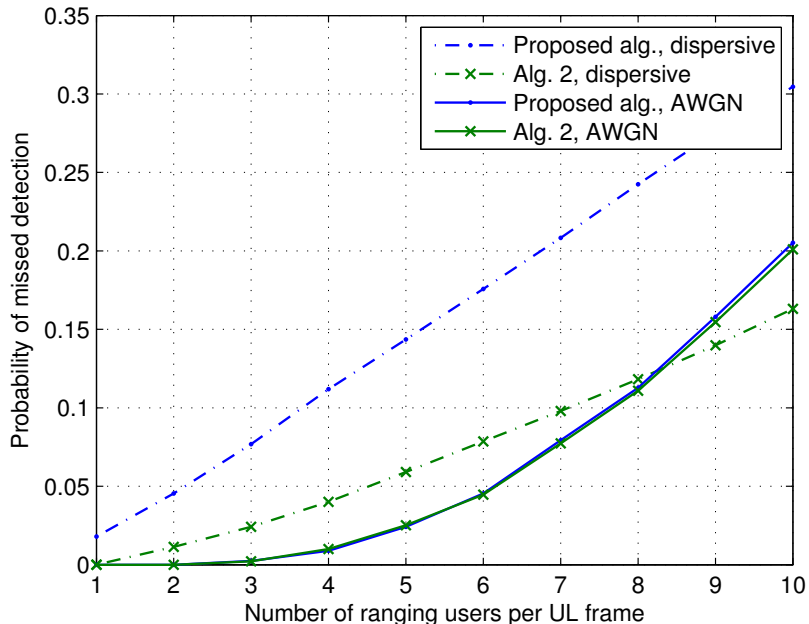
Figure 3.6 Probability of missed detection.

thresholds $(\eta_1, \eta_2, \eta_3)$ for the proposed algorithm are chosen to be $(3, 0.2, 6)$ for AWGN channels and $(3, 0.1, 6)$ for dispersive channels. Fig. 3.6 and Fig. 3.7 show the probability of missed detection and the probability of false alarm, respectively, for both the proposed algorithm and algorithm 2, and for different numbers of ranging users per UL frame. Over AWGN channels, both algorithm performances are almost identical with zero probability of false alarm. Over dispersive channels, the proposed algorithm suffers from a higher probability of missed detection compared to algorithm 2. The difference between the two algorithms increases as the number of users increases. On the other hand, the proposed algorithm shows a much lower probability of false alarm than algorithm 2 especially for low number of ranging users. Even with up to 8 ranging users per UL frame, the proposed algorithm is able to detect more than 75% of received codes with a false alarm probability less than 0.2%.

An important measure of the ranging algorithm quality is the timing estimation accuracy. For dispersive channels, the timing error definition is ambiguous [81]. In this study, we consider the timing error relative to the channel tap with maximum average power, or first tap in the considered dispersive channel. The standard deviations for the timing estimator errors for both the proposed algorithm and algorithm 2 are shown in Fig. 3.8. Both algorithms show zero timing errors for AWGN
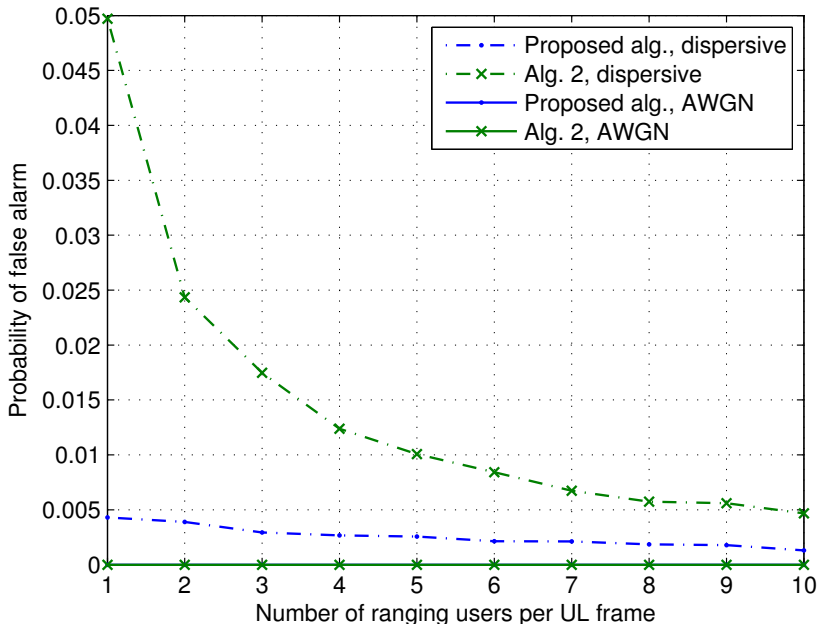
Figure 3.7  Probability of false alarm.

channels. Over dispersive channels, the proposed algorithm timing estimator shows a higher error standard deviation than that of algorithm 2. Overall, both algorithms show an accurate timing estimation capability with an average standard deviation of 5 and 3 for the proposed algorithm and algorithm 2, respectively. A more important measure of ranging accuracy is the probability of the timing error falling outside a given interval. For example, if we assume the timing errors to be a normally-distributed random variable with zero mean [81], the probability of the timing error to exceed 32 samples (25% of the CP) is less than 1% for both algorithms.

Next, we consider the computational complexity of the proposed algorithm. For both algorithms under consideration, correlating the received signal with all possible ranging codes constitutes the majority of the algorithm computations. As such, the number of times this function is called by the ranging algorithm is used as a measure of how complex the algorithms are. In this regard, algorithm 2 has a fixed computation complexity regardless of the number of ranging opportunities or the number of ranging users within the received UL frame as shown in section 3.5. The reduction of computational complexity gained by using the proposed algorithm over algorithm 2 is evaluated and the results are shown in Fig. 3.9. The computational complexity are normalized by the number of detected codes $(1 - P_{md})$ to take into consideration the different probabilities of missed detection
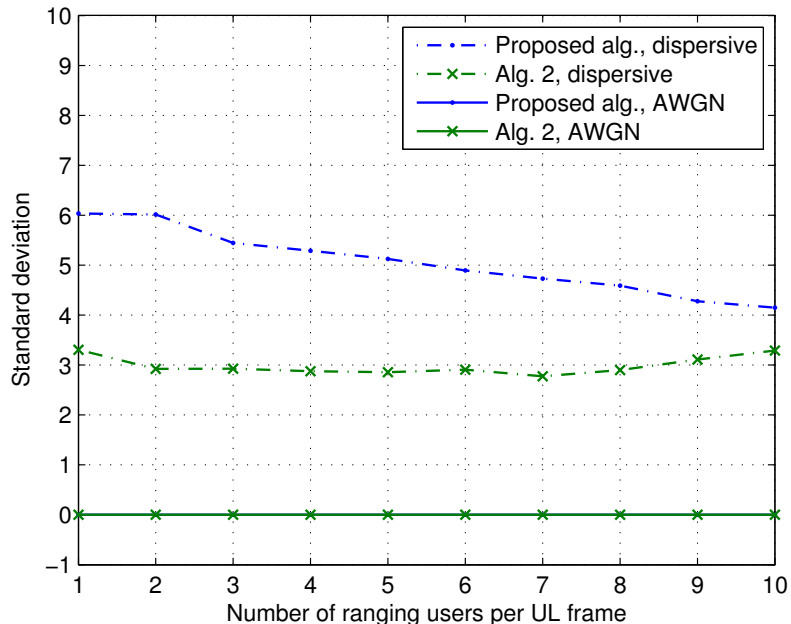
Figure 3.8  Standard deviation of timing errors.

between both methods. The proposed algorithm reduces the computational complexity by over 98% over AWGN channels. Over dispersive channels, the complexity reduction ranges from 96% to 80% depending on the number of ranging users per UL frame.

Finally, another set of system parameters from the WiMAX system profiles is considered to verify the performance of the proposed algorithm. The new set of system parameters are: $N = 512$, $N_g = 32$ samples. In accordance to the standard, the signal bandwidth, in this case, is 5 MHz and the sampling frequency is 5.6 MHz. For fairness of comparison, the maximum RTD, the number of OFDMA symbols per UL frame, and the number of frames used to evaluate the simulation results remain constant. The probabilities of missed detection and false alarm for the first and second sets of system parameters are compared in Fig. 3.10. In both system profiles, the performances are almost identical. This is due to the fact that WiMAX standard maintains fixed subcarrier spacing regardless of the signal bandwidth or FFT size. As a result, the ranging channel, which consists of a fixed number of subcarriers, has a fixed bandwidth for different signal bandwidths. In Fig. 3.11, the standard deviations of timing errors for both cases as well as for both considered ranging algorithms are compared. Note that as the bandwidth is reduced, the sampling time is increased which leads
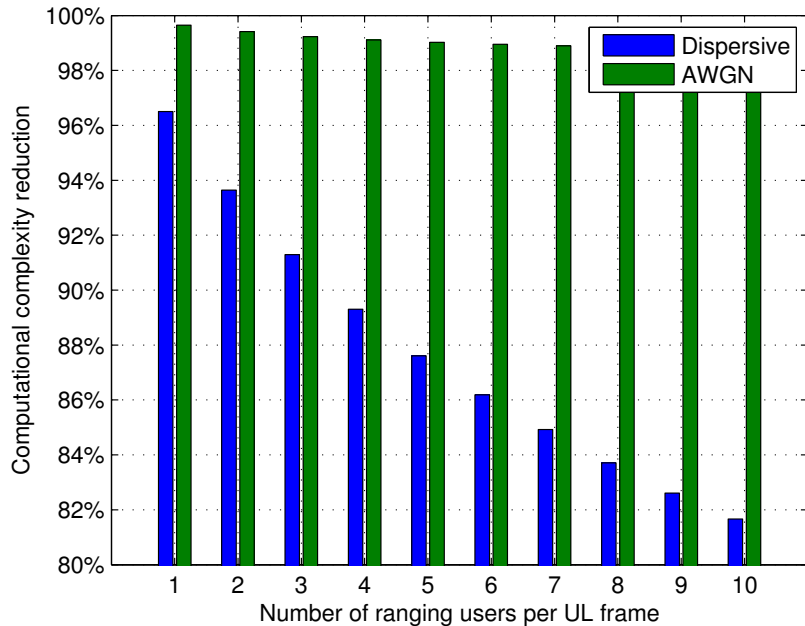
Figure 3.9  Computational complexity reduction using the proposed algorithm.

to a reduction in timing errors (in samples). In this case, the timing estimation performances of the proposed algorithm and algorithm 2 are almost equal.

## 3.7    Conclusions

A novel algorithm for OFDMA initial ranging process based on the IEEE 802.16e-2005 standard is proposed. The proposed algorithm performs multiuser code detection and timing offset estimation for ranging users. The algorithm is divided into three stages. In the first stage, the system detects OFDMA symbols carrying ranging users. The second stage is responsible for detection of codes and estimation of timing offsets for each user within current OFDMA symbol. Finally, the last stage identifies user ranging codes. The proposed algorithm performance was evaluated for both AWGN channels and dispersive channels. A complexity comparison between the proposed algorithm and other existing algorithms was carried out as well. The results show that proposed algorithm reduces the computational complexity by 80% to 96% depending on the number of ranging users while maintaining the timing error standard deviation under 5% of the guard interval. Simulation results showed that the proposed algorithm can perform well with as high as 10 users per ranging channel
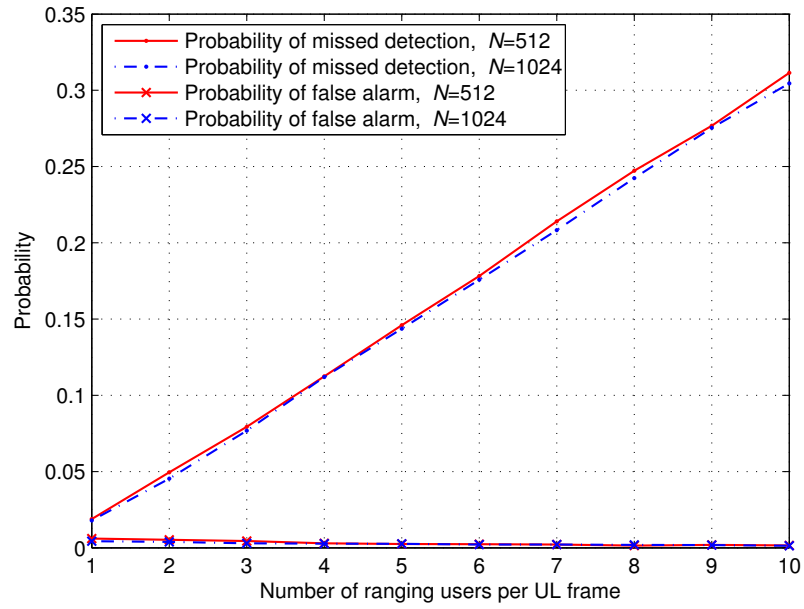
Figure 3.10  Probabilities of missed detection and false alarm for $N = 1024$ and $N = 512$.

in a given UL frame. Hence, it is believed that the proposed algorithm can be realized in practical OFDMA-based BSs.
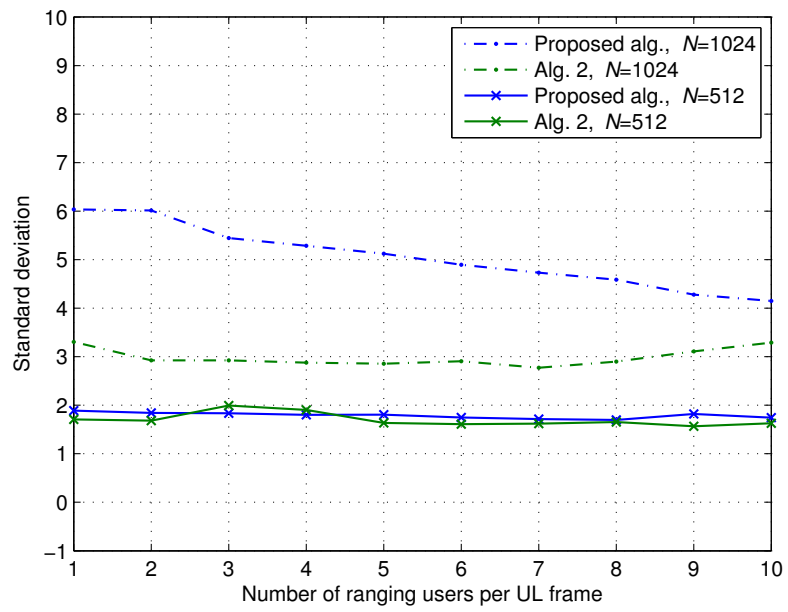
Figure 3.11  Standard deviation of timing errors for $N = 1024$ and $N = 512$.

# CHAPTER 4

# SPECTRUM SHAPING OF OFDM-BASED COGNITIVE RADIO SIGNALS

## 4.1 Introduction

Recently, opportunistic usage of licensed frequency bands has been proposed as a solution to spectral crowding problem by using cognitive radio (CR) systems [2, 60]. A CR system would be able to operate in licensed bands by utilizing vacant parts of these bands. A key point for the success of CR is the ability to shape its signal spectrum to achieve minimum interference to licensed users (LU). Orthogonal frequency division multiplexing (OFDM) has been proposed as a candidate signaling technology for such applications. By dividing the spectrum into subbands that are modulated with orthogonal subcarriers, OFDM spectrum can be shaped with more ease compared to other signaling techniques. However, modulated OFDM subcarriers suffer from high sidelobes, which result in adjacent channel interference (ACI). Thus, disabling a set of OFDM subcarriers to create a spectrum null may not be sufficient to avoid interference to LU. On the other hand, using filters can increase the system complexity and introduce long delays. Using guard bands on both sides of used OFDM spectrum and windowing the time domain signal have been investigated in [64]. In [65–67], the use of interference cancellation carriers (CC) is proposed. Other proposed methods include the use of subcarrier weighting [74] or multiple-choice sequences [75].

In this chapter, we discuss some of the current methods and techniques proposed in the literature for spectrum shaping of an OFDM signal to avoid or minimize interference to LUs. We investigate the effect of various system parameters (such as the LU bandwidth, cyclic prefix (CP) length, and number of CCs) and their effects on the system performance in terms of interference level, spectral efficiency, computational complexity, and power consumption. Simulation results showing the system performance are provided along with discussions of the advantages and disadvantages of each technique. We then propose a new method, referred to as adaptive symbol transition (AST), to suppress OFDM sidelobes and shape the signal spectrum. Similar to the windowing technique,

the OFDM symbols are extended in time to reduce the effect of symbol transition. However, instead of using a predefined filter shape, the transition signal is optimized adaptively based on transmitted data and detected LU bands to reduce the interference to LUs.

## 4.2   System Model

Throughout this chapter, we assume a CR system employing OFDM as the signaling technique. The CR is assumed to be aware of the surrounding environment and the radio channel characteristics. After scanning the channel, the CR should be able to identify LUs operating within the targeted band [92]. The goal is to exploit identified spectrum opportunities and achieve highest possible spectral efficiency while keeping the interference to detected LUs to minimum. In the system, the encoded data is modulated and then fed to an $N$-point inverse fast Fourier transform (IFFT) unit. We define $\mathbf{F}_{N_1,N_2} = \{F_{n_1,n_2}\}$ as the $N_1$-point Fourier transform matrix of a vector of length $N_2$, where

$$F_{n_1,n_2} = \exp\left(\frac{-j2\pi n_1 n_2}{N_1}\right).$$  (4.1)

The time domain signal at the output of the IFFT is

$$\mathbf{x} = \frac{1}{N}\mathbf{F}^*_{N,N}\mathbf{X},$$  (4.2)

where $N$ is the IFFT size, $(\cdot)^*$ is the complex conjugate operator, $\frac{1}{N}\mathbf{F}^*$ is the inverse Fourier transform matrix, and $\mathbf{X} = [X(1), X(2), ..., X(N)]^T$ is the modulated data vector. The signal is then extended using a CP consisting of $N_g$ samples. The signal goes through a pulse shaping filter before being sent through the communication channel.

## 4.3   Active Cancellation Carriers

Active CCs technique was proposed in [65–67] where a few tones at both edges of the spectrum hole are used to cancel the interference to LUs. First, we start by examining the performance of CCs with no cyclic extension or pulse shaping used to simplify the analysis. However, the effect of CP is discussed later in Section 4.3. The time domain signal is upsampled by a factor of $\zeta$ and the signal spectrum is calculated as follows

$$\mathbf{S} = \mathbf{F}_{\zeta N \times N}\mathbf{x} = \mathbf{Q}\mathbf{X},$$  (4.3)

where

$$\mathbf{Q} = \frac{1}{N}\mathbf{F}_{\zeta N \times N}\mathbf{F}_{N \times N}^*. \tag{4.4}$$

Note that $\zeta$ corresponds also to the number of points per sidelobe that are considered in the spectrum shaping process. Unless otherwise mentioned, the value of $\zeta$ is set to eight. A LU is detected within the OFDM band spanning over $B$ subcarriers $X(i+1), X(i+2), ..., X(i+B)$, where $i\Delta f$ is the LU signal offset with respect to the OFDM signal, $B\Delta f$ is the LU signal bandwidth, and $\Delta f$ is the frequency subcarrier separation. If the above subcarriers are disabled and remaining subcarriers are used for data transmission, the interference to LU band is

$$\mathcal{I}_L = \mathbf{Q}_B\mathbf{X}_B, \tag{4.5}$$

where $\mathbf{Q}_B$ is a subset of $\mathbf{Q}$ containing only the rows of $\mathbf{Q}$ that corresponds to the LU band, $\zeta(i+1)$ to $\zeta(i+B)$, and $\mathbf{X}_B$ is the same as $\mathbf{X}$ but with interference subcarriers, $X(i+1)$ to $X(i+B)$, set to zero. Assume $c$ CCs on each edge of the spectrum gap are used to cancel the interference to LU band. In this case, subcarriers $X(i+1-c)$ to $X(i+B+c)$ are set to zero in $\mathbf{X}_B$ to measure the interference to LU band. With the use of CCs, interference power to LU is,

$$\mathbf{P}_\mathcal{I} = \parallel \mathbf{Q}_\mathcal{I}\mathbf{X}_\mathcal{I} + \mathcal{I}_L \parallel^2. \tag{4.6}$$

where $\mathbf{Q}_\mathcal{I}$ is a subset of $\mathbf{Q}_B$ containing only the columns corresponding to disabled subcarriers, $i+1-c$ to $i+B+c$, and $\mathbf{X}_\mathcal{I}$ is a vector of required values of disabled subcarriers to minimize the interference. The mean-squared-error (MSE) solution to the above equation is,

$$\mathbf{X}_\mathcal{I} = -(\mathbf{Q}_\mathcal{I}^H\mathbf{Q}_\mathcal{I})^{-1}\mathbf{Q}_\mathcal{I}^H\mathcal{I}_L, \tag{4.7}$$

where $(\cdot)^H$ is the Hermitian transpose. From (4.5), (4.7) can be written as

$$\mathbf{X}_\mathcal{I} = \mathbf{W}_\mathcal{I}\mathbf{X}_B, \tag{4.8}$$

where $\mathbf{W}_\mathcal{I} = -(\mathbf{Q}_\mathcal{I}^H\mathbf{Q}_\mathcal{I})^{-1}\mathbf{Q}_\mathcal{I}^H\mathbf{Q}_B$. Note that $\mathbf{W}_\mathcal{I}$ needs to be calculated only once for the same spectrum shape while $\mathbf{X}_\mathcal{I}$ is calculated for every OFDM symbol [65].
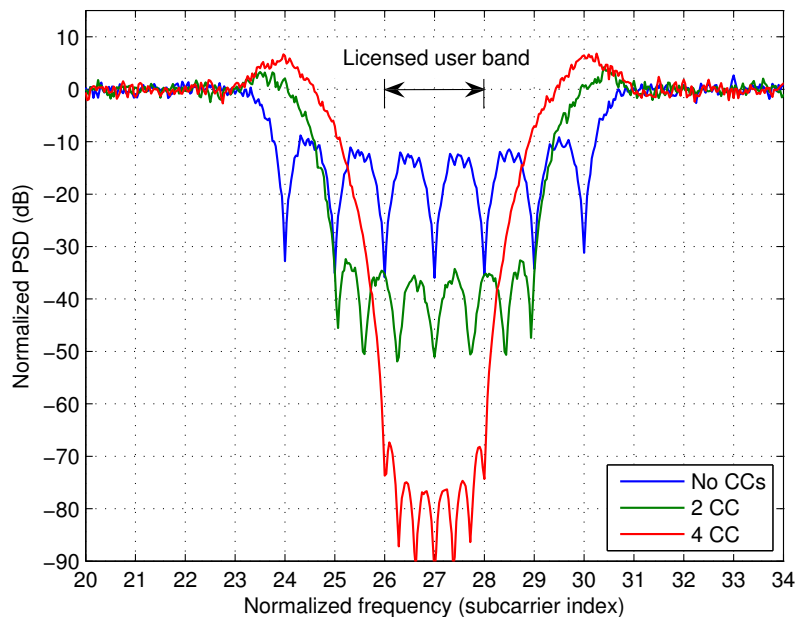
Figure 4.1  Number of CC effect on the signal PSD.

To examine the performance of the CC technique, an OFDM system with $N = 256$ is considered. The DC subcarrier $X(0)$ is disabled. A LU is detected spaning the band between subcarriers $X(26)$ and $X(28)$. To keep spectrum efficiency constant, seven subcarriers are disabled, $X(24)$ to $X(30)$, in all considered cases. First, the normalized power spectral density (PSD) is estimated with disabled subcarriers set to zero and data subcarriers carrying binary phase shift keying (BPSK) signals. Next, two and four CCs are considered, with half of CCs on each side of the gap. The results are shown in Fig. 4.1. When CCs are not used, the interference level is kept under $-10\,\text{dB}$ of the original signal power level. Two and four CCs reduce the interference level to around $-35\,\text{dB}$ and $-75\,\text{dB}$, respectively. CC technique reduces the interference significantly at the cost of an increase in the computational complexity and symbol energy.

Next, the effect of the LU bandwidth is considered. For a fixed number of four CCs, the PSD of the transmitted signal with a gap of 7, 17, and 27 subcarriers, assuming LUs with bandwidths of 3, 13, and 23 subcarriers, are shown in Fig. 4.2. As the gap bandwidth increases, the efficiency of CCs is reduced. Moreover, peaks emerge on the signal spectrum just before the spectrum gap. These peaks' power increases as the gap bandwidth increases indicating that more power is used by the CCs. To further investigate this effect, increases in the average symbol energy $E_r$ due to CCs is

67
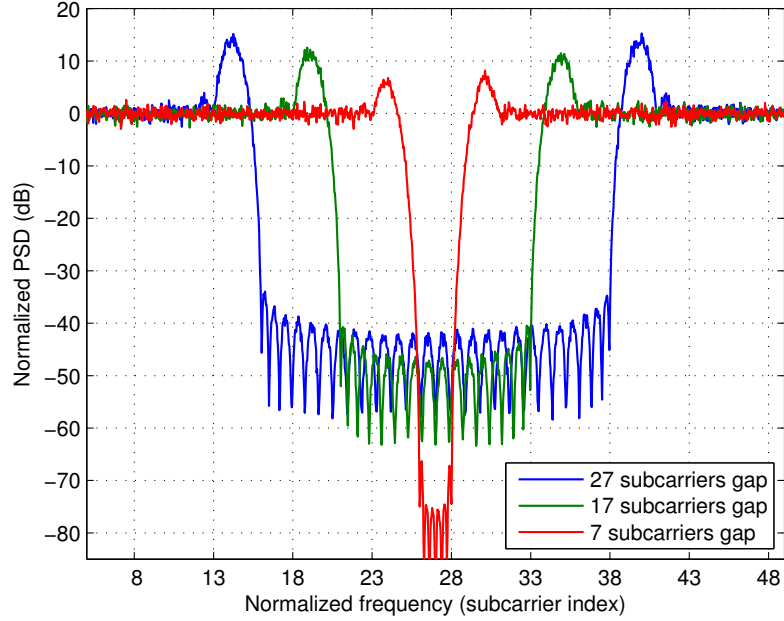
Figure 4.2  Gap size effect on effect on the signal PSD.

Table 4.1  Increase in average OFDM symbol energy $E_r$.

| Disabled subcarriers | 2 CCs | 4 CCs |
|---|---|---|
| 7 | 1% | 3% |
| 17 | 2% | 15% |
| 27 | 25% | 26% |

measured (see Table 4.1), where $E_r = (\acute{E}_S - E_S)/E_S$, $E_S$ is the average symbol energy with no CCs, and $\acute{E}_S$ is the average symbol energy with CCs. For a fixed overall symbol energy, the increase in energy consumed by CCs reduces the useful data energy leading to a decrease in the system efficient signal-to-noise ratio (SNR). This may result in an increase in the bit error rate (BER). Thus, a CR system faces a tradeoff between reducing the interference level to LU and keeping the spectrum efficiency and the overall BER of the system within acceptable levels.

### 4.4   Cyclicly Extended OFDM Signals

In practical OFDM systems, symbols are cyclically extended to mitigate inter-symbol interference (ISI) and synchronization errors [93]. The effects of CP on CCs are presented in [72] but a very short CP value was considered in the simulation (0.04 of symbol time). CP extension results in a loss of

orthogonality between OFDM subcarriers. Note that at the receiver, the CP is removed prior to the fast Fourier transform (FFT) block and thus the orthogonality is restored. Since orthogonality is lost in transmitted signal, sidelobes of adjacent subcarriers are misaligned. This reduces the ability of one subcarrier to reduce the interference, caused by the sidelobes, of adjacent subcarriers. In fact, only sidelobes of subcarriers with $N/N_g$ separation are aligned to each other. One last note is that increasing the CP interval causes the PSD of sidelobes to decay faster.

To take the CP effect into account in the CC technique, we define

$$\mathbf{C} = \begin{pmatrix} \mathbf{0}_{N_g \times N-N_g} & \mathbf{I}_{N_g} \\ \mathbf{I}_{N-N_g} & \mathbf{0}_{N-N_g \times N_g} \\ \mathbf{0}_{N_g \times N-N_g} & \mathbf{I}_{N_g} \end{pmatrix}_{N+N_g \times N}, \tag{4.9}$$

where $\mathbf{0}$ is the zero matrix and $\mathbf{I}$ is the identity matrix. The signal spectrum is then modified to be

$$\mathbf{S} = \mathbf{F}_{\zeta N \times N+N_g} \mathbf{C} \mathbf{x}, \tag{4.10}$$

For (4.3) to hold, $\mathbf{Q}$ in (4.4) is modified based on (4.10) to be

$$\mathbf{Q} = \frac{1}{N} \mathbf{F}_{\zeta N \times N+N_g} \mathbf{C} \mathbf{F}_{N \times N}^*. \tag{4.11}$$

Fig. 4.3 shows the normalized PSD of the transmitted signal for the same system used to generate Fig. 4.1 with 4 CCs and different CP sizes. For $N_g/N = 1/32$, 1/8, 1/4, and 1/2, $E_r$ was found to be 3%, 75%, 29%, and 1% respectively. The figure shows that a short CP, as in the case of $N_g/N = 1/32$, has a negligible effect on the system performance in both power and interference level. A longer CP with $N_g/N = 1/8$ reduces the CCs effectiveness by around $20\,\mathrm{dB}$ and, even worse, increases the energy consumed by CCs to a significantly higher value of 75%. As $N_g/N$ increases, the performance loss due to the CP decreases and so does $E_r$. This can be explained as follows. For $N_g/N = 1/8$, none of the CCs sidelobes are aligned for the case under consideration. As a result, the CCs spectra are added non-coherently and thus some parts of their signals are cancelled out which reduces the system efficiency. As a result, more power is needed to achieve minimum interference level. On the other hand, for $N_g/N = 1/4$, subcarriers $X(25)$ and $X(29)$ are aligned and thus the system regain some of the performance loss. However, more power is still needed by the CCs since
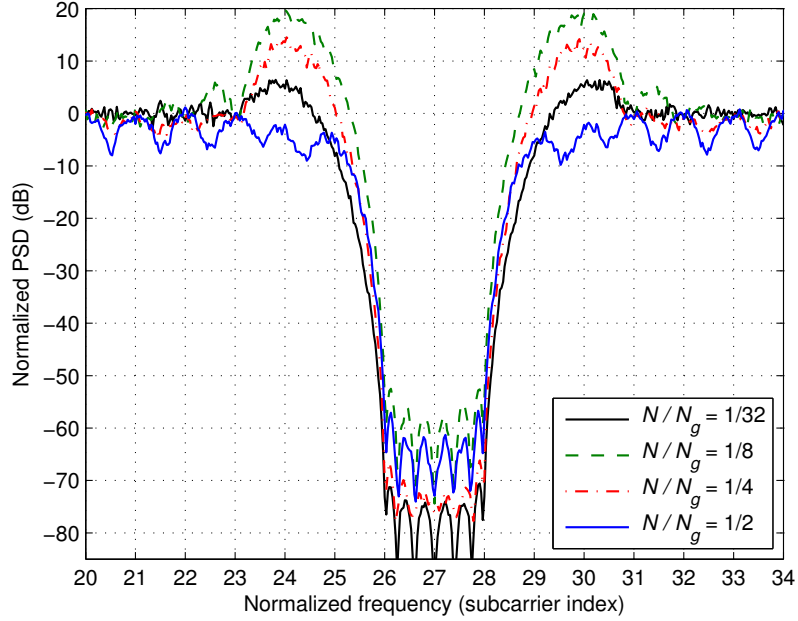
Figure 4.3 CP size effect on the signal PSD.

the other two subcarriers are not matched. Finally, for $N_g/N = 1/2$, all CCs are matched and thus both the performance loss and consumed power are low. In fact, the power consumed by CCs for $N_g/N = 1/2$ is even less than for the case of no CP. This is due to the fact that a long CP results in lower interference levels to adjacent bands. A conclusion can be made that CP length, gap location and CCs locations are all parameters that can significantly affect both the performance and power consumption of CCs.

## 4.5   Raised Cosine Windowing

A possible technique to reduce the interference to LU is the use of time windowing. The time domain OFDM symbols are multiplied with a shaping window to improve the spectrum characteristics of the signal [64]. Raised cosine (RC) windows are usually used, where the filter vector $\mathbf{g} = \{g_n\}$ is defined as:

$$
g_n = \begin{cases} \frac{1}{2} + \frac{1}{2}\cos\left(\pi + \frac{\pi n}{\beta N_T}\right), & \text{for } 0 \leq n < \beta N_T \\ 1, & \text{for } \beta N_T \leq n < N_T \\ \frac{1}{2} + \frac{1}{2}\cos\left(\pi \frac{n - N_T}{\beta N_T}\right), & \text{for } N_T \leq n < (1+\beta)N_T, \end{cases} \tag{4.12}
$$

where $N_T = N + N_g$ is the symbol length (in samples) and $\beta$ is the rolloff factor. The total symbol length is $(1 + \beta)N_T$. However, adjacent symbols partially overlap over a length of $\beta N_T$ from each side, causing the actual symbol time to be $N_T$. To maintain the orthogonality between the OFDM subcarriers and the system resistance to ISI, the symbols are extended using both prefix and postfix. The durations for both the prefix and postfix extensions ($N_{\text{pre}}$ and $N_{\text{post}}$ respectively) are chosen such that they cover the overlapping period of the symbols. The advantage of windowing is its low complexity and simple implementation. The drawback is the time extension of the symbol which reduces the system throughput.

The system performance was evaluated for different values of $\beta$. The system had seven disabled subcarriers, $N/N_g = 1/32$, $N_{\text{post}} = \beta N_T$, and $N_{\text{pre}} = \beta N_T + N_g$. Thus, $N_T = (N + N_g)/(1 - \beta)$. The results are shown in Fig. 4.4. The average interference level (in dB) within LU band was found to be $-23$, $-40$, $-55$ for $\beta = 0.12$, $0.25$, and $0.4$, respectively. The increase in symbol energy was calculated for all cases. For $\beta = 0.12$, $0.25$, and $0.4$, $E_r$ was found to be 10%, 25%, and 51%, respectively. Moreover, the symbol time increased by 14%, 33%, and 67%. Compared to the results in Fig. 4.1, it appears that CCs are superior to windowing in both spectral efficiency and power. However, it is important to point out that windowing requires much less computations than CCs. In addition, windowing is more robust since it is independent of the gap position, width, or symbol data values. Note that windowing reduces the sidelobes of all OFDM subcarriers which improves not only the target gap but also the out-of-band emissions as well. Fig. 4.5 shows the RC windowed system with $\beta = 0.25$, and various gap sizes. It is seen that as the gap bandwidth increases, the interference level decreases. Since windowing increases the decay rate of modulated subcarrier sidelobes, this technique performs better with larger gaps. Compared to CCs shown in Fig. 4.2, windowed system achieves $10\,\text{dB}$ lower interference level for a 27 subcarriers gap with almost the same power consumption. However, CCs have the advantage of maintaining an almost flat spectrum over the LU band.
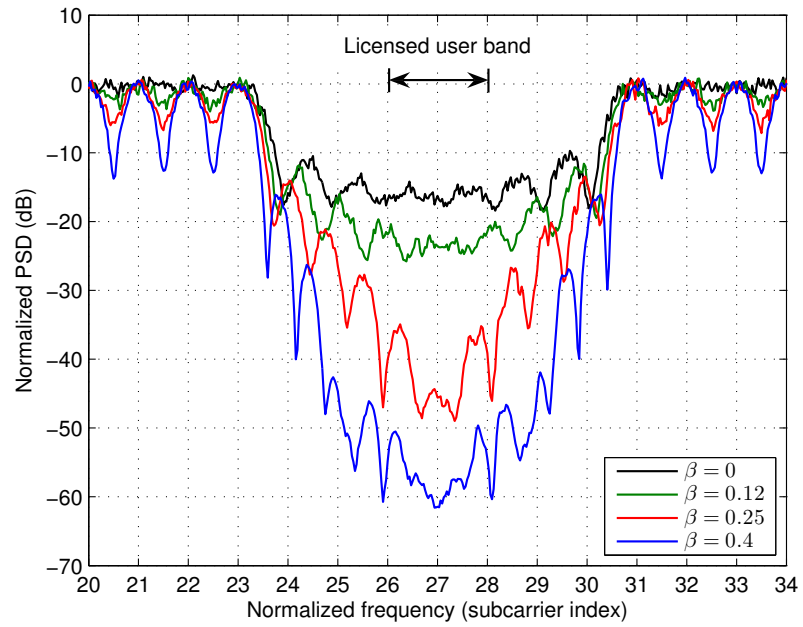
Figure 4.4 Rolloff factor effect on the RC-windowed signal PSD.
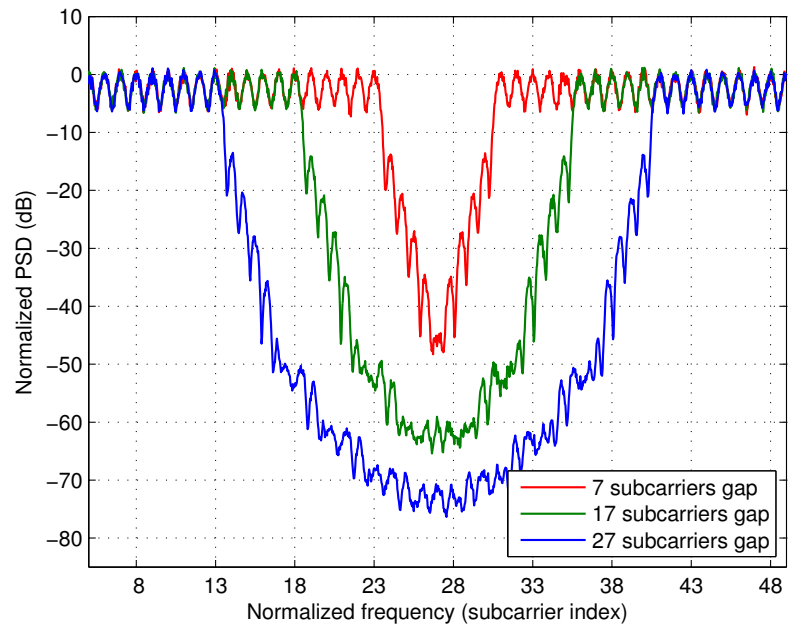


Figure 4.5 Gap size effect on the RC-windowed signal PSD.

## 4.6 Combining Cancellation Carriers and Raised Cosine Windowing

In this section, the combination of both CCs and RC windowing is considered. The CCs calculation is modified to take the RC windowing into account. We define

$$\mathbf{D} = \begin{pmatrix} \mathbf{0}_{N_{\mathrm{pre}} \times N - N_{\mathrm{pre}}} & \mathbf{I}_{N_{\mathrm{pre}}} \\ \mathbf{I}_{N - N_{\mathrm{pre}}} & \mathbf{0}_{N - N_{\mathrm{pre}} \times N_{\mathrm{pre}}} \\ \mathbf{0}_{N_{\mathrm{pre}} \times N - N_{\mathrm{pre}}} & \mathbf{I}_{N_{\mathrm{pre}}} \\ \mathbf{I}_{N_{\mathrm{post}}} & \mathbf{0}_{N_{\mathrm{post}} \times N - N_{\mathrm{post}}} \end{pmatrix}_{(1+\beta)N_T \times N}, \tag{4.13}$$

where $\mathbf{D}$ models the effect of adding both prefix and postfix to the time signal. We also define $\mathbf{R}_C = \mathrm{diag}\{\mathbf{g}\}$, where $\mathbf{R}_C$ is a diagonal matrix holding the elements of $\mathbf{g}$ as its main diagonal. The value of $\mathbf{S}$ and $\mathbf{Q}$ are then modified accordingly to

$$\mathbf{S} = \mathbf{F}_{\zeta N \times (1+\beta)N_T} \mathbf{R}_C \mathbf{D} \mathbf{x}, \tag{4.14}$$

and

$$\mathbf{Q} = \frac{1}{N} \mathbf{F}_{\zeta N \times (1+\beta)N_T} \mathbf{R}_C \mathbf{D} \mathbf{F}^*_{N \times N}. \tag{4.15}$$

Again, a LU spanning three subcarriers is considered and a gap of seven subcarriers is used. $N_g/N = 1/8$ and $\beta = 0.25$. The PSDs of the system using only RC windowing and using combination of RC and CCs technique are shown in Fig. 4.6. The figure also shows the PSD for a gap of 17 subcarriers. Note that in this case, RC windowing increases the symbol time by 33% and $E_r$ to 13%. In the case of seven subcarriers gap, the combined system reduces the interference level by an extra $20\,\mathrm{dB}$. In addition, the increase in $E_r$ due to CCs is around 0.02%. In other words, CCs cause almost no increase in symbol energy. However, for the wider gap of 17 subcarriers, there is almost no gain for the combined system over the RC system. Thus, combining CC technique with RC windowing is only beneficial for the system to combine CCs and RC windowing for small gaps.

## 4.7 Proposed Algorithm

In previous sections, sidelobe suppression techniques such as CC technique, RC windowing, and a combination of both, were considered. On one hand, a low complexity technique such as the RC windowing does not provide sufficient sidelobe suppression. On the other hand, the CC technique,
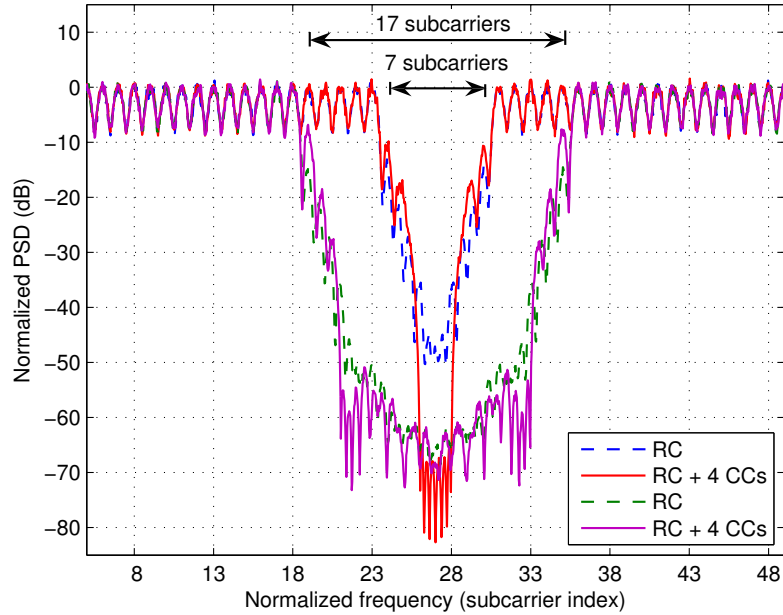
Figure 4.6  Combined RC windowing and CC effect on the signal PSD.

which provide significant sidelobe suppression for smaller gaps, is ineffective for larger gap sizes. In addition, CC technique results in an increase in the system peak-to-average-power ratio (PAPR), and the performance is sensitive to the CP size. Due to the higher power used for the CCs, using this technique affects the spectral flatness of the transmitted signal and can increase the inter-carrier interference (ICI) in case of a Doppler spread or a frequency offset error at the receiver. Other methods that were not considered in this study such as the subcarrier weighting method [74] causes an increase in the system BER, and the interference reduction is not as significant as it is with the CC method.

In this section, we propose a new method, referred to as adaptive symbol transition (AST), to suppress OFDM sidelobes and shape the signal spectrum. Similar to the windowing technique, the OFDM symbols are extended in time to reduce the effect of symbol transition. However, instead of using a predefined filter shape, the transition signal is optimized adaptively based on transmitted data and detected LU bands to reduce the interference to LUs.
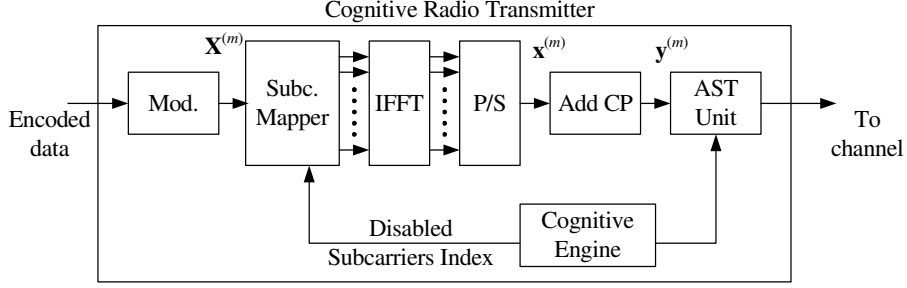
Figure 4.7  System Model.

### 4.7.1  Proposed System Model

The proposed system model is shown in Fig. 4.7. The encoded data is modulated and fed to an $N$-point IFFT unit. The signal is then extended with a CP consisting of $N_g$ samples and the extended symbols $\mathbf{y}^{(m)}$ are fed to the AST block. Meanwhile, the cognitive engine passes required information regarding LUs operating in the same band to both the subcarrier mapper and the AST block. This information is used to disable subcarriers operating in the LU bands and to suppress the interference –caused by OFDM sidelobes– to LUs as explained in the following section.

### 4.7.2  Adaptive Symbol Transition

In [64], windowing of OFDM symbols was investigated as a method to suppress OFDM sidelobes. The time domain symbols are passed through a filter (usually RC filters are used), and consecutive symbols are allowed to overlap. The process smooths the transition between OFDM symbols and thus improves the spectral characteristics of the OFDM signal. To keep the orthogonality between OFDM subcarriers, the symbols are cyclically extended to cover the overlapping region. The advantage of this approach is its low computational complexity. The disadvantage is the reduced spectral efficiency due to the symbol extension. Similar to windowing, the AST technique suppresses OFDM sidelobes by extending OFDM symbols and using the extensions to smooth the transition between consecutive symbols. However, instead of using a predefined window shape, such RC, we propose an adaptive method that calculates the value of the symbol extension based on LUs center frequency and bandwidth.

Once again, we assume the CR system detects an LU signal spanning over $K$ subcarriers $X(i+1)$, $X(i+2),\ldots X(i+K)$. The above subcarrier set is disabled to avoid interfering with the LU. To further suppress the interference, the AST block adds an extension $\mathbf{a}^{(m)} = [a(1)^{(m)},\ a(2)^{(m)},\ldots a(C)^{(m)}]^T$

75

to every OFDM symbol $\mathbf{y}^{(m)}$ as shown in Fig. 4.8, where $(m)$ is the symbol index and $C$ is the number of samples in $\mathbf{a}^{(m)}$. $\mathbf{y}^{(m)}$ and $\mathbf{y}^{(m-1)}$ are used to calculate $\mathbf{a}^{(m)}$ in the following manner.

First, we examine the interference to the LU. The signal is upsampled by a factor $\zeta$, or in other words, we consider $\zeta$ points per subcarrier. The signal spectrum of two consecutive symbols can be obtained as,

$$\mathbf{S}^{(m)} = \mathbf{F}_{\zeta N,\beta} \underbrace{\begin{bmatrix} \mathbf{y}^{(m-1)} \\ \mathbf{a}^{(m)} \\ \mathbf{y}^{(m)} \end{bmatrix}}_{\mathbf{z}^{(m)}}, \tag{4.16}$$

where $\beta = 2N + 2N_g + C$. The interference to the LU is then,

$$\boldsymbol{\mathcal{I}}_L = \boldsymbol{\mathcal{F}}_K \mathbf{z}_K^{(m)}, \tag{4.17}$$

where $\boldsymbol{\mathcal{F}}_K$ is a subset of $\mathbf{F}_{\zeta N,\beta}$ containing only the rows that corresponds to the LU band (rows $\zeta(i+1)$ to $\zeta(i+K)$) and $\mathbf{z}_K^{(m)}$ is the same as $\mathbf{z}^{(m)}$ but with $\mathbf{a}^{(m)} = [\mathbf{0}]_{C \times 1}$. To minimize interference power, the AST block chooses $\mathbf{a}^{(m)}$ such that,

$$\mathfrak{a}^{(m)} = \arg\min_{\mathbf{a}^{(m)}} \left\| \boldsymbol{\mathcal{F}}_I \mathbf{a}^{(m)} + \boldsymbol{\mathcal{I}}_L \right\|^2, \tag{4.18}$$

where $\boldsymbol{\mathcal{F}}_I$ is a subset of $\boldsymbol{\mathcal{F}}_K$ containing only the columns that corresponds to $\mathbf{a}^{(m)}$; columns $N + N_g$ to $N + N_g + C - 1$.

The MSE solution to (4.18) was found to result in very high values for $||\mathfrak{a}^{(m)}||$. This leads to increase in the extension power. As a result, the useful symbol energy is reduced compared to the total symbol energy resulting in an increase in the system BER. To mitigate this effect, we add a constraint on the minimization in (4.18) such that the symbol extension power is below a given level $\alpha^2$,

$$\left\| \mathbf{a}^{(m)} \right\|^2 \leq \alpha^2 \tag{4.19}$$

Input: conventional OFDM symbols



Output: extended OFDM symbols
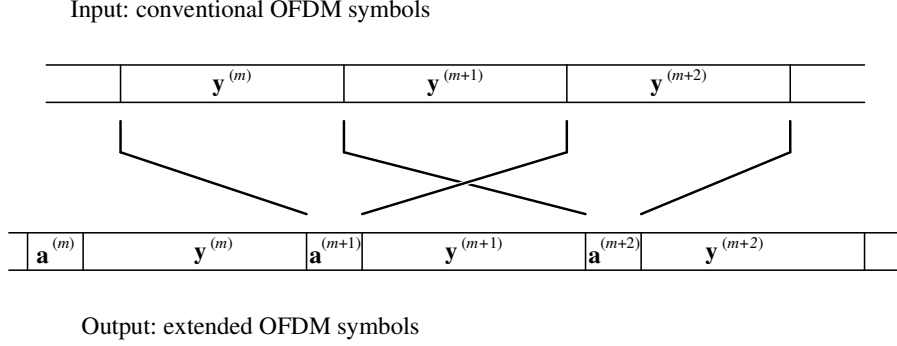
Figure 4.8  Output of the AST block.

The optimization in (4.18) and (4.19) is known as linear least squares problem with a quadratic inequality constraint [94]. Using singular value decomposition (SVD), we get,

$$\mathbf{U}^H \boldsymbol{\mathcal{F}}_I \mathbf{V} = \begin{bmatrix} \mathbf{D}_{\mathcal{F}_I} \\ \mathbf{0} \end{bmatrix} \tag{4.20}$$

and,

$$\mathbf{D}_{\mathcal{F}_I} = \text{diag}(v_1, \ldots, v_C), \qquad v_i \geq 0, \tag{4.21}$$

where $[\mathbf{U}]_{\Upsilon \times \Upsilon}$ and $[\mathbf{V}]_{C \times C}$ are unitary, and $\Upsilon = \zeta(K-1) + 1$. Using the method of Lagrange multipliers we get the following equation,

$$f(\lambda) = \sum_{i=1}^{C} \frac{v_i^2 |\tilde{\mathcal{I}}_{L,i}|^2}{(v_i^2 + \lambda)^2} = \alpha^2, \tag{4.22}$$

where $\tilde{\boldsymbol{\mathcal{I}}}_L = \mathbf{U}^H \boldsymbol{\mathcal{I}}_L = [\tilde{\mathcal{I}}_{L,1}, ..., \tilde{\mathcal{I}}_{L,\Upsilon}]^T$. If a solution exist to the optimization problem, the function $f(\lambda)$ will have a unique positive root and it has been shown that this is the desired root [94]. The solution can then be obtained as,

$$\mathfrak{a}^{(m)} = \mathbf{V}[-v_1 \tilde{\mathcal{I}}_{L,1}/(v_1^2 + \tilde{\lambda}), \ldots, -v_C \tilde{\mathcal{I}}_{L,C}/(v_C^2 + \tilde{\lambda})]^T, \tag{4.23}$$

where $\tilde{\lambda}$ is the unique positive root of (4.22). Fortunately, for a given spectrum shape, $\boldsymbol{\mathcal{F}}_I$ is fixed and thus, only $\boldsymbol{\mathcal{I}}_L$ needs to be updated for every OFDM symbol. The computational complexity of the optimization problem is reduced significantly due to this fact.

An important parameter for OFDM systems is the PAPR which affects the dynamic range over which the system should be linear. By choosing $\alpha^2$ such that,

$$\alpha^2 = C/(N + N_g)E_S, \tag{4.24}$$

the signal average power is kept at the same level, where $E_S$ is the symbol energy prior to the AST block. Since the AST signal is optimized to smooth the symbol transition, it does not introduce any peaks to the signal (confirmed by simulation results) and, thus, the PAPR of the system does not increase. Nevertheless, the AST reduces the useful symbol energy. Using (4.24), the maximum SNR loss $\gamma$ is,

$$\gamma = 10 \log_{10} \left( \frac{E_S + \alpha^2}{E_S} \right) = 10 \log_{10} \left( 1 + \frac{C}{N + N_g} \right) \text{dB}. \tag{4.25}$$

By controlling $C$ and for a fixed PAPR, the system has a tradeoff between reducing $\gamma$ (by reducing $C$), or improving the interference suppression (by increasing $C$).

Note that since AST technique is performed on time-domain symbols, the performance is not sensitive to the CP size. In addition, the AST does not introduce any ISI to the system as the leakage from the symbol extension is contained in the CP. The intended receiver can remove the AST extension along with the CP to maintain an ISI-free signal.

### 4.7.3 Simulation Results

In this section, the performance of the proposed method is investigated using computer simulations. We consider an OFDM-based CR system with $N = 256$ and $N_g = 16$. The AST method is used with $C = 16$, $\zeta = 16$, and, based on (4.24), $\alpha^2 = 0.06E_S$. The DC subcarrier is disabled. Data subcarriers are modulated with a quadrature phase shift keying (QPSK) signal. All results shown are averaged over $10,000$ OFDM symbols. We consider two cases for performance evaluation. In the first case, an LU is detected spaning 24 OFDM subcarriers. The system disables 32 subcarriers leaving a guard band of 4 subcarriers on each side of the LU band. The guard bands are to allow the signal power to decay while the AST block performs the optimization over the 24–subcarrier band. The normalized PSD of the signal at the output of the AST block is measured and the results are shown in Fig. 4.9. The system performance is compared with a conventional OFDM system without any symbol extension, and with an OFDM system using RC windowing and a symbol duration equal to the AST system. The conventional OFDM system suffers an interference level of $-22\,\text{dB}$. The
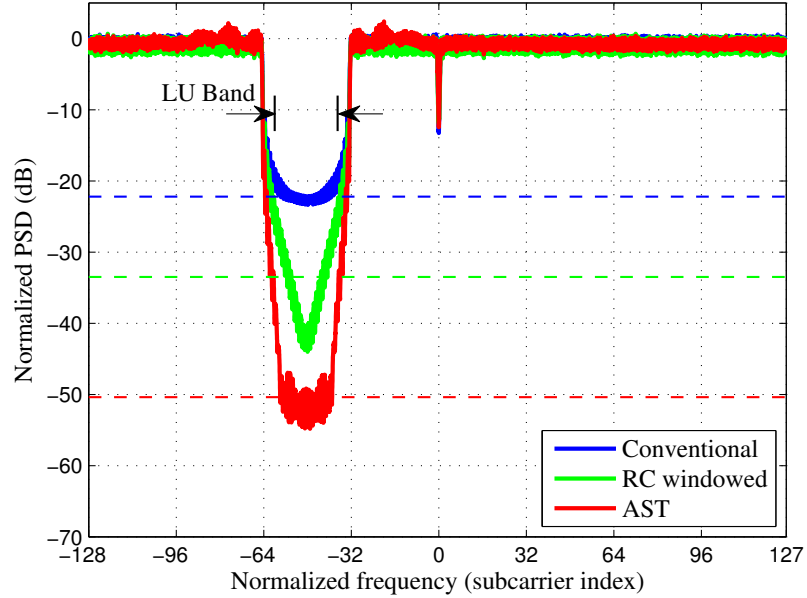
Figure 4.9  Spectrum of an OFDM signal with 32 subcarriers gap.

RC-windowed system suppresses the interference to $-33$ dB, while the AST reduces the interference further to less than $-50$ dB. The AST method achieves a 28 dB gain over conventional systems while keeping the SNR loss less than 0.25 dB.

Finally, we consider the second case where AST method is used to reduce the number of disabled subcarriers used as guard bands in current OFDM systems. For example, a worldwide interoperability for microwave access (WiMAX) system employing a 256 subcarriers OFDM system disables 55 subcarriers (28 and 27 on the left and right sides, respectively) to limit out-of-band radiations. Using sidelobe suppression techniques, the required guard band can be reduced for an increase in system complexity. We consider using 24 subcarriers (12 on each side) as guard bands. $N$, $N_g$, $C$, $\zeta$, and $\alpha^2$ are the same as the first case. The normalized PSD of the left side of the signal is shown in Fig. 4.10. The AST method suppresses the signal power to $-50$ dB by the end of the in-band signal compared to $-32$ dB for RC-window method and $-20$ dB for conventional systems.

## 4.8    Conclusions

In this chapter, we investigated three techniques for OFDM spectrum shaping. CCs technique has the advantage of lower interference level especially for small gap sizes. However, CC performance
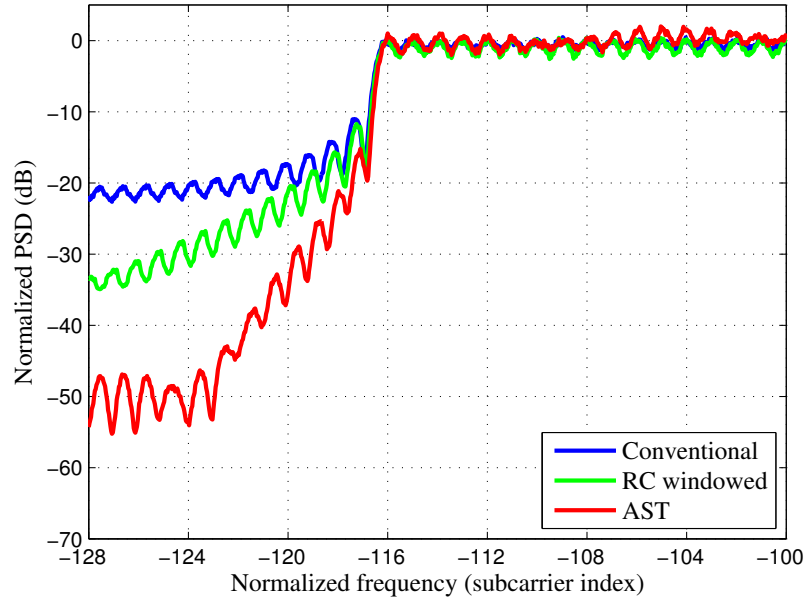
Figure 4.10  Spectrum of an OFDM signal with 12 subcarriers guard band.

is sensitive to the CP size, and as the gap size increases, the performance degradation, and the consumed power by CCs increases. Alternatively, RC windowing technique is a more robust solution with lower complexity. The sidelobe suppression comes at the cost of an increase in the symbol duration which reduces the spectral efficiency. However, RC windowing is inferior to CCs for small gap sizes. The combined CCs and RC windowing technique performs very well for small gaps regardless of the CP size. Moreover, the power consumed by CCs is minimal in this case. The disadvantage is that the system exhibits both low spectral efficiency due to symbol extension and higher computational complexity due to the use of CC. In addition, the combined technique does not introduce any gain over RC windowing for large gap sizes.

Based on the above observations, we investigated a new method that can overcome the drawbacks of RC windowing and CC technique. The proposed AST method extends OFDM symbols and uses the extension to reduce ACI to other users operating in the same band. Simulation results show that AST can achieve a significant gain over conventional sidelobe suppression techniques while maintaining low increase in symbol energy. Moreover, AST does not increase the signal PAPR and the performance is not sensitive to the CP size.

# CHAPTER 5

## ANALYSIS AND OPTIMIZATION OF OFDMA UPLINK SYSTEMS OVER TIME-VARYING FREQUENCY-SELECTIVE RAYLEIGH FADING CHANNELS

### 5.1 Introduction

Due to its attractive features, orthogonal frequency division multiple access (OFDMA) has been proposed for a various wireless standards such as WiMAX [9], LTE-Advanced [14], and IST-WINNER [15]. Most of these systems are expected to provide broadband services for mobile users. As such, it is expected that receivers will suffer from time-varying frequency-selective propagation effects. The quality of channel estimation, in such case, can significantly impact the overall system performance.

To support multiple user access in OFDMA uplink (UL) systems, the OFDMA signal is divided into smaller units, called tiles or chunks, consisting of a number of subcarriers that are adjacent in time and frequency. One or more of these tiles can be assigned to multiple users by the scheduler in an adaptive or random manner. Since adjacent tiles are not necessarily assigned to the same user, it is expect that different tiles are received over different wireless channels. As such, the channel estimation and equalization needs to be performed on a tile-by-tile basis [95, 96]. Pilots are placed within each tile to enable the channel estimation process. The optimum allocation of pilots within a tile to reduce the channel estimation mean-squared-error (MSE) is investigated in [97, 98] considering the frequency and time dimensions. The authors concluded that pilots should be placed at the corners of the tile at low signal-to-noise ratio (SNR) values and at $1/\sqrt{3}$ of the tile duration/bandwidth at high SNR values. In this work, pilots placement at the corners of each tile is considered [9].

The structure of pilot assignments in OFDMA UL in the time-frequency grid is analogous to that of pilot-symbol-aided modulation (PSAM) in single user orthogonal frequency division multiplexing (OFDM). However, since in OFDMA UL systems, pilots in adjacent tiles cannot be used for channel estimation, optimum algorithms such as 2D Wiener filtering [99] or higher order algorithms such

as sinc interpolation cannot be used [100]. In addition, techniques such as minimum mean-square error (MMSE) channel estimation [101] are inapplicable, since the number of pilot symbols per user/channel is not necessarily sufficient to reliably estimate the channel statistics. One approach for channel estimation in this case is to obtain least squares (LS) estimates at pilot symbols and use a first order time-frequency interpolation (bilinear interpolation) to estimate the channel at data symbols. Another approach is to use iterative channel estimation methods which utilize data symbols to improve the channel estimation process [95]. The drawback of this approach is the increased complexity, and consequently the delay, needed to perform multiple iterations. This is especially true for larger tile sizes, since the receiver needs to buffer the entire tile duration (up to 7560 subcarriers in some cases). In [96], the authors propose to use basis expansion model (BEM) to describe the time-frequency selectivity of the channel within each tile, instead of a linear model. While this method can improve the channel estimation performance, the channel Doppler spread and delay spread values are needed to correctly model the channel. Hence, from a practical point of view, using bilinear interpolation may be the most attractive approach for OFDMA UL systems [97]. In all the aforementioned studies, analysis of the bit error rate (BER) or optimum pilot insertion rate for tile-based OFDMA UL system are not considered.

In this chapter, the performance of OFDMA UL system over time-varying frequency-selective Rayleigh fading channels is considered. It is assumed that the system uses a tile-based channel estimation and equalization approach. Considering time-frequency interpolation filter, the variances of the channel estimates and channel estimation errors are evaluated. Expressions for the BER performance under channel estimation errors for quadrature phase shift keying (QPSK) and quadrature amplitude modulation (QAM) signals are derived. Based on the presented results, an analysis of optimum tile dimensions (or equivalently pilot insertion rate) that maximize the overall system throughput is investigated.

The remainder of this chapter is organized as follows. In Section 5.2, the system model and considered channel model are introduced. Evaluation of the channel estimation and equalization using time-frequency interpolation is presented in Section 5.3. Analysis of the BER performance for QPSK and QAM signals is derived in Section 5.4. In Section 5.5, optimum tile dimensions for maximum system throughput is discussed. Simulation results are used to verify the theoretically results in Section 5.6. Finally, concluding remarks are presented in Section 5.7.

## 5.2   System Model

### 5.2.1   Channel Model

The complex baseband representation of a mobile wireless channel impulse response (CIR) is described as [101],

$$h(t, \tau) = \sum_\ell h_\ell(t)\delta(t - \tau_\ell), \tag{5.1}$$

where $\tau_\ell$ is the delay of the $l$th path and $h_\ell(t)$ is the corresponding complex amplitude. Note that $h_\ell(t)$'s are wide-sense stationary (WSS) narrowband complex Gaussian processes, and are independent for different paths. Without the loss of generality, the channel is assumed to be normalized such that

$$\sum_\ell \sigma_\ell^2 = 1 \tag{5.2}$$

where

$$\sigma_\ell^2 = E\left\{|h_\ell(t)|^2\right\} \tag{5.3}$$

and $E\{\cdot\}$ is the expectation operator. The channel frequency response (CFR) at time $t$ is,

$$H(t, f) = \sum_\ell h_\ell(t) \exp\left(-\jmath 2\pi f \tau_\ell\right). \tag{5.4}$$

The channel fading in time is modeled using the classical Doppler spectrum [102]. Thus, for an OFDM system with symbol duration $T_S$ and subcarrier spacing $\Delta f$, the correlation function between the channel responses at two subcarriers $(n, k)$ and $(n + \Delta n, k + \Delta k)$ is [101],

$$R_H(\Delta n, \Delta k) = J_0(2\pi \Delta n f_d) \sum_\ell \sigma_\ell^2 \exp\left(-\jmath 2\pi \Delta k \Delta f \tau_\ell\right) \tag{5.5}$$

where $J_0$ is the zeroth-order Bessel function of the first kind, $f_d$ is the maximum Doppler shift, and $n$ and $k$ are the symbol index and subcarrier index, respectively, such that

$$R_H(\Delta n, \Delta k) \equiv R_H(\Delta n T_S, \Delta k \Delta f). \tag{5.6}$$

### 5.2.2 Signal Model

In OFDMA systems, used subcarriers are divided into smaller blocks, also known as tiles or chunks, which represent the minimum allocation unit. The tiles are then assigned to subchannels either randomly or depending on user channels. The overall received UL frame is a sum of all current user signals, which are transmitted over different communication channels.

An example of how the UL frame is divided into tiles is shown in Fig. 5.1. Used subcarriers are divided into $Q$ tiles, usually with equal number of tiles on each side of the DC subcarrier. Three different tile structures are shown in the figure, where tile dimensions are three symbols by four subcarriers. In this example, the tile bandwidth, $B_{\text{tile}} = 3\Delta f$, and the tile duration, $T_{\text{tile}} = 2T_S$. For the remainder of this chapter, Tile C structure is considered. Note that a similar frame structure is employed by the mobile worldwide interoperability for microwave access (WiMAX) standard [9].

An OFDMA-UL system employing $N$ subcarriers per symbol is considered. The DC subcarrier and guard subcarriers are disabled. The remaining subcarriers $N_u$ are used for data transmission with equal number of subcarriers on each side of the DC subcarrier. The above assumptions are common for most practical implementations of OFDMA systems.

Considering the output of the fast Fourier transform (FFT) unit at the receiver, the received signal of a user $u$ at subcarrier $(n, k)$ is

$$Y(n,k) = H^{(u)}(n,k)X^{(u)}(n,k) + I(n,k) + W(n,k), \tag{5.7}$$

where $X^{(u)}(n,k)$ and $H^{(u)}(n,k)$ are the $u$th user transmitted signal and CFR at subcarrier $(n,k)$, respectively, $W(n,k)$ is the additive white Gaussian noise (AWGN) with zero mean and variance $\sigma_n^2 = N_0/2$, and $I(n,k)$ is the inter-carrier interference (ICI) due to Doppler spreading. It is shown in [103] that,

$$I(n,k) = \frac{1}{N} \sum_{i=0,i\neq k}^{N} X(n,i) \sum_{m=0}^{N-1} H(n,i,m) \exp(j2\pi m(i-k)/N) \tag{5.8}$$

where $H(n,i,m)$ is the CFR at subcarrier $(n,i)$ and sampling instant $m$, as the channel is assumed to be time variant. Whenever the sampling index is dropped, it is to indicate averaging is performed
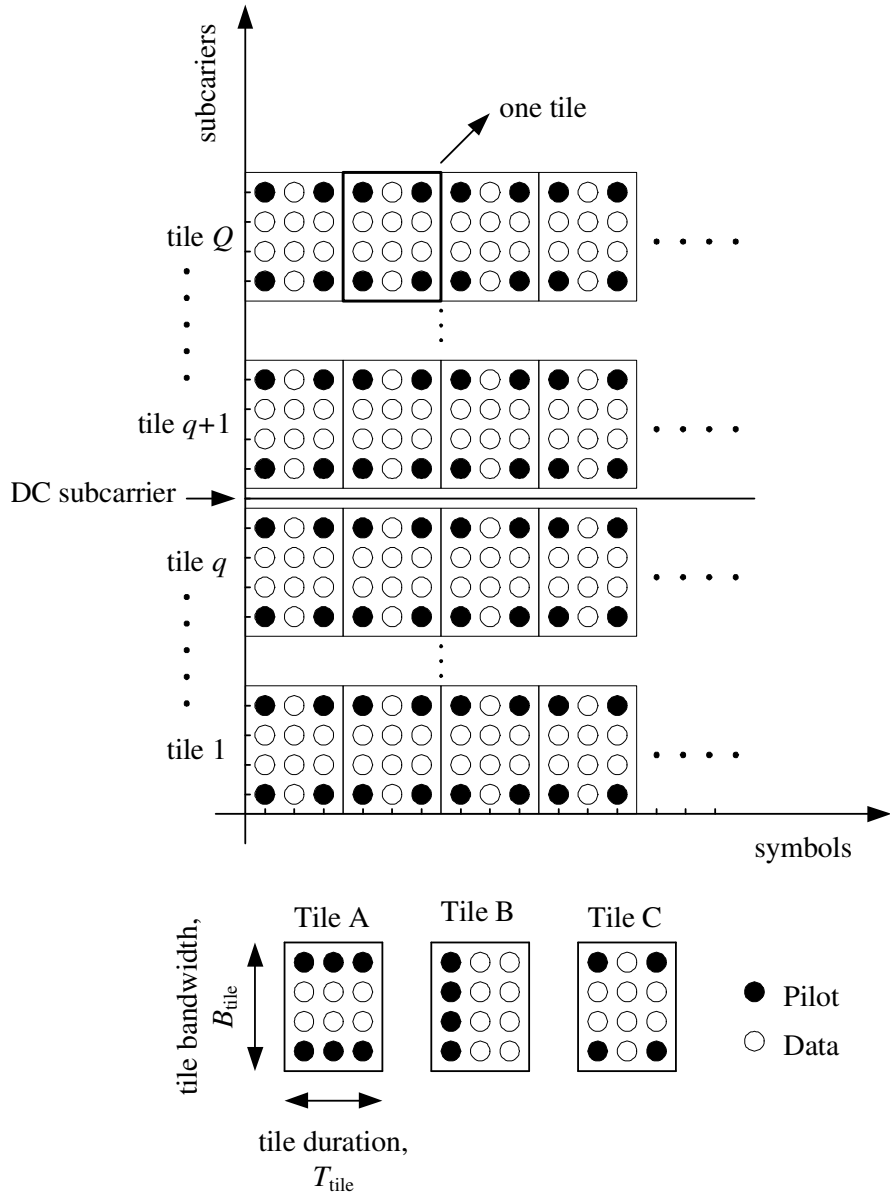
Figure 5.1  UL frame structure and subcarrier mapping to tiles.

over all samples of the current symbol, such that in (5.7)

$$H^{(m)}(n,k) = \frac{1}{N} \sum_{m=0}^{N-1} H^{(m)}(n,k,m). \tag{5.9}$$

It is assumed that one or more tiles can be assigned to any given user in the system but a single tile can only be assigned to one user. In addition, it is assumed that the process of tile assignment
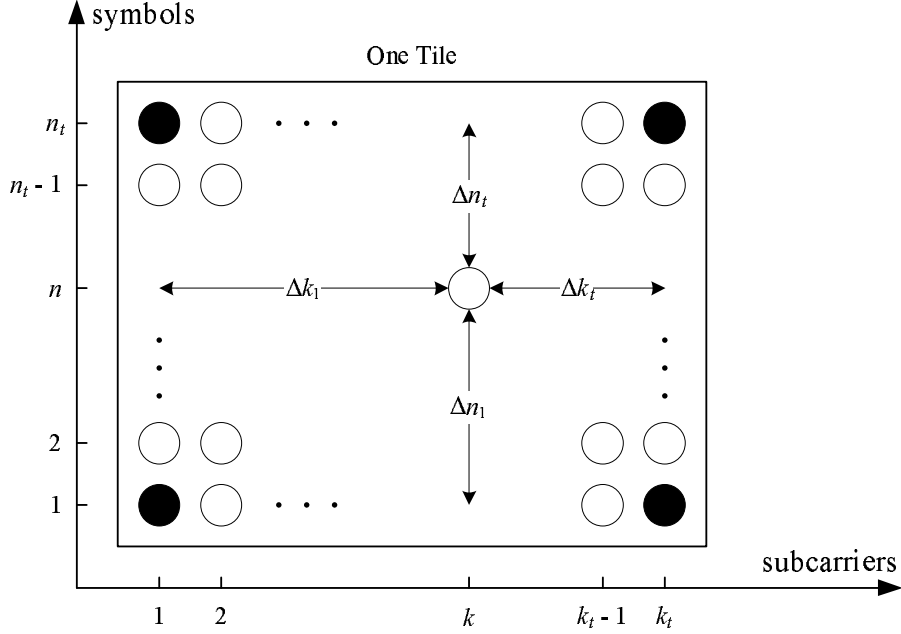
Figure 5.2  The subindex of one OFDMA UL tile.

to multiple users is done in a random fashion, such that adjacent tiles do not necessarily belong to the same user. Thus, the receiver performs the channel estimation and equalization on a tile-by-tile basis. Finally, channel statistics such as the number of paths, the delay spread, or Doppler spread of each user's channel is assumed to be unknown to the receiver. For the remainder of this chapter, the user superscript $(u)$ is dropped for simplicity.

## 5.3 Channel Estimation and Equalization

In this section, the process of channel estimation and equalization in an OFDMA UL system is examined. Since each tile is processed separately, the subindex of subcarriers within each tile is considered. Thus, if the tile size is chosen to be $n_t$ symbols by $k_t$ subcarriers, then pilots are assigned to subcarriers $(1, 1)$, $(1, k_t)$, $(n_t, 1)$, and $(n_t, k_t)$ as shown in Fig. 5.2.

The channel LS estimates are calculated by dividing the received subcarriers $Y(n, k)$ at pilot locations with known pilot symbols $P(n, k)$. From (5.7), the LS estimate of the channel is

$$\hat{H}_{\text{LS}}(n, k) = H(n, k) + \frac{I(n, k)}{P(n, k)} + \frac{W(n, k)}{P(n, k)} \tag{5.10}$$

86

where $n \in \{1, n_t\}$ and $k \in \{1, k_t\}$, for each tile. Without the loss of generality, it is assumed that data symbols and pilot symbols are normalized such that $E\{|X(n,k)|^2\} = E\{|P(n,k)|^2\} = 1$. Thus, the second order statistics of $I(n,k)$ and $W(n,k)$ are not changed when divided by $P(n,k)$. The ICI can be modeled as an additive Gaussian process with zero mean and variance $\sigma^2_{\text{ICI}}$ [104]. An upper bound on $\sigma^2_{\text{ICI}}$ for the classical Doppler spectrum is introduced in [105] as

$$\sigma^2_{\text{ICI}} \leq \frac{1}{24}(2\pi f_d T_s)^2. \tag{5.11}$$

Assuming the ICI and AWGN values at each subcarrier are independent and identically distributed (i.i.d.), the correlation function between the LS estimates at two subcarriers $(n,k)$ and $(n+\Delta n, k+ \Delta k)$ can be shown, using (5.10) and (5.6), to be

$$R_{H,\text{LS}}(\Delta n, \Delta k) = \begin{cases} \sigma^2_H + \sigma^2_{\text{ICI}} + \sigma^2_n, & \text{for } \Delta n = \Delta k = 0, \\ R_H(\Delta n, \Delta k), & \text{otherwise} \end{cases} \tag{5.12}$$

where

$$\sigma^2_H = E\left[|H(n,k)|^2\right]. \tag{5.13}$$

Since the channel is assumed to be normalized, then from (5.2), we conclude that $\sigma^2_H = 1$.

The receiver estimates the channel at data subcarriers using bilinear interpolation and the four LS estimates. For a data subcarrier $(n,k)$ that belongs to the current tile, the bilinear channel estimate is calculated as follows

$$\hat{H}_{\text{BL}}(n,k) = \frac{1}{\Delta n_T \Delta k_T} \begin{bmatrix} \Delta n_t & \Delta n_1 \end{bmatrix} \begin{bmatrix} \hat{H}_{\text{LS}}(1,1) & \hat{H}_{\text{LS}}(1,k_t) \\ \hat{H}_{\text{LS}}(n_t,1) & \hat{H}_{\text{LS}}(n_t,k_t) \end{bmatrix} \begin{bmatrix} \Delta k_t \\ \Delta k_1 \end{bmatrix} \tag{5.14}$$

where

$$\Delta n_1 = n - 1, \qquad \Delta n_t = n_t - n, \qquad \Delta n_T = n_t - 1,$$

$$\Delta k_1 = k - 1, \qquad \Delta k_t = k_t - k, \qquad \Delta k_T = k_t - 1, \tag{5.15}$$

87

as shown in Fig. 5.2. Using zero-forcing (ZF) equalizer, the equalized OFDMA subcarrier is given by

$$
\begin{aligned}
\hat{X}(n,k) &= \frac{Y(n,k)}{\hat{H}_{\mathrm{BL}}(n,k)} \\
&= X(n,k) - \frac{\epsilon(n,k)}{\hat{H}_{\mathrm{BL}}(n,k)} X(n,k) + \frac{I(n,k)}{\hat{H}_{\mathrm{BL}}(n,k)} + \frac{W(n,k)}{\hat{H}_{\mathrm{BL}}(n,k)}
\end{aligned}
\tag{5.16}
$$

where

$$
\epsilon(n,k) = \hat{H}_{\mathrm{BL}}(n,k) - H(n,k)
\tag{5.17}
$$

is the channel estimation error at data subcarrier $(n,k)$.

## 5.4 Bit Error Rate Analysis

In this section, the BER of OFDMA UL systems operating in multipath slow fading channels is evaluated. The BER of systems, including OFDM systems, under channel estimation errors has been studied in the literature [100, 106–112]. Evaluation of BER, assuming the channel envelop and phase are two independent random processes, is introduced in [106] without considering ICI and in [107, 110] while taking ICI into consideration. In [110, 111], the BER is evaluated while taking into account the correlation between the envelop and the phase of the channel. In [100], the results are extended to Ricean fading channels and multichannel receivers. However, the calculation of BER in most of the above references involves the evaluation of three-fold (or even four-fold) integral and yields highly-complex expressions. An approximation of the BER for OFDM-based wireless local area network (WLAN) systems with channel estimation errors is introduced in [108]. The authors assumed that for relatively small channel estimation errors, the estimated channel response and the channel estimation errors are uncorrelated. In this work, we use the results introduced in [108], since they yield simplified expressions with minimal error margin for considered application (as verified by computer simulations in Section 5.6).

From (5.16), it can be seen that the sources of degradation are the bilinear channel estimates, the channel estimation error, the ICI, and the AWGN, with powers (or variances) $\sigma_{\mathrm{BL}}^2$, $\sigma_\epsilon^2$, $\sigma_{\mathrm{ICI}}^2$, and $\sigma_n^2$, respectively. Note that the symbol power is not considered here, since it is assumed that symbols are normalized. To evaluate the BER, the instantaneous SNR is obtained at any subcarrier

$(n, k)$ using (5.16) such that

$$\text{SNR}(n, k) = \frac{\left|\hat{H}_{\text{BL}}(n, k)\right|^2}{\left|\epsilon(n, k)\right|^2 + \sigma_{\text{ICI}}^2 + \sigma_n^2}. \tag{5.18}$$

The instantaneous BER is evaluated for a given modulation type using (5.18), and the average BER is obtained by averaging over the probability density functions (PDF) of both the channel estimation error and the channel estimates. The BER for a QPSK signal is [108]

$$P_{\text{QPSK}} \approx \frac{1}{2}\left[1 - \sqrt{\frac{\pi\sigma_{\text{BL}}^2}{2\sigma_\epsilon^2}}\exp(\xi)\,\text{erfc}\left(\sqrt{\xi}\right)\right] \tag{5.19}$$

where $\text{erfc}(\cdot)$ is the complementary error function and

$$\xi = \frac{\sigma_{\text{BL}}^2 + 2\sigma_{\text{ICI}}^2 + 2\sigma_n^2}{2\sigma_\epsilon^2}. \tag{5.20}$$

For square QAM signals, i.e. with even number of bits per symbol, and with Gray bit mapping, the BER is [108]

$$P_{\text{QAM}} \approx \frac{2}{\log_2 M}\left(1 - \frac{1}{\sqrt{M}}\right)\left[1 - \sqrt{\frac{3\pi\sigma_{\text{BL}}^2}{2(M-1)\sigma_\epsilon^2}}\exp(\xi_M)\,\text{erfc}\left(\sqrt{\xi_M}\right)\right] \tag{5.21}$$

where $M$ is the modulation order and

$$\xi_M = \frac{3\sigma_{\text{BL}}^2 + 2(M-1)(\sigma_{\text{ICI}}^2 + \sigma_n^2)}{2(M-1)\sigma_\epsilon^2}. \tag{5.22}$$

For low channel estimation errors, $\xi$ and $\xi_M$ yield large values, as can be seen from (5.20) and (5.22). However, evaluating the $\text{erfc}(\cdot)$ of large values can lead to inaccurate results. To overcome this problem, we further simplify the expressions in (5.19) and (5.21) by using an approximation of the $\text{erfc}(\cdot)$. It can be shown from [113] that the $\text{erfc}(\cdot)$ is bounded by

$$L_0(x) < \text{erfc}(x) \leq R_0(x) \tag{5.23}$$

89

where

$$L_0(x) = \frac{2 \exp(-x^2)}{\sqrt{\pi} \left( x + \sqrt{x^2 + 2} \right)} \tag{5.24}$$

and

$$R_0(x) = \frac{2 \exp(-x^2)}{\sqrt{\pi} \left( x + \sqrt{x^2 + 4/\pi} \right)}. \tag{5.25}$$

For large vaules of $x$, such as in considered application, we note that

$$\mathrm{erfc}(x) \approx L_0(x). \tag{5.26}$$

Applying (5.26) to (5.19) and (5.21), the BER for QPSK signals reduces to

$$P_{\mathrm{QPSK}} \approx \frac{1}{2} \left[ 1 - \sqrt{\frac{2\sigma_{\mathrm{BL}}^2}{\sigma_\epsilon^2}} \frac{1}{\sqrt{\xi} + \sqrt{\xi + 2}} \right] \tag{5.27}$$

and for QAM signals reduces to

$$P_{\mathrm{QAM}} \approx \frac{2}{\log_2 M} \left( 1 - \frac{1}{\sqrt{M}} \right) \left[ 1 - \sqrt{\frac{6\sigma_{\mathrm{BL}}^2}{(M-1)\sigma_\epsilon^2}} \cdot \frac{1}{\sqrt{\xi_M} + \sqrt{\xi_M + 2}} \right]. \tag{5.28}$$

The above two expressions for the BER have the advantages of being much simpler compared with exact BER expressions in the literature, can be evaluated accurately for low channel estimation errors (no $\mathrm{erfc}(\cdot)$), and provide very close results to the exact BER as shown in Section 5.6.

To use the BER expressions presented in (5.27) and (5.28), the power of the channel estimates $\sigma_{\mathrm{BL}}^2$ and channel estimation errors $\sigma_\epsilon^2$ need to be calculated. The value of $\sigma_{\mathrm{BL}}^2$ is expressed as

$$\sigma_{\mathrm{BL}}^2 = \frac{1}{n_t k_t - 4} \sum_n \sum_k \sigma_{\mathrm{BL}}^2(n, k) \tag{5.29}$$

and

$$\sigma_{\mathrm{BL}}^2(n, k) = E \left\{ \left| \hat{H}_{\mathrm{BL}}(n, k) \right|^2 \right\} \tag{5.30}$$

where the summations are over all data subcarriers within the tile and $\sigma_{\mathrm{BL}}^2(n,k)$ is the variance of the channel estimates at subcarrier $(n,k)$. From (5.10) and (5.14), and since $I(n,k)$ and $W(n,k)$ are i.i.d. zero mean random variables, it can be shown that

$$\sigma_{\mathrm{BL}}^2(n,k) = \frac{1}{\Delta n_T^2 \Delta k_T^2} \Bigg[ (\Delta n_t^2 \Delta k_t^2 + \Delta n_1^2 \Delta k_t^2 + \Delta n_t^2 \Delta k_1^2 + \Delta n_1^2 \Delta k_1^2) \Re\{R_{\mathrm{H,LS}}(0,0)\}$$

$$+ 2\Delta n_1 \Delta n_t (\Delta k_1^2 + \Delta k_t^2) \Re\{R_{\mathrm{H,LS}}(\Delta n_T, 0)\} + 2\Delta k_1 \Delta k_t (\Delta n_1^2 + \Delta n_t^2) \Re\{R_{\mathrm{H,LS}}(0, \Delta k_T)\}$$

$$+ \Delta n_1 \Delta n_t \Delta k_1 \Delta k_t \Re\{R_{\mathrm{H,LS}}(\Delta n_T, \Delta k_T)\} \Bigg] \quad (5.31)$$

where $\Re\{x\}$ is the real part of $x$. The above relation can be expressed in matrix form as follows

$$\sigma_{\mathrm{BL}}^2(n,k) = \frac{1}{\Delta n_T^2 \Delta k_T^2} \overline{n} \Re\{\boldsymbol{R}_A\} \overline{k} \quad (5.32)$$

where

$$\overline{n} = \begin{bmatrix} \Delta n_1^2 + \Delta n_t^2 & 2\Delta n_1 \Delta n_t \end{bmatrix}, \quad (5.33)$$

$$\boldsymbol{R}_A = \begin{bmatrix} R_{\mathrm{H,LS}}(0,0) & R_{\mathrm{H,LS}}(0, \Delta k_T) \\ R_{\mathrm{H,LS}}(\Delta n_T, 0) & R_{\mathrm{H,LS}}(\Delta n_T, \Delta k_T) \end{bmatrix}, \quad (5.34)$$

and

$$\overline{k} = \begin{bmatrix} \Delta k_1^2 + \Delta k_t^2 \\ 2\Delta k_1 \Delta k_t \end{bmatrix}. \quad (5.35)$$

Note that $\boldsymbol{R}_A$ is independent of the subcarrier index $(n,k)$. The value of $\boldsymbol{R}_A$ can be related to channel correlation function $R_H(\Delta n, \Delta k)$ using (5.12) such that

$$\boldsymbol{R}_A = \begin{bmatrix} \sigma_H^2 + \sigma_{\mathrm{ICI}}^2 + \sigma_n^2 & R_H(0, \Delta k_T) \\ R_H(\Delta n_T, 0) & R_H(\Delta n_T, \Delta k_T) \end{bmatrix}. \quad (5.36)$$

Similar to $\sigma_{\mathrm{LS}}^2$, the variance of the channel estimation error can be calculated from (5.17) as follows

$$\sigma_\epsilon^2 = \frac{1}{n_t k_t - 4} \sum_n \sum_k \sigma_\epsilon^2(n, k) \tag{5.37}$$

and

$$\sigma_\epsilon^2(n, k) = \sigma_H^2 + \sigma_{\mathrm{BL}}^2 - 2\Re\Big\{ \underbrace{E\left[ H^*(n, k)\hat{H}_{\mathrm{BL}}(n, k) \right]}_{R_B(n,k)} \Big\}. \tag{5.38}$$

From (5.14), it can be shown that

$$R_B(n, k) = \frac{1}{\Delta n_T \Delta k_T} \begin{bmatrix} \Delta n_t & \Delta n_1 \end{bmatrix} \begin{bmatrix} R_H(\Delta n_1, \Delta k_1) & R_H(\Delta n_1, \Delta k_t) \\ R_H(\Delta n_t, \Delta k_1) & R_H(\Delta n_t, \Delta k_t) \end{bmatrix} \begin{bmatrix} \Delta k_t \\ \Delta k_1 \end{bmatrix}. \tag{5.39}$$

Based on the results in (5.29), (5.32), (5.36), (5.37), (5.38), and (5.39); the values of $\sigma_{\mathrm{BL}}^2$ and $\sigma_\epsilon^2$ can be calculated using the channel autocorrelation function and the considered tile dimensions ($n_t$ and $k_t$).

## 5.5  Optimum Tile Dimensions

Next, optimization of the tile dimensions, using the results presented is this chapter, is considered. For the system under consideration, it is assumed that hard decision detection and decoding is used at the receiver. Similar analysis can be applied to the soft decision detection case. However, calculations of soft decision metrics over Rayleigh channels with channel estimation errors is quite complicated [114, 115] and is out of the scope of this work. Two approaches are considered under hard decision criteria. The first approach is to choose the tile dimension that maximizes the system throughput, assuming optimum channel coding. The second approach is to consider the tile dimensions that maximize the system effective throughput under practical channel coding conditions.

With sufficient interleaving, the channel can be modeled as a binary symmetric channel (BSC) with BER $P_b$ which can be obtained using (5.27) and (5.28). In this case, the channel capacity

is [89, p. 382]

$$C = P_b \log_2(2P_b) + (1 - P_b) \log_2 2(1 - P_b). \tag{5.40}$$

From the noisy channel coding theorem [116], the maximum coding rate that can achieve error-free transmission is equal to $C$. Thus, for given tile dimensions $(n_t, k_t)$, the maximum achievable throughput is

$$T_{\max} = C \log_2 M \; \frac{n_t k_t - 4}{n_t k_t} \; \frac{N_u}{T_S}. \tag{5.41}$$

It can be seen from (5.41) that increasing the tile dimensions, which effectively reduces the pilot insertion rate, can increase the system throughput. However, larger tile dimensions degrade the channel estimation performance leading to high BER, $P_b$ and consequently lower channel capacity, $C$. As such, there is an optimum value for $n_t$ and $k_t$ at which the throughput is maximized. The optimum tile dimensions in that sense can be obtained using numerical methods as shown in Section 5.6.

Achieving the channel capacity using channel coding is usually very difficult in practice. Thus, using the above approach may result in tile dimensions that are not optimum for a practical system. In this case, the system design may consider choosing the tile dimensions that maximize the system effective throughput, where the effective throughput is defined as

$$T_{\mathrm{eff}} = r_c(1 - P_f) \log_2 M \; \frac{n_t k_t - 4}{n_t k_t} \; \frac{N_u}{T_S}, \tag{5.42}$$

where $r_c$ is the channel coding rate, which is usually predefined in a practical system, and $P_f$ is the frame error rate (FER). The above expression is based on the fact that for practical systems, the decoded frames are checked for errors and erroneous frames are dropped. Thus, the actual system throughput is based on the rate of frames that are received successfully. Similar to the previous approach, while increasing the tile dimensions can increase the system throughput, it leads to higher FER which may cancel any increase to the overall system throughput. Therefore, it is expected that there should be optimum tile dimensions, that maximize the effective throughput.

Table 5.1  Simulation parameters for a typical OFDMA UL system I.

| Parameter | Value |
| --- | --- |
| Carrier frequency | $2.5\,\text{GHz}$ |
| FFT size | 1024 |
| CP size | 128 |
| Number of used subcarriers | 840 |
| Sampling frequency | $11.2\,\text{MHz}$ |

## 5.6  Simulation Results

An OFDM UL system that is based on the WiMAX standard [9] is considered. Typical simulation parameters are chosen based on [90] and are summarized in Table 5.1. Similar to WiMAX OFDMA systems, it is assumed that each tile spans three symbols $n_t = 3$, and four subcarriers $k_t = 4$. Based on the above tile dimensions, the UL frame size in symbols is always considered as an integer multiple of three. There are 210 tiles per three OFDMA symbols which are assigned randomly to one or more users. The modulation schemes considered for data subcarriers are QPSK, 16QAM, and 64QAM. The system is tested over three channels based on the ITU channel models [91]: Indoor A, Pedestrian B, and Vehicular A, with Doppler spread of $0\,\text{Hz}$ ($0\,\text{km/h}$), $6.9\,\text{Hz}$ ($3\,\text{km/h}$), and $138.9\,\text{Hz}$ ($60\,\text{km/h}$), respectively. It is assumed that the channel is independent between different frames and between different users. The receiver processes each frame individually. At the receiver, the uncoded BER is measured and averaged over all users. For comparison, the theoretical BER curves based on the results presented in (5.27) and (5.28) are considered. The results for both simulations and theoretical values are presented in Fig. 5.3, Fig. 5.4, and Fig. 5.5 for Pedestrian B, Vehicular A, Indoor A channel models, respectively. The figures show that derived BER values are in very good agreement with simulation results with only little mismatch at higher BER values.

Next, we investigate the optimum tile dimensions for two operation profiles. The first profile is for an OFDMA UL system operating in a Vehicular A channel with 64QAM modulation. In the second profile, the system is operating in Pedestrian B channel with QPSK modulation. In both cases, the system uses a convolutional code with rate $r_c = 1/2$, constraint length of 7, and generator polynomials of (133, 171) in octal form. This code achieves the maximum free distance for the given rate and constraint length [117]. The conding block is chosen to be $70\,\text{bytes}$. At the receiver, hard decision Viterbi decoder is used to decode the demodulated symbols. In search for optimum tile dimensions, the maximum and effective throughputs for various tile sizes are evaluated using (5.41)
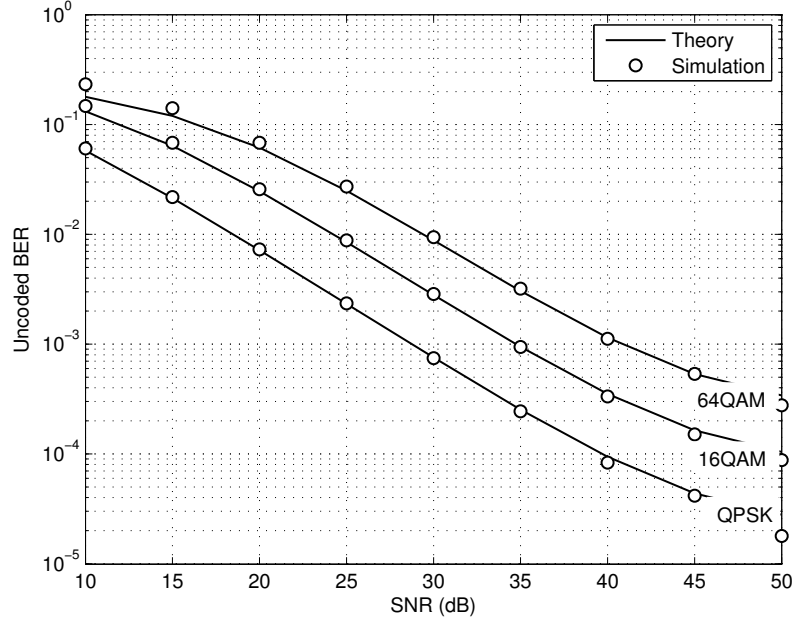
Figure 5.3  Uncoded BER of OFDMA UL system over Pedestrian B channel.
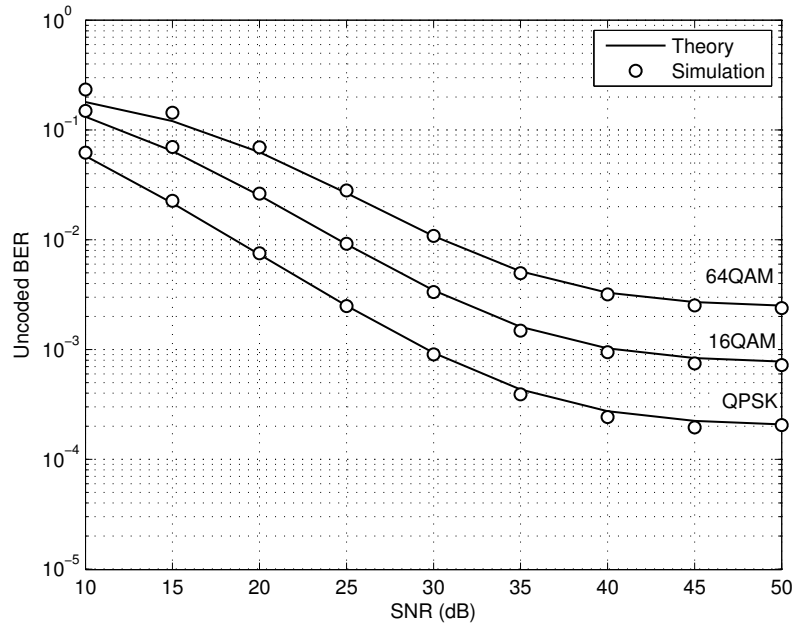


Figure 5.4  Uncoded BER of OFDMA UL system over Vehicular A channel.
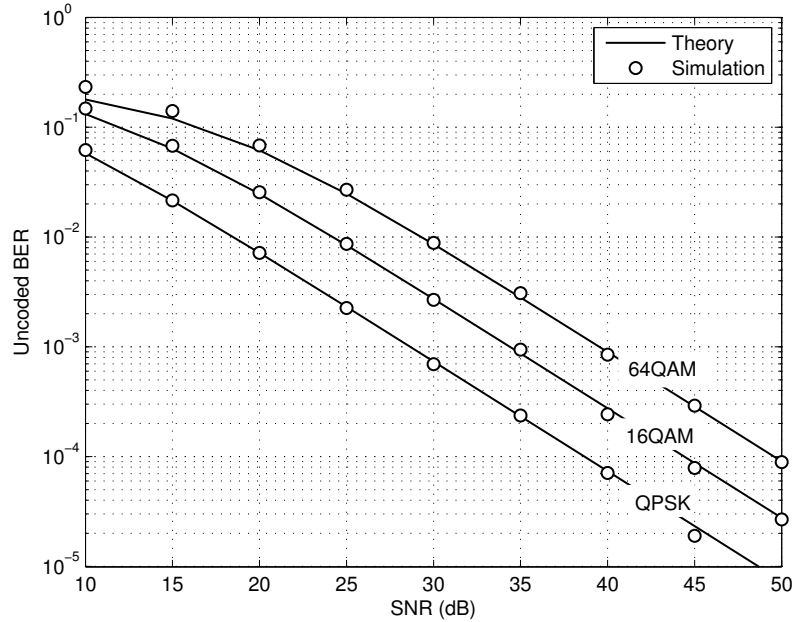
Figure 5.5  Uncoded BER of OFDMA UL system over Indoor A channel.

and (5.42), respectively. To evaluate the effective throughput, the FER needs to be calculated. Unfortunately, there are no exact expressions for the coded BER and the FER for convolutional codes. Thus, upper bounds on the BER and the FER are calculated using results from [89, 118]. The disadvantage of using union bounds is that they diverge for higher BER values (or relatively low SNR values). The maximum and effective throughput for the first and second profile are shown in Fig. 5.6, Fig. 5.7, Fig. 5.8, and Fig. 5.9, respectively. In all figures the throughput surface shows a convex shape which indicates a maximum value at a given tile dimensions. These results are in agreement with the conclusions drawn in Section 5.5. The figures also show that the optimum tile dimensions are quite larger that the one used initially (i.e. $n_t = 3$, $k_t = 4$).

To verify the above results, computer simulations were generated for both profiles. Note that when choosing the tile dimensions for the OFDMA system, there are some limitations. First, the tile duration in symbols $n_t$ is limited by the total allowed frame duration. Second, the number of used subcarriers $N_u$ should be an integer multiple of the tile bandwidth in subcarriers $k_t$. Based on these limitations, the best possible tile dimensions for both system profiles under consideration were found to be $n_t = 9$ and $k_t = 12$. Considering the second system profile, simulation results for the uncoded BER, coded BER, and the FER are shown in Fig. 5.10 and Fig. 5.11 for tile dimensions
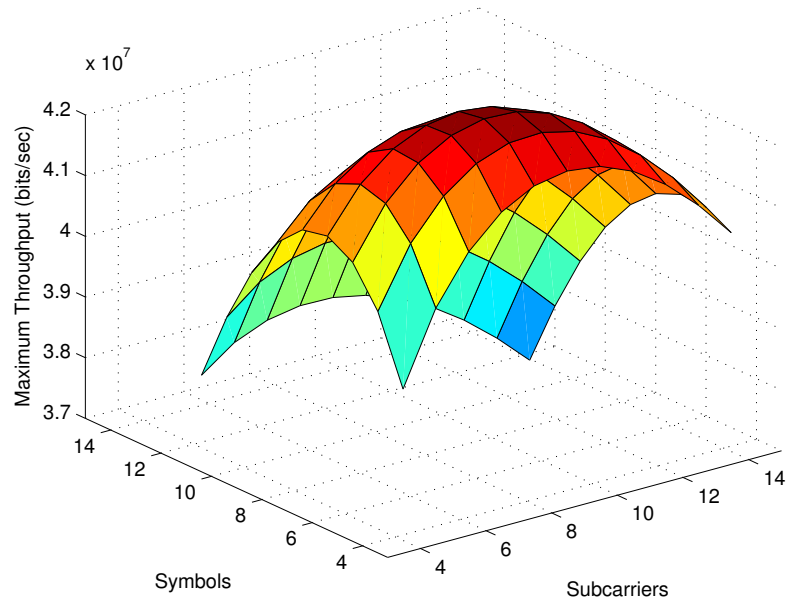
Figure 5.6 Maximum throughput of OFDMA UL system with 64QAM modulation at SNR = 35 dB over Vehicular A channel.



Figure 5.7 Effective throughput of OFDMA UL system with 64QAM modulation and rate 1/2 convolution coding, at SNR = 35 dB over Vehicular A channel.
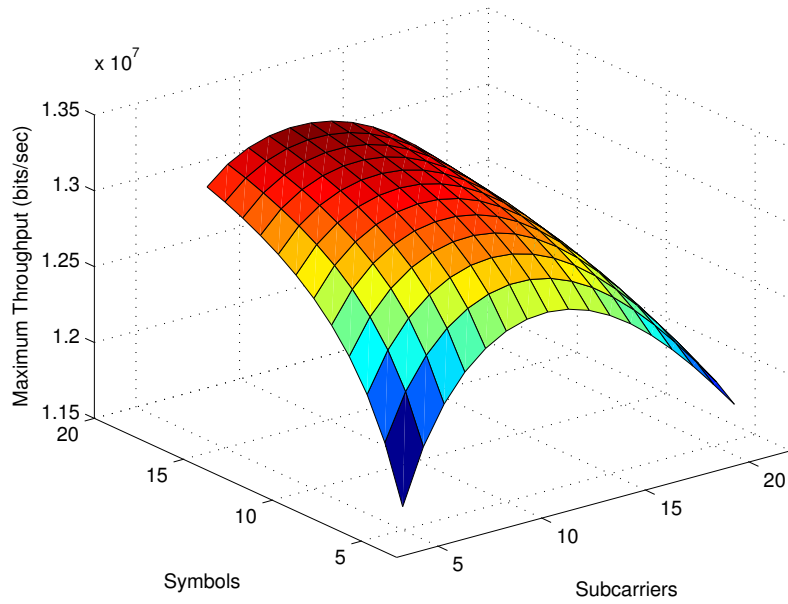
Figure 5.8  Maximum throughput of OFDMA UL system with QPSK modulation at SNR = 15 dB over Pedestrian B channel.
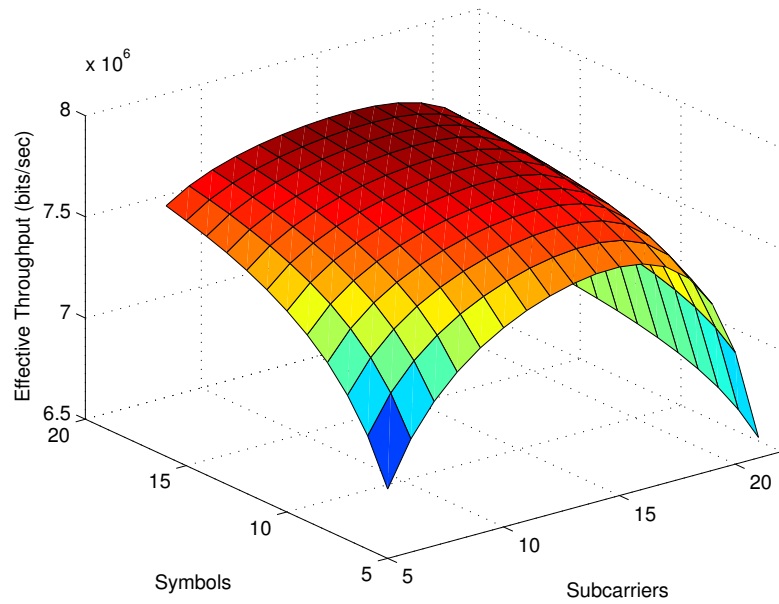


Figure 5.9  Effective throughput of OFDMA UL system with QPSK modulation and rate 1/2 convolution coding, at SNR = 15 dB over Pedestrian B channel.
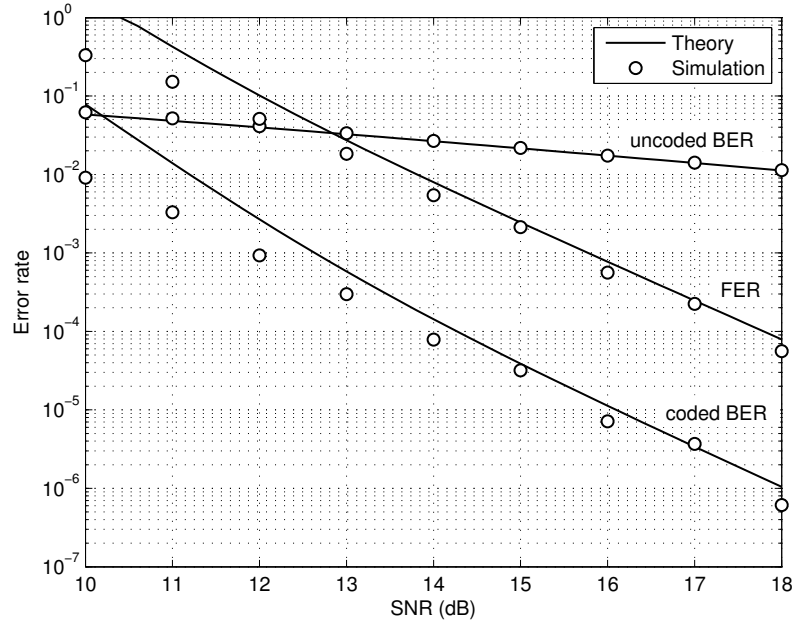
Figure 5.10  Uncoded BER, coded BER, and FER of OFDMA UL system with QPSK modulation over Pedestrian B channel where $n_t = 3$ and $k_t = 4$.

$(n_t = 3, k_t = 4)$ and $(n_t = 9, k_t = 12)$, respectively. Theoretical values for the uncoded BER as well as upper bounds for the coded BER and the FER are included for reference. The theoretical and simulated values for the uncoded BER are matching well. The upper bounds converges with simulated results at higher SNR values.

Finally, simulation results of the effective throughputs for both system profiles and both considered tile dimensions are shown in Fig. 5.12 and Fig. 5.13. Due to the use of upper bounds for the FER, the theoretical results for the effective throughput act as lower bounds for simulated values. The lower bounds converge with simulated results at higher SNR values. The results show that a significant increase in the system throughput (around 40% increase) can be achieved by carefully choosing the used tile dimensions.

## 5.7    Conclusion

In this chapter, channel estimation in OFDMA UL systems over time-varying multipath Rayleigh fading channels is considered. Tile-based channel estimation is assumed with no knowledge of multiple user channel statistics such as Doppler and delay spreads. Approximate expressions of
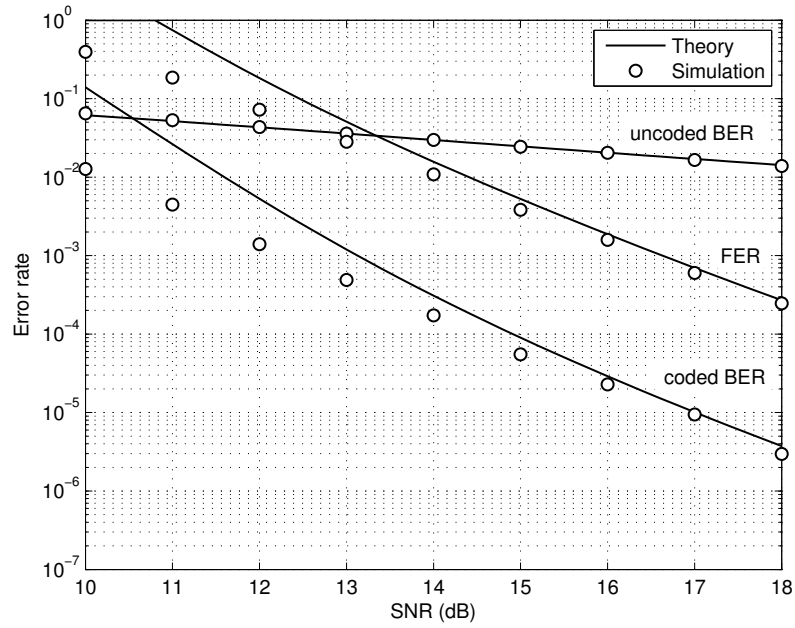
Figure 5.11  Uncoded BER, coded BER, and FER of OFDMA UL system with QPSK modulation over Pedestrian B channel where $n_t = 9$ and $k_t = 12$.
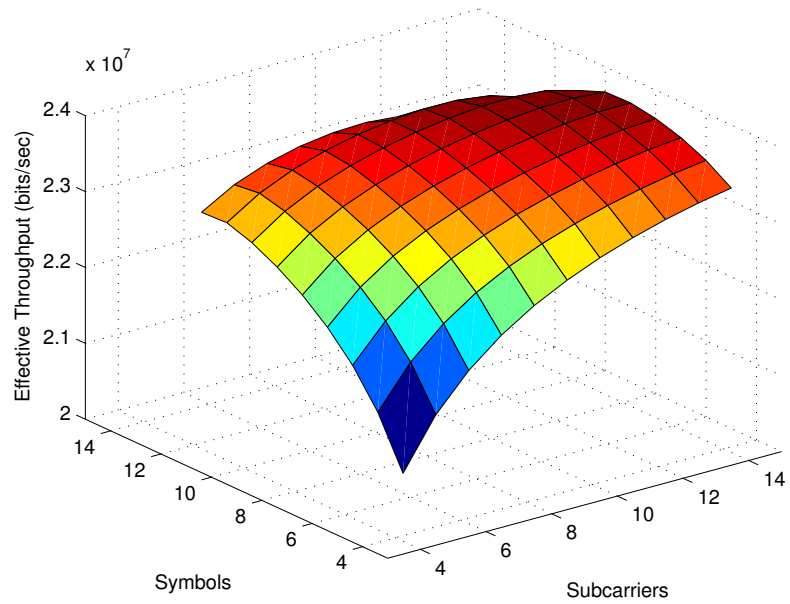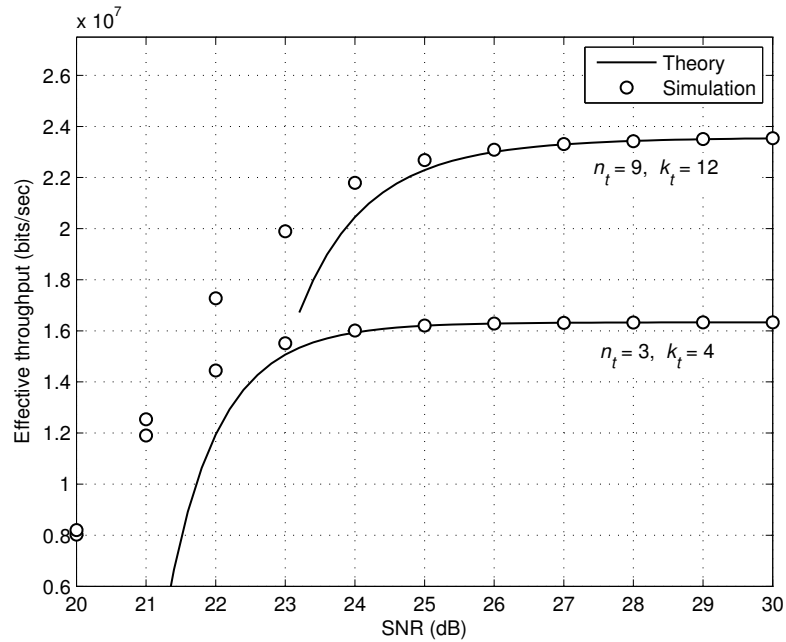


Figure 5.12  Effective throughput of OFDMA UL system with 64QAM modulation and rate 1/2 convolution coding over Vehicular A channel.
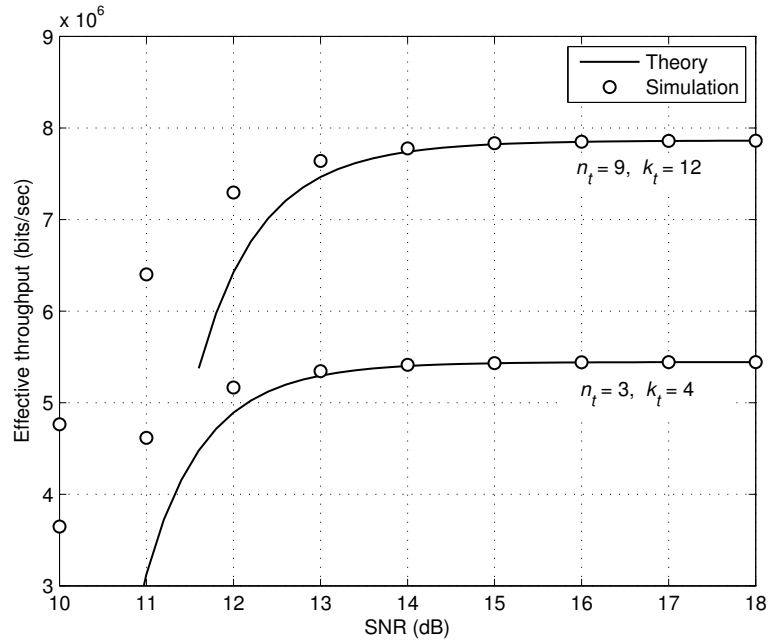
Figure 5.13  Effective throughput of OFDMA UL system with QPSK modulation and rate 1/2 convolution coding over Pedestrian B channel.

the BER for QPSK and QAM signals with channel estimation errors are derived when bilinear interpolation is used for channel estimation. Using BER theoretical expressions, the optimum tile dimensions (or optimum pilot insertion rate) in the time-frequency grid are investigated. Both analytical and simulated results show that careful choice of the tile dimensions can significantly increase the system throughput (up to 40% in some cases).

# CHAPTER 6

# IQ IMBALANCE CORRECTION FOR OFDMA UPLINK SYSTEMS

## 6.1   Introduction

The direct conversion receiver is an attractive architecture for the physical layer (PHY) of orthogonal frequency division multiple access (OFDMA) systems since it avoids costly intermediate frequency (IF) filters, reduces power consumption, and allows for easier integration than superheterodyne structure [17]. However, direct conversion receivers cause more distortions to the baseband signal due to the imbalance between the inphase (I) and quadrature (Q) branches. The IQ imbalance results in a degradation in the system performance. This drawback of direct conversion receivers becomes more significant with orthogonal frequency division multiplexing (OFDM) systems as they are known to be sensitive to receiver front-end non-idealities [18]. Thus, there is a need for methods to nullify or reduce the IQ distortions.

Several techniques have been proposed to reduce the degradation caused by IQ imbalance in OFDM-based systems [119]. In [120–122], the IQ imbalance caused by the receiver front-end is investigated. The combined effects of IQ imbalance at the transmitter and receiver front-ends is investigated in [123–126]. An interesting approach that uses the influence of IQ imbalance to obtain diversity gain is proposed in [127].

In all of the above, the effects of IQ imbalance on multiuser OFDM systems are not considered. In OFDMA-uplink (UL) systems, IQ imbalance problem becomes more complicated. First, the non-idealities in multiple user front-ends are expected to be different. Second, the total IQ imbalance effects on OFDMA systems results in multiuser interference (MUI) as opposed to inter-carrier interference (ICI) in OFDM systems. In addition, in OFDMA-UL systems, preambles are not used for channel estimation. Instead, the channel is divided into subchannels -that can be assigned to users- with dedicated pilots for each subchannel. Without preambles, many of proposed algorithms above are inapplicable.

In this chapter, we consider the effect of IQ imbalance on the OFDMA-UL system. The received signal as a function of multiuser transmitted signals, IQ parameters, and communication channels is mathematically formulated. This signal model is then used to investigated methods to estimate and equalized both the multiuser channels and IQ distortions. A novel pilot pattern is designed which is then used by two proposed methods to efficiently mitigate signal distortions caused by the combined effect of multipath dispersive channels and IQ imbalances of multiple users. The proposed methods are shown to significantly reduce the impact of IQ imbalance on OFDMA signals.

## 6.2 System Model

We consider an OFDMA-UL system employing $N$ subcarriers per symbol. The DC subcarrier and guard subcarriers are disabled. The remaining subcarriers $N_u$ are used for data transmission with equal number of subcarriers on each side of the DC subcarrier. The above assumptions are common for most practical implementations of OFDMA systems. Used subcarriers are divided into $M$ subchannels, the indexes of each subchannel $m$ is in the set $\mathcal{M}_m$. Subchannels can then be assigned to multiple users. Every user $m$ generates a sequence of modulated symbols $x_m$ which are mapped to subcarriers of assigned subchannels. The signal in then fed to an inverse fast Fourier transform (IFFT) block and the cyclic prefix (CP) is added. The $n$th sample of the transmitted symbol of user $m$ is,

$$s_m(n) = \sum_{k \in \mathcal{M}_m} x_m(k) \exp\left(\frac{\jmath 2\pi nk}{N}\right), \qquad -N_g \leq n \leq N-1 \tag{6.1}$$

where $N_g + N$ is the total number of samples per symbol and $N_g$ is the size of the CP.

The IQ imbalance distorts the ideal Tx signal as follows [121],

$$\widetilde{s}_m = \alpha_m s_m + \beta_m s_m^*, \tag{6.2}$$

where $(\cdot)^*$ is the complex conjugate, and $\alpha_m$ and $\beta_m$ are related to the IQ imbalance as follows,

$$\alpha_m = \cos \Delta\phi_m + j\epsilon_m \sin \Delta\phi_m, \tag{6.3a}$$

$$\beta_m = \epsilon_m \cos \Delta\phi_m - j \sin \Delta\phi_m, \tag{6.3b}$$

where $\epsilon_m$ and $\Delta\phi_m$ are the gain imbalance and the phase mismatch, respectively. For the remainder of the chapter, $\alpha_m$ and $\beta_m$ are referred to as the IQ parameters. At the receiver, the sum of all transmitted user signals is received,

$$y(n) = \sum_{m=1}^{K} r_m(n) + w(n), \tag{6.4}$$

where $K$ is the total number of users in the system at the current symbol, $w(n)$ is thermal noise, and $r_m$ is the received signal of the $m$th user.

$$r_m(n) = \sum_{i} s_m(i) h_m(n - i), \tag{6.5}$$

where $h_m(n)$ is the sampled channel impulse response (CIR) of the $m$th user at time $t = nT_S$ and $T_S$ is the sampling time of received signal. In order to eliminate any interference between adjacent OFDMA symbols, i.e. inter-symbol interference (ISI), the CP size, $N_g$ is chosen such that $N_g T_S$ is larger that the maximum delay spread of the channel for all users. At the receiver, the CP is removed and the signal is fed to an $N$-point fast Fourier transform (FFT) block. The output of the FFT can be expressed as,

$$Y(k) = \sum_{n=0}^{N-1} y(n) \exp\left(-\frac{\jmath 2\pi nk}{N}\right), \qquad 0 \le k \le N - 1, \tag{6.6}$$

where $k$ is the subcarrier index. If received signal is ISI free, then received subcarriers of user $u$ are,

$$Y(k) = \alpha_u H_u(k) x_u(k) + \beta_v H_v(k) x_v^*(\bar{k}) + \eta(k), \qquad k \in \mathcal{M}_u \tag{6.7}$$

where $\eta(k)$ is modeled as additive white Gaussian noise (AWGN) with zero mean and variance $N_0/2$, $\bar{k}$ is the mirrored subcarrier of $k$ over the DC subcarrier, $v \in \{1, \ldots, K\}$ is the index of user which subcarrier $\bar{k}$ is assigned to, and $H_m$ is the $m$th user channel frequency response (CFR). If $H_u$ is perfectly known to the receiver, then the equalized signal of user $u$ is,

$$\widetilde{Y}(k) = \underbrace{\alpha_u x_u(k)}_{\text{desired signal}} + \underbrace{\beta_v \frac{H_v(k)}{H_u(k)} x_v^*(\bar{k}) + \frac{\eta(k)}{H_u(k)}}_{\text{interference}}, \qquad k \in \mathcal{M}_u. \tag{6.8}$$

It can be seen from the above equation that the first term is the desired signal with an attenuation $\alpha_u$, the second term represents the ICI for $v = u$ or the MUI for $v \neq u$, and the last term represents the noise. The interference term can be canceled by jointly detecting $x_u(k)$ and $x_v^*(\bar{k})$. In such a case, the receiver needs to estimate $H_m$ for $m = 1, \ldots, K$. The pilot subcarriers $N_p$ are divided among users/subchannels.

In an IQ distortion free OFDMA system, the system estimates the channel response at $N_u$ subcarriers using $N_p$ pilots. However, for a system suffering from IQ distortion, every user $m$ transmitting over subcarriers $k \in \mathcal{M}_m$ causes interference at $\bar{k}$ as well, as shown in (6.7). This means that in worst case scenario, where $\bar{k} \notin \mathcal{M}_m \forall k$, the user effectively transmits over twice the number of assigned subcarriers. Receiver then needs to estimate two user channels per subcarrier or a total of $2N_u$ channel responses using the same number of pilots. In addition, estimation of $K$ sets of IQ parameters $\{\alpha_m, \beta_m\}$ is needed to fully cancel the interference introduced by image carriers as shown in (6.8).

## 6.3 Channel/IQ Equalization

In this section, equalization of the channel effects and IQ distortions in the received signal is discussed. First, the UL frame structure needs to be introduced. In OFDMA systems, used subcarriers are divided into smaller units, also known as tiles or chunks, which represent the minimum allocation unit (see Fig. 6.1). The tiles are then assigned to subchannels either randomly or depending on user channels. The overall received UL frame is a sum of all current user signals, which are transmitted over different communication channels. The use of sophisticated channel estimation algorithms at the receiver can significantly increase the system complexity and processing delay. Therefore, pilots are assigned within each tile. The receiver can then perform channel estimation on each tile individually using low complexity channel estimation techniques such as bilinear interpolation.

An example of how the UL frame is divided into tiles is shown in Fig. 6.1. Used subcarriers are divided into $Q$ tiles, with equal number of tiles on each side of the DC subcarrier. This means that for every tile $q$, there is an image tile $\bar{q} = Q - q + 1$. Three different tile structures are shown in the figure, where one tile dimensions are three symbols by four subcarriers. The tile bandwidth, $B_{\text{tile}} = 3\Delta f$, where $\Delta f$ is the subcarrier spacing, and the tile duration, $T_{\text{tile}} = 3T_{\text{sym}}$, where $T_{\text{sym}} = (N + N_g)T_S$ is the symbol duration. For the remainder of this chapter, Tile C structure is used. Note that a
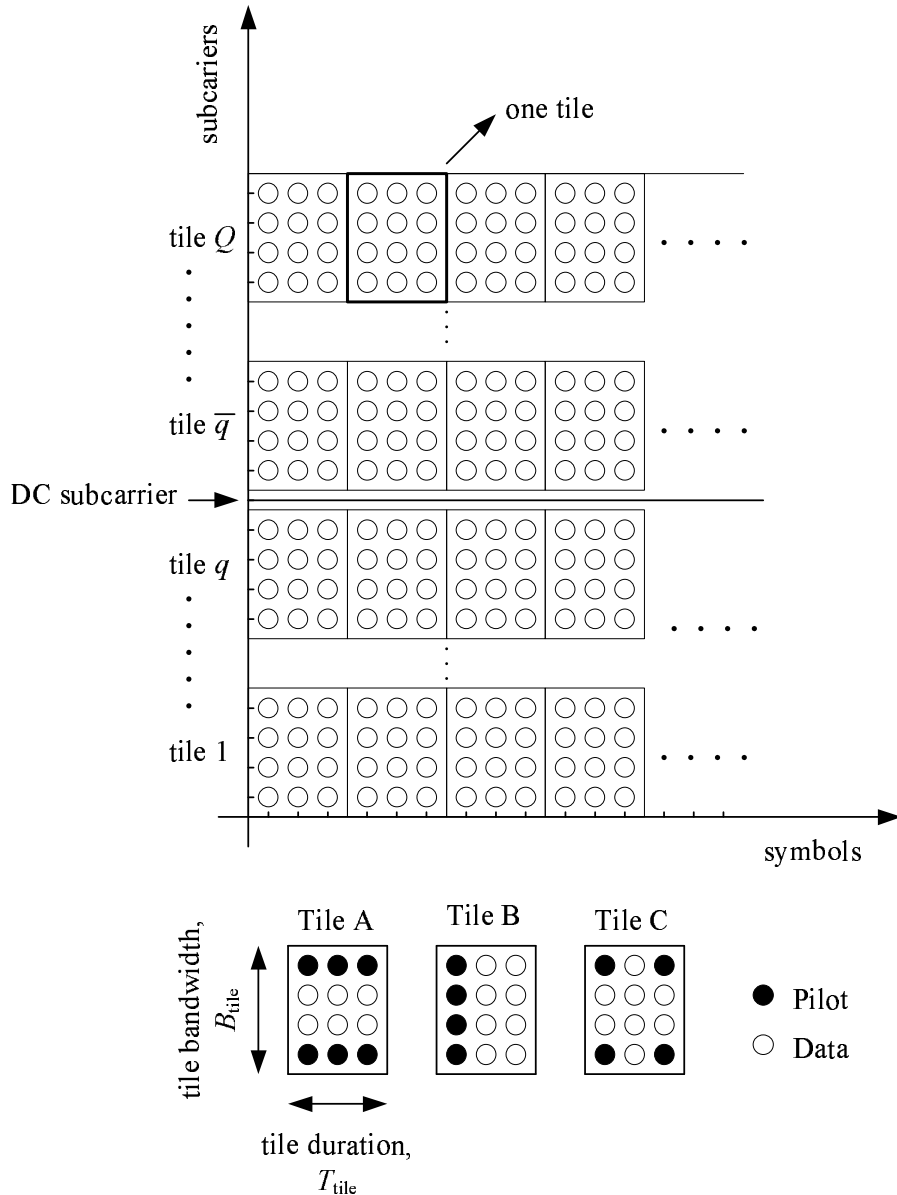
Figure 6.1  UL frame structure and subcarrier mapping to tiles.

similar frame structure is employed by the mobile worldwide interoperability for microwave access (WiMAX) standard [9].

In a system with no IQ distortion, the receiver would consider each tile independently. The four pilots within a tile would be used to obtain least squares (LS) estimates. The LS estimates are then used to estimate the channel at the remaining data subcarriers using bilinear interpolation. If the received signal is distorted by the IQ imbalance, the receiver processes each tile $q$ along with its
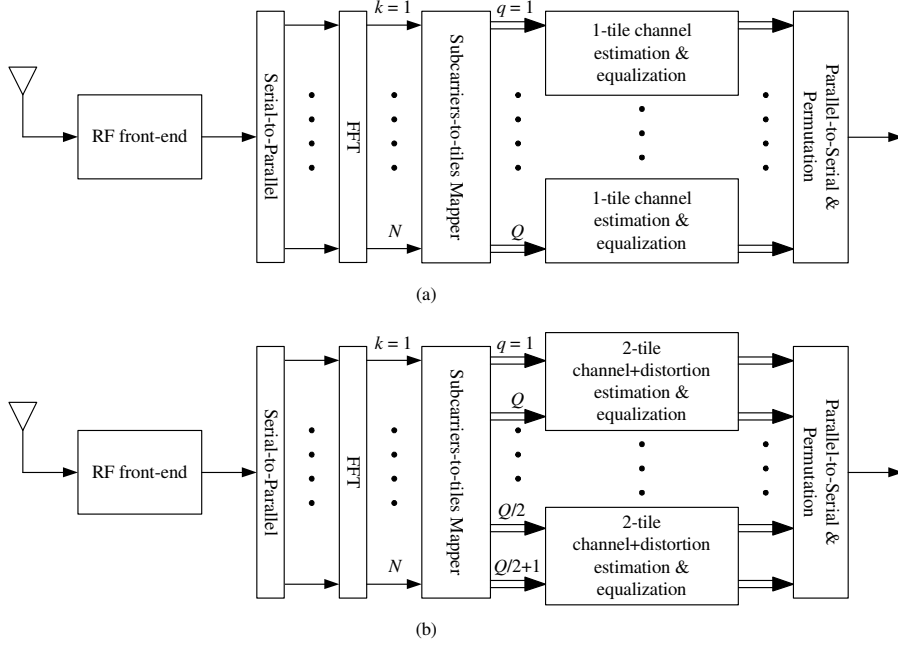
Figure 6.2 Receiver block diagram of (a) conventional OFDMA-UL system, and (b) An OFDMA-UL system for signals with IQ distortion.

image tile $\bar{q}$. Simplified block diagrams of both a conventional OFDMA receiver and an IQ distorted OFDMA receiver are depicted in Fig. 6.2. Without the loss of generality, we assume that tile $q$ is assigned to user $u$ and tile $\bar{q}$ is assigned to user $v \neq u$. The received subcarriers of tile $q$ and $\bar{q}$ are,

$$y(i,j) = \alpha_u H_u(i,j)x(i,j) + \beta_v H_v(i,j)x^*(i,\bar{j}), \qquad y(i,j) \in q, \tag{6.9a}$$

$$y(i,\bar{j}) = \alpha_v H_v(i,\bar{j})x(i,\bar{j}) + \beta_u H_u(i,\bar{j})x^*(i,j), \qquad y(i,\bar{j}) \in \bar{q}, \tag{6.9b}$$

where the index $(i,j)$ represents the $i$th OFDMA symbol and $j$th subcarrier as shown in Fig. 6.3. Using (6.9a) and (6.9b), the received signals as function of transmitted signals, users' CFR, and users' IQ parameters is expressed as,

$$\begin{bmatrix} y(i,j) \\ y^*(i,\bar{j}) \end{bmatrix} = \underbrace{\begin{bmatrix} \alpha_u H_u(i,j) & \beta_v H_v(i,j) \\ \beta_u^* H_u^*(i,\bar{j}) & \alpha_v^* H_v^*(i,\bar{j}) \end{bmatrix}}_{\mathbf{Z}(i,j)} \begin{bmatrix} x(i,j) \\ x^*(i,\bar{j}) \end{bmatrix} \tag{6.10}$$

To jointly detect transmitted subcarrier $x(i,j)$ and its image $x(i,\bar{j})$, the receiver needs to estimate eight unknowns (four CFR samples and four IQ parameters), if the estimation of the channel re-

107
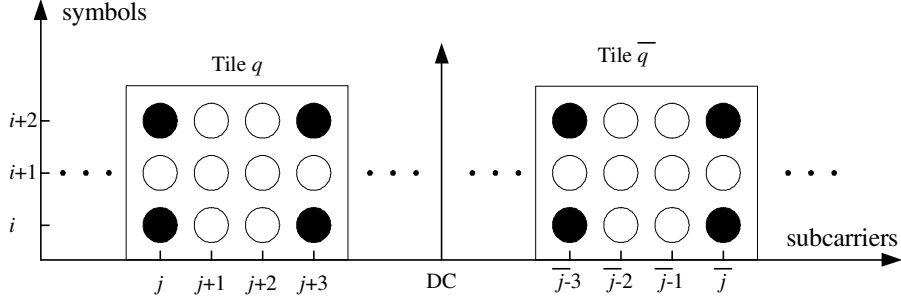
Figure 6.3 Subcarrier indexing of a tile pair.

sponses and IQ imbalances are done separately. Alternatively, the receiver can estimate only the four unknowns of $\mathbf{Z}(i, j)$, if the effects of the channels and IQ imbalances are estimated jointly. However, in this case, the receiver does not have an estimate of the IQ distortion introduced by each user. The LS estimation of transmitted signal is given by,

$$\begin{bmatrix} x(i,j) \\ x^*(i,\bar{j}) \end{bmatrix} = \mathbf{Z}^{-1}(i,j) \begin{bmatrix} y(i,j) \\ y^*(i,\bar{j}) \end{bmatrix} \tag{6.11}$$

## 6.4 Channel/IQ Estimation

Let's assume that $x(i, j)$, $x(i, \bar{j})$, $x(i, j+3)$, and $x(i, \bar{j}-3)$ are pilots as shown in Fig. 6.3. Knowing the value of the two pilots in (6.10) is not sufficient to estimate the channel/IQ parameters matrix $\mathbf{Z}(i, j)$. Two methods are proposed to solve this problem. The first proposed method, Method A, assumes that the tile bandwidth, $B_{\text{tile}}$ is less than the channel coherence bandwidth, $B_C$, for all users. In this case, the CFR over the tile band is almost constant, i.e. $H_m(i, j) \approx H_m(i, j + 3)$ for $m \in \{1, \ldots, K\}$. Based on the above assumption, the second pair of pilots at symbol $i$ and subcarriers $\{j + 3, \bar{j} - 3\}$ can be represented as,

$$\begin{bmatrix} y(i, j + 3) \\ y^*(i, \bar{j} - 3) \end{bmatrix} = \begin{bmatrix} \alpha_u Hu(i, j + 3) & \beta_v H_v(i, j + 3) \\ \beta_u^* H_u^*(i, \bar{j} - 3) & \alpha_v^* H_v^*(i, \bar{j} - 3) \end{bmatrix} \begin{bmatrix} x(i, j + 3) \\ x^*(i, \bar{j} - 3) \end{bmatrix}$$

$$\approx \mathbf{Z}(i, j) \begin{bmatrix} x(i, j + 3) \\ x^*(i, \bar{j} - 3) \end{bmatrix} \tag{6.12}$$

108

Using (6.10) and (6.12), the system can solve for $\mathbf{Z}(i,j)$. The same procedure is then repeated for the two pilot pairs at symbol $i+2$ to obtain $\mathbf{Z}(i+2,j)$. To insure that this set of equations has a unique solution, pilot vector pairs are chosen to be orthogonal [128, 129] such that,

$$\begin{bmatrix} x(i,j) & x^*(i,\bar{j}) \end{bmatrix} \begin{bmatrix} x(i,j+3) \\ x^*(i,\bar{j}-3) \end{bmatrix} = 0, \tag{6.13a}$$

$$\begin{bmatrix} x(i+2,j) & x^*(i+2,\bar{j}) \end{bmatrix} \begin{bmatrix} x(i+2,j+3) \\ x^*(i+2,\bar{j}-3) \end{bmatrix} = 0. \tag{6.13b}$$

Next, $\mathbf{Z}(i+1,j)$ can be estimated using 1-D interpolation between $\mathbf{Z}(i,j)$ and $\mathbf{Z}(i+2,j)$. Finally, using (6.11), $\{\mathbf{Z}(i,j), \mathbf{Z}(i+1,j), \mathbf{Z}(i+2,j)\}$ are used to estimate the remaining data subcarriers at symbols $\{i, i+1, i+2\}$, in this order. The receiver repeats this process for each pair of tiles ($Q/2$ times).

The second proposed method, Method B, assumes that the tile duration, $T_{\text{tile}}$ is less than the coherence time of the channel, $T_C$, for all users. In this case, $H_m(i,j) \approx H_m(i+2,j)$ for $m \in \{1,\ldots,K\}$. Based on the above assumption, the second pair of pilots (to be coupled with (6.10)) at symbols $\{i, i+2\}$ and subcarriers $\{j, \bar{j}\}$ can be represented as,

$$\begin{bmatrix} y(i+2,j) \\ y^*(i+2,\bar{j}) \end{bmatrix} \approx \mathbf{Z}(i,j) \begin{bmatrix} x(i+2,j) \\ x^*(i+2,\bar{j}) \end{bmatrix} \tag{6.14}$$

Using (6.10) and (6.14), the system solves for $\mathbf{Z}(i,j)$. Similarly, the pilot pairs at subcarriers $\{j+3, \bar{j}-3\}$ can be used to solve for $\mathbf{Z}(i,j+3)$. Next, the receiver uses linear interpolation to calculate $\{\mathbf{Z}(i,j+1), \mathbf{Z}(i,j+2)\}$ from $\{\mathbf{Z}(i,j), \mathbf{Z}(i,j+3)\}$. Finally, the above values of $\mathbf{Z}$ are used to estimate the remaining data subcarriers in both tiles. The procedure is then repeated for each pair of tiles. The pilots orthogonality is achieved as follows,

$$\begin{bmatrix} x(i,j) & x^*(i,\bar{j}) \end{bmatrix} \begin{bmatrix} x(i+2,j) \\ x^*(i+2,\bar{j}) \end{bmatrix} = 0, \tag{6.15a}$$

$$\begin{bmatrix} x(i,j+3) & x^*(i,\bar{j}-3) \end{bmatrix} \begin{bmatrix} x(i+2,j+3) \\ x^*(i+2,\bar{j}-3) \end{bmatrix} = 0. \tag{6.15b}$$

Table 6.1  Simulation parameters for a typical OFDMA UL system II.

| Parameter | Value |
|---|---|
| Carrier frequency | 2.5 GHz |
| FFT size, $N$ | 1024 |
| CP size, $N_g$ | 128 |
| Number of used subcarriers, $N_u$ | 840 |
| Sampling frequency, $1/T_S$ | 11.2 MHz |
| Number of tiles, $Q$ | 210 |
| Number of subchannels, $M$ | 35 |

To enable the receiver to use either methods, we propose to use the following pilot pattern, which satisfies the conditions in (6.13a), (6.13b), (6.15a), and (6.15b).

$$\begin{bmatrix} x(i,j) & x(i,j+3) \\ x(i+2,j) & x(i+2,j+3) \end{bmatrix} = \begin{bmatrix} -d_2^* & d_1 \\ d_1 & d_2^* \end{bmatrix}, \tag{6.16a}$$

$$\begin{bmatrix} x(i,\bar{j}-3) & x(i,\bar{j}) \\ x(i+2,\bar{j}-3) & x(i+2,\bar{j}) \end{bmatrix} = \begin{bmatrix} d_2 & d_1^* \\ -d_1^* & d_2 \end{bmatrix}, \tag{6.16b}$$

where $d_1$ and $d_2$ are arbitrary symbols that belong to the modulation symbol set used for pilots. The above pilot pattern achieves orthogonality between pilot pairs in both the subcarrier dimension and the symbol dimension. Thus, the receiver can improve the system performance by adaptively using either Method A or Method B depending on the user channel conditions (i.e. delay spread and Doppler spread) or by using both methods and choosing the estimates with the least error vector magnitude (EVM) values.

## 6.5   Simulation Results

A system based on the WiMAX standard [9] is considered. Typical simulation parameters are chosen based on [90] and are summarized in Table 6.1. We assume three users are transmitting in all UL frames. The available 35 subchannels are divided among users with 12, 12, and 11 subchannels assigned to user 1, user 2, and user 3, respectively. Subchannels assigned to UL users are randomized for every frame. The modulation used for data subcarriers is quadrature phase shift keying (QPSK), and for pilots, binary phase shift keying (BPSK) is used ($d_1 = d_2 = 1$). The system is tested over three channels based on the ITU channel models [91]: Indoor A, Pedestrian B, and Vehicular A, with Doppler spread of 0 Hz (0 km/h), 6.9 Hz (3 km/h), and 138.9 Hz (60 km/h), respectively. It

is assumed that the channel is independent between different frames and between different users. The receiver processes each frame individually. At the receiver, the uncoded bit error rate (BER) is measured and averaged over all users.

For all generated simulations, it is first assumed that there are no IQ imbalances introduced to the signal. The receiver uses all pilots per tile to estimate and equalize only the channel effects using 2-D linear interpolation technique. This case is labeled as "Ideal IQ". Next, the UL user signals are distorted by IQ imbalances. The IQ gain imbalance and phase mismatch of user 1, user 2, and user 3 are $\{0.2, 2°\}$, $\{0.35, 5°\}$, and $\{0.5, 8°\}$, respectively. The uncoded BER is measured while the receiver operates assuming no IQ imbalance is present. The results are labeled as "IQ Imbalance/ No compensation". Finally, Method A and Method B are used to estimate and equalize the combined channel and IQ distortions. The results are shown in Fig. 6.4, Fig. 6.5, and Fig. 6.6. In all figures, the system performance degrades significantly when the receiver ignores the IQ distortions to the signal. At a signal-to-noise ratio (SNR) of $35\,\mathrm{dB}$, the IQ distortions increase the BER by two orders of magnitude. On the other hand, proposed methods manage to reduce the BER considerably. For the results over the Pedestrian B channel in Fig. 6.4, the delay spread is high while the Doppler spread is low. As a result, Method B outperforms Method A, since it assumes low Doppler spreading. Method B significantly reduces the IQ distortion effect on the signal. The loss is around $2\,\mathrm{dB}$ from the ideal IQ case at $\mathrm{BER} = 10^{-3}$. For the results over the Vehicular A channel in Fig. 6.5, both delay spread and Doppler spread are high. In this case, Method A slightly outperforms Method B, since its approximation is more accurate. While both methods A and B improve the BER significantly, the loss from the ideal IQ case is considerable. Under such highly selective channels and with IQ distortions, the system can choose to reduce signal bandwidth which leads to an improved performance of Method A. Finally, for the results over the Indoor A channel in Fig. 6.6, both delay spread and Doppler spread are low. As expected in this case, both methods A and B perform very well. The BER degradation due to the IQ distortions is recovered with around $2.5\,\mathrm{dB}$ loss from the ideal IQ case at $\mathrm{BER} = 10^{-3}$. Note that there is a loss from the ideal IQ case even in channels with low Doppler spread and delay spread. This loss is a result of the noise averaging effect. In ideal case, the estimation of channel response, which is almost constant over slot bandwidth and/or slot duration, is averaged by the bilinear interpolation over twice the number of pilots compared to proposed methods. A receiver capable of detecting the presence of IQ distortions
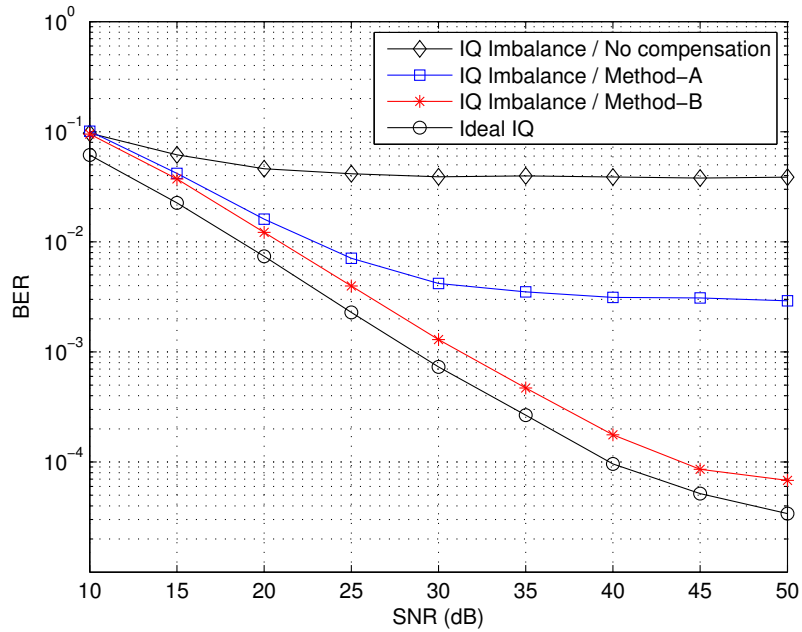
Figure 6.4 Average uncoded BER of QPSK signals received over Pedestrian B channel and with IQ impairments.

can avoid this loss by switching to conventional channel estimator if received signal is free from IQ distortions.

## 6.6  Conclusion

In this chapter, a model for OFDMA-UL systems with IQ impairments is introduced. The received signal as a function of transmitted signals, IQ parameters, and communication channels is mathematically formulated. The signal model is used to design a novel two-dimensional orthogonal pilot pattern. Two low complexity methods are proposed to equalize and detect IQ distorted signals using designed pilot pattern. Proposed methods were shown to improve the system performance significantly over conventional detection methods for signals suffering from multiple user IQ distortions.
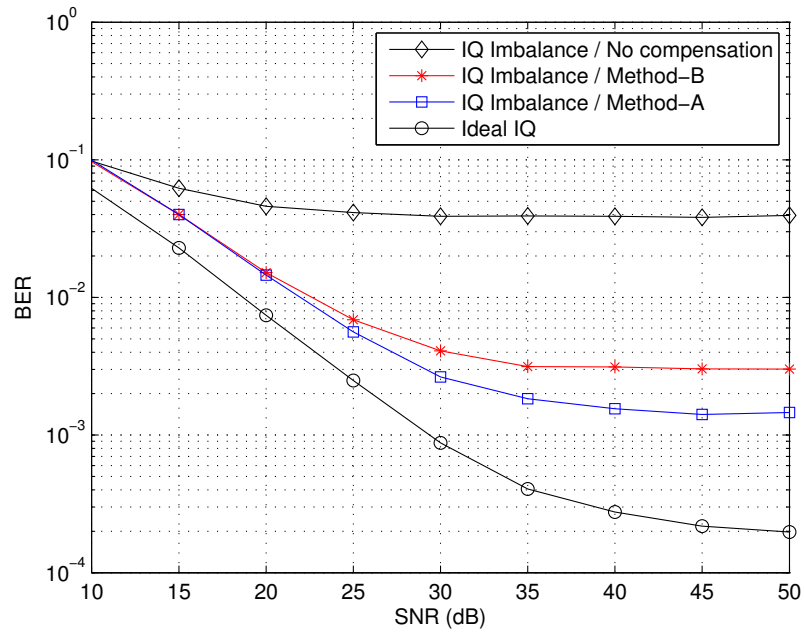
Figure 6.5  Average uncoded BER of QPSK signals received over Vehicular A channel and with IQ impairments.
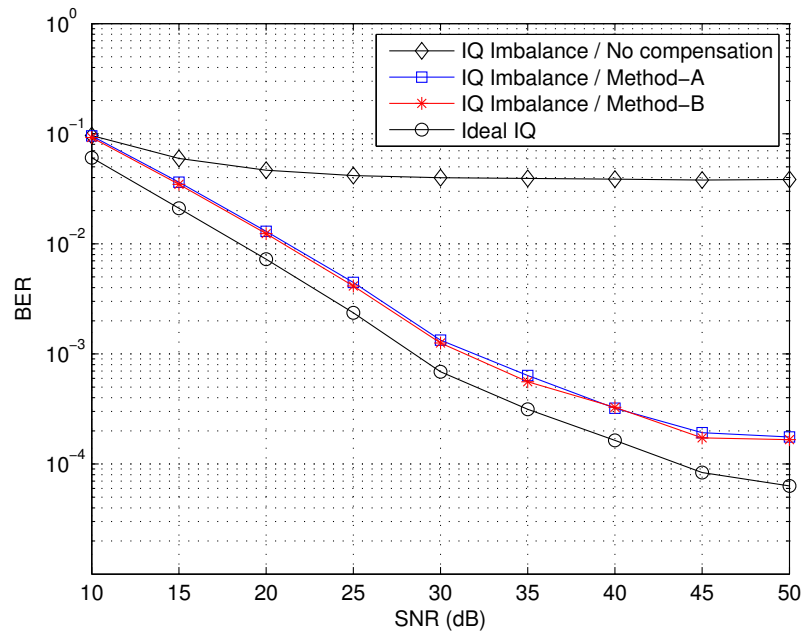


Figure 6.6  Average uncoded BER of QPSK signals received over Indoor A channel and with IQ impairments.

# CHAPTER 7

# ERROR VECTOR MAGNITUDE BASED SNR ESTIMATION IN BLIND RECEIVERS

## 7.1  Introduction

In wireless communication systems, complex digital modulation schemes are used for meeting stringent spectral and signal-to-noise ratio (SNR) requirements [130]. In such systems, the overall quality of the transmission and reception are determined by various baseband and RF system specifications. Among these, bit error rate (BER) and error vector magnitude (EVM) are two primary specifications that determine the performance of the wireless system in terms of transmitted and received symbols corresponding to a given digital modulation scheme. While BER is useful as a conceptual figure of merit, it suffers from a number of practical drawbacks that compromise its value as a standard test in manufacturing or maintenance [131]. Calculation of BER requires dedicated equipment, thus increasing the cost and complexity of the test system. In addition, it has limited diagnostic value. If the BER value measured exceeds accepted limits, it offers no clue regarding the probable cause or source of signal degradation.

For measurements and testing devices, EVM is a viable alternative test method when looking for a figure of merit in non-regenerative transmission links. EVM can offer insightful information on the various transmitter imperfections, including carrier leakage, IQ mismatch, nonlinearity, local oscillator (LO) phase noise and frequency error [19]. Requirements on EVM are already part of most wireless communications standards such as the IEEE 802.11a-1999 standard [6] and the IEEE 802.16e-2005 worldwide interoperability for microwave access (WiMAX) standard [9]. EVM measurements and simulations can be found in [131–133]. The impact of IQ imbalance, as well as LO phase noise on EVM is investigated in [134] and EVM as a function of these impairments is derived. This work has been expanded in [19], where the effects of carrier leakage, nonlinearity and LO frequency error on EVM are considered.

Relating EVM to other performance metrics such as SNR and BER is an important research topic, as well [135, 136]. These relations are quite useful since it allows the reuse of already available EVM measurements to infer more information regarding the communication system. Moreover, using EVM measurements could reduce the system complexity by getting rid of the need to have separate modules to estimate or measure other metrics. When relating EVM to SNR, one assumption that has been made is that the EVM is measured using known data sequences (e.g. preambles or pilots) or that the SNR is high enough that symbol errors are negligible [135, 136]. Another assumption was that one or two system imperfections are dominant; the remaining imperfections are modeled as Gaussian noise [19, 134]. However, the above analyses did not consider measuring EVM blindly for low SNR levels where symbol errors are possible. With new technologies for spectrum detection and utilization [4, 92], there is a need to detect signals at medium to very low SNR values. The signal quality metrics including EVM and SNR are possibly measured over unknown data sequences (nondata-aided) as well.

In this chapter, we consider the relation between EVM and SNR for nondata-aided receivers. The signal degradation sources are modeled as additive white Gaussian noise (AWGN), Rayleigh fading channels, and IQ imbalances. It is shown that for higher modulation orders or low SNR values, using previously made assumptions leads to inaccurate results. The exact value of EVM for nondata-aided symbol detection is derived and expressed in terms of the SNR. The derived relations are then used to estimate the SNR using measured EVM values for QAM and PAM signals and over limited number of symbols. The results show that SNR can be accurately estimated using measured EVM even when symbol sequences are unknown, and the SNR level is low.

The remainder of this chapter is organized as follows. In Section 7.2, the signal model and assumptions are presented. The EVM is defined and mathematically expressed in Section 7.3. Relation between EVM and SNR for data-aided receivers and its application to nondata-aided receivers are discussed in Section 7.4. In Section 7.5, the EVM relation to SNR is derived for QAM and PAM signals. Computer-based simulations are performed to examine the correctness of derived expressions; those results are discussed in Section 7.6. Finally, concluding remarks are given in Section 7.7.

## 7.2 Signal Model

We assume a digital baseband signal $x$ is transmitted over a communication channel with a channel impulse response (CIR) $h$. In addition, the received signal is corrupted by complex AWGN, $w$. Thus, the $n$th received baseband symbol can be expressed as follows,

$$r(n) = \sum_{l=-\infty}^{\infty} x(l)h(n-l) + w(n). \tag{7.1}$$

Note that $h$ can also include the effects of transmitter/receiver filters in addition to the channel. If a modulation order of $M$ is used, then $x(n) \in \{S_1, S_2, ...S_M\}$. Throughout the chapter, it is assumed that all symbols are sent with equal probability.

The receiver, usually a measurement instrument such as vector signal analyzers (VSA), acquires the signal, performs synchronization, and channel estimation and equalization. The detected signal can be represented by,

$$y(n) = g(n)x(n) + \eta(n), \tag{7.2}$$

where $g(n)$ and $\eta(n)$ represent the multiplicative and additive impairments to detected signal. The multiplicative impairments can be a result of channel estimation errors or IQ imbalances, for example. The additive impairments is usually due to thermal noise and are modeled as an independent and identically distributed (i.i.d.) complex AWGN samples with power spectral density (PSD) of $N_0/2$.

In this chapter, three models are considered for the detected signal. The first case is when the additive noise is the dominant degradation source and $g(n) \approx 1$. The second case is for signals detection over Rayleigh fading channels. Finally, the third case is for signals detection with other impairments such as channel estimation errors, interference, or IQ imbalances.

## 7.3 Error Vector Magnitude

EVM can be defined as the root-mean-squared (RMS) value of the difference between a collection of measured symbols and ideal symbols [136]. The value of the EVM is averaged over typically a large number of symbols and it is often expressed as a percentage (%) or in dB. The EVM can be

represented as [137],

$$\text{EVM}_{\text{RMS}} = \sqrt{\frac{\frac{1}{N} \sum_{n=1}^{N} |S_r(n) - S_t(n)|^2}{P_0}},$$ (7.3)

where $N$ is the number of symbols over which the value of EVM is measured, $S_r(n)$ is the normalized received $n$th symbol which is corrupted by Gaussian noise, $S_t(n)$ is the ideal/transmitted value of the $n$th symbol $x(n)$, and $P_0$ is either the maximum normalized ideal symbol power or the average power of all symbols for the chosen modulation. For the remainder of this chapter, the latter definition of $P_0$ is used. In such case,

$$P_0 = \frac{1}{M} \sum_{m=1}^{M} |S_m|^2.$$ (7.4)

The EVM value is normalized with the average symbol energy to remove the dependency of EVM on the modulation order. In (7.3), $S_r(n)$ is the detected symbol $y(n)$ and $S_t(n)$ could be either known to the receiver (data-aided) if pilots or preambles are used to measure the EVM, or estimated from $y(n)$ (nondata-aided) if data symbols are used instead.

## 7.4   Relating EVM to SNR

Let us consider the case where the signal is only corrupted by AWGN. For data-aided EVM calculations, (7.3) is reduced to,

$$\text{EVM}_{\text{RMS}} = \sqrt{\frac{\frac{1}{N} \sum_{n=1}^{N} |\eta(n)|^2}{P_0}}.$$ (7.5)

If the EVM is measured over large values of $N$, then [135, 136, 138],

$$\text{EVM}_{\text{RMS}} \approx \sqrt{\frac{N_0}{P_0}} = \sqrt{\frac{1}{\text{SNR}}},$$ (7.6)

where $N_0/2 = \sigma_n^2$ is the noise PSD.

The above EVM-SNR relation, however, only holds for data-aided receivers. For nondata-aided receivers, the transmitted symbols are estimated and those estimates $\hat{x}(n)$ are used to measure the

117

EVM value. Thus, for low SNR values, errors are made when estimating $x(n)$. The measured EVM value in this case is expected to be less than its actual value as the symbol estimator tends to assign received symbols to their closest possible constellation point. For a BPSK signal, the symbol estimator criterion is as follows,

$$\hat{x}(n) = \begin{cases} S_1, & \text{if } y_\Re(n) > 0, \\ S_2, & \text{if } y_\Re(n) < 0, \end{cases} \tag{7.7}$$

where $y_\Re(n)$ is the real part of $y(n)$. Note that for $y_\Re(n) = 0$, $\hat{x}(n) = S_1$ or $S_2$ with equal probability. As such, errors in estimating $x(n)$, and consequently in measuring the EVM, occurs every time a constellation point passes to another point decision region. To further illustrate the effect of such errors on the EVM-SNR relation, the EVM versus SNR curves for various modulation orders are plotted in Fig. 7.1. The results are averaged over $100,000$ modulated symbols. The ideal value of EVM ($= 1/\sqrt{\text{SNR}}$) is also plotted for reference. Two observations can be drawn from this figure. First, the measured EVM values are less than the ideal EVM, as expected. Second, the measured EVM deviation from its ideal value increases with the modulation order. This is due to the fact that for higher modulation orders, and for the same SNR level, the probability of a symbol error is higher [89],

$$P_S = 1 - \left[ 2 \left( 1 - \frac{1}{\sqrt{M}} \right) Q \left( \sqrt{\frac{3}{M-1} \text{SNR}} \right) \right]^2, \tag{7.8}$$

where $P_S$ is the symbol error rate (SER), $M$ is the modulation order, $Q(v) = 1/2 \, \text{erfc}(v/\sqrt{2})$, and $\text{erfc}(\cdot)$ is the complementary error function. Note that the above equation holds for QAM signals but not for BPSK signals. Based on the above, the measured EVM for nondata-aided receivers becomes dependent on the modulation order even with the normalization in (7.3). Moreover, using the measured EVM as an indication of the SNR as in (7.6) can be misleading, especially for low SNR levels. Thus, there is a need for a more accurate EVM to SNR relation for nondata-aided receivers.
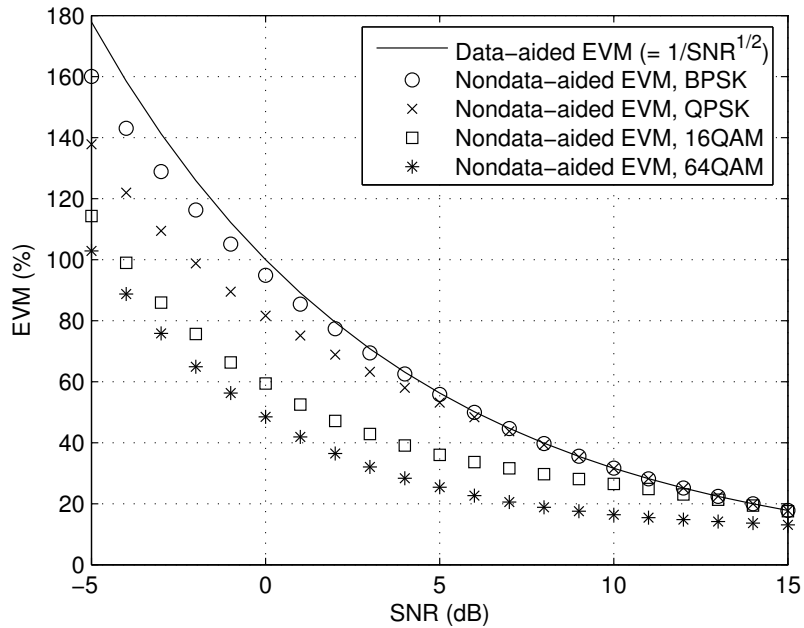
Figure 7.1 Measured versus ideal EVM measurements in nondata-aided receivers.

## 7.5 EVM-SNR for Nondata-Aided Receivers

### 7.5.1 Detection Over AWGN Channels

Consider the detected signal in (7.2) where $g(n) \approx 1$. For nondata-aided receivers, the EVM is,

$$\text{EVM}_{\text{RMS}} = \sqrt{\frac{\frac{1}{N}\sum_{n=1}^{N}|y(n) - \hat{x}(n)|^2}{P_0}}. \qquad (7.9)$$

For large values of $N$, the numerator in (7.9) can be approximated as,

$$\frac{1}{N}\sum_{n=1}^{N}|y(n) - \hat{x}(n)|^2 \approx E\left\{|y(n) - \hat{x}(n)|^2\right\}, \qquad (7.10)$$

where $E\{x\}$ is the expected value of $x$. For simplicity, the index $n$ is dropped for the remainder of this chapter.

119

We first start by considering BPSK signals. In this case, $x$ and $\hat{x}$ are real signals. Thus, we can rewrite (7.10) as follows,

$$E\left\{|y - \hat{x}|^2\right\} = E\left\{(y_\Re - \hat{x})^2\right\} + E\left\{\eta_\Im^2\right\},\tag{7.11}$$

where $y_\Re = x + \eta_\Re$, and the subscripts $\Re$ and $\Im$ represent the real and imaginary components of the signal, respectively. Note that $\eta_\Re$ and $\eta_\Im$ are uncorrelated random processes that have a Gaussian distribution with zero mean and $\sigma_n^2$ variance. Thus,

$$E\left\{\eta_\Im^2\right\} = \sigma_n^2.\tag{7.12}$$

To evaluate $E\{(y_\Re - \hat{x})^2\}$, the statistical properties of $y_\Re$ is examined. Since BPSK modulation is considered, then $x \in \{-a, a\}$, where $a$ is the symbol amplitude. Thus, the conditional probability density function (PDF) of received signal is,

$$f(y_\Re|x = S_i) = \frac{1}{\sigma_n}\phi\left(\frac{y_\Re - S_i}{\sigma_n}\right),\tag{7.13}$$

where,

$$\phi(v) = \frac{1}{\sqrt{2\pi}}\exp\left(-\frac{v^2}{2}\right)\tag{7.14}$$

and $\phi(\cdot)$ the PDF of a standard normal distribution. Based on the criterion in (7.7), the probability of $\hat{x} = a$ is,

$$P(\hat{x} = a) = P(x = -a)\int_0^\infty f(y_\Re|x = -a)\,\mathrm{d}y_\Re + P(x = a)\int_0^\infty f(y_\Re|x = a)\,\mathrm{d}y_\Re.\tag{7.15}$$

It is assumed that,

$$P(x = -a) = P(x = a) = \frac{1}{2}.\tag{7.16}$$

As such, it can be shown that,

$$f(y_\Re|\hat{x} = a) = \frac{1}{C}\Big(f(y_\Re|x = -a) + f(y_\Re|x = a)\Big), \quad y_\Re > 0,\tag{7.17}$$

and

$$f(y_\Re|\hat{x} = -a) = \frac{1}{C}\Big(f(y_\Re|x = -a) + f(y_\Re|x = a)\Big), \quad y_\Re < 0, \tag{7.18}$$

where $C$ is a constant chosen such that,

$$\int_{-\infty}^{\infty} f(y_\Re|\hat{x} = S_i) \, dy_\Re = 1. \tag{7.19}$$

In this case, $C = 1$. Using (7.17) and (7.18),

$$E\left\{(y_\Re - \hat{x})^2\right\} = P(\hat{x} = -a) \int_{-\infty}^{\infty} (y_\Re + a)^2 f(y_\Re|\hat{x} = -a) \, dy_\Re$$

$$+ P(\hat{x} = a) \int_{-\infty}^{\infty} (y_\Re - a)^2 f(y_\Re|\hat{x} = a) \, dy_\Re. \tag{7.20}$$

Since the decision point $(y_\Re = 0)$ is equally spaced between the two possible values of $x$ and since $f(y_\Re|x = S_i)$ is symmetric around $x$, then,

$$P(\hat{x} = -a) = P(\hat{x} = a) = \frac{1}{2}. \tag{7.21}$$

Since $f(y_\Re|\hat{x} = -a) = f(-y_\Re|\hat{x} = a)$, then by exchanging $y_\Re$ with $-y_\Re$ in the second integral in (7.20) and with some manipulation it can be shown that,

$$\int_{-\infty}^{\infty} (y_\Re + a)^2 f(y_\Re|\hat{x} = -a) \, dy_\Re = \int_{-\infty}^{\infty} (y_\Re - a)^2 f(y_\Re|\hat{x} = a) \, dy_\Re. \tag{7.22}$$

Thus, using (7.21) and (7.22), (7.20) can be reduced to,

$$E\left\{(y_\Re - \hat{x})^2\right\} = \int_{-\infty}^{\infty} (y_\Re - a)^2 f(y_\Re|\hat{x} = a) \, dy_\Re. \tag{7.23}$$

From (7.18) and (7.13), the integral in (7.23) can be expressed as,

$$E\left\{(y_\Re - \hat{x})^2\right\} = \frac{1}{\sigma_n} \int_0^{\infty} (y_\Re - a)^2 \phi\left(\frac{y_\Re + a}{\sigma_n}\right) \, dy_\Re + \frac{1}{\sigma_n} \int_0^{\infty} (y_\Re - a)^2 \phi\left(\frac{y_\Re - a}{\sigma_n}\right) \, dy_\Re,$$

$$= \frac{1}{\sigma_n} \int_{-a}^{\infty} v^2 \phi\left(\frac{v + 2a}{\sigma_n}\right) \, dv + \frac{1}{\sigma_n} \int_{-a}^{\infty} v^2 \phi\left(\frac{v}{\sigma_n}\right) \, dv, \tag{7.24}$$

where $v = y_\Re - a$. The last two integrals in (7.24) are related to $E\{V^2\}$ where $V$ is a random variable that has a low-truncated normal distribution [139]. To solve (7.24), we define a new function $z(A, \mu, \sigma)$, where,

$$z(A, \mu, \sigma) \equiv \frac{1}{\sigma} \int_A^\infty v^2 \phi\left(\frac{v - \mu}{\sigma}\right) dv \qquad (7.25)$$

It is shown in Appendix C that,

$$z(A, \mu, \sigma) = \sigma(A + \mu)\phi\left(\frac{A - \mu}{\sigma}\right) + (\mu^2 + \sigma^2)Q\left(\frac{A - \mu}{\sigma}\right) \qquad (7.26)$$

Using (7.25), the solution to (7.24) is,

$$\begin{aligned}
E\left\{(y_\Re - \hat{x})^2\right\} &= z(-a, -2a, \sigma_n) + z(-a, 0, \sigma_n) \\
&= -3a\sigma_n\phi\left(\frac{a}{\sigma_n}\right) + (4a^2 + \sigma_n^2)Q\left(\frac{a}{\sigma_n}\right) - a\sigma_n\phi\left(\frac{-a}{\sigma_n}\right) + \sigma_n^2 Q\left(\frac{-a}{\sigma_n}\right). \quad (7.27)
\end{aligned}$$

Note that $\phi(v) = \phi(-v)$ and $Q(-v) + Q(v) = 1$. As such, (7.27) is reduced to,

$$E\left\{(y_\Re - \hat{x})^2\right\} = \sigma_n^2 - 4a\sigma_n\phi\left(\frac{a}{\sigma_n}\right) + 4a^2 Q\left(\frac{a}{\sigma_n}\right) \qquad (7.28)$$

Then, substituting (7.28) and (7.12) into (7.11),

$$E\left\{|y - \hat{x}|^2\right\} = 2\sigma_n^2 - 4a\sigma_n\phi\left(\frac{a}{\sigma_n}\right) + 4a^2 Q\left(\frac{a}{\sigma_n}\right). \qquad (7.29)$$

Without the loss of generality, we assume that the average symbol power, $P_0 = 1$ (i.e. $a = 1$). Therefore

$$\text{SNR} = \frac{P_0}{N_0} = \frac{1}{2\sigma_n^2}. \qquad (7.30)$$

To relate EVM to SNR for nondata-aided receivers and for BPSK signaling, the results from (7.29), (7.30) are substituted into (7.9) as follows,

$$\text{EVM}_{\text{BPSK}} = \left[\frac{1}{\text{SNR}} - \frac{4}{\sqrt{2\text{SNR}}}\phi\left(\sqrt{2\text{SNR}}\right) + 4Q\left(\sqrt{2\text{SNR}}\right)\right]^{1/2}, \qquad (7.31)$$

122

or more conveniently using the exponential and error functions as,

$$\text{EVM}_{\text{BPSK}} = \left[ \frac{1}{\text{SNR}} - \frac{2}{\sqrt{\pi \text{SNR}}} \exp(-\text{SNR}) + 2\,\text{erfc}\left(\sqrt{\text{SNR}}\right) \right]^{1/2}.$$ (7.32)

Note that the first square-rooted term in (7.32) represents the ideal EVM value. The second and last terms represent the errors caused by the symbol estimation process. For high values of SNR, the last two terms converge to zero and the EVM approaches its ideal value. This is explained by the fact that for high SNR values, the probability of symbol error goes to zero. This is also confirmed by the simulation results in Fig. 7.1. The validity of (7.32) is further investigated in Section 7.6.

Next, we consider square QAM signals (i.e. with even number of bits per symbol such as QPSK, 16QAM, 64QAM, etc). For a QAM signal of order $M$, the modulated symbols are,

$$x = (2i - k)a + \jmath(2m - k)a, \quad i, m = 0, 1, \ldots, k$$ (7.33)

where $k = \sqrt{M} - 1$. In this case,

$$E\{|y - \hat{x}|^2\} = E\{(y_{\Re} - \hat{x}_{\Re})^2\} + E\{(y_{\Im} - \hat{x}_{\Im})^2\}.$$ (7.34)

Due to the independence and symmetry between the real and imaginary parts of the signal, $E\{(y_{\Re} - \hat{x}_{\Re})^2\} = E\{(y_{\Im} - \hat{x}_{\Im})^2\}$. Thus, it is sufficient to calculate only one of the above expectations. For non-square QAM signals, the above equality does not hold. It is shown later in this section how to calculate the expected EVM value in such case.

In the following analysis, the real part of the signal is considered. Generalizing the expression in (7.20), $E\{(y_{\Re} - \hat{x}_{\Re})^2\}$ can be obtained by averaging over all possible values of $\hat{x}_{\Re}$ as follows,

$$\begin{aligned}
E\{(y_{\Re} - \hat{x}_{\Re})^2\} &= \sum_{i=0}^{k} P(\hat{x}_{\Re} = S_i) E\{(y_{\Re} - S_i)^2 | \hat{x}_{\Re} = S_i\} \\
&= \sum_{i=0}^{k} P(\hat{x}_{\Re} = S_i) \int_{-\infty}^{\infty} (y_{\Re} - S_i)^2 f(y_{\Re} | \hat{x}_{\Re} = S_i) \mathrm{d}y_{\Re},
\end{aligned}$$ (7.35)

where $S_i = (2i - k)a$, is the real value of the modulation symbol. Similar to (7.17), it be shown that for any arbitrary value of $i$,

$$f(y_\Re|\hat{x}_\Re = S_i) = \frac{1}{C_i} \left[ \sum_{j=0}^{k} f(y_\Re|x_\Re = S_j) \right], \quad y_\Re \in D_i$$

$$= \frac{1}{C_i} \left[ \sum_{j=0}^{k} \frac{1}{\sigma_n} \phi \left( \frac{y_\Re - S_j}{\sigma_n} \right) \right], \quad y_\Re \in D_i \qquad (7.36)$$

where $D_i$ is the decision region for symbol $S_i$ such that,

$$\text{for} \quad i = 0, \qquad \qquad -\infty < D_0 \leq S_0 + a,$$

$$\text{for} \quad 1 \leq i \leq k - 1, \qquad \qquad S_i - a < D_i \leq S_i + a,$$

$$\text{and for} \quad i = k, \qquad \qquad S_k - a < D_k < \infty. \qquad (7.37)$$

To satisfy the condition in (7.19), the normalization constant $C_i$ is found to be,

$$C_i = \int_{D_i} \left[ \sum_{j=0}^{k} \frac{1}{\sigma_n} \phi \left( \frac{y_\Re - S_j}{\sigma_n} \right) \right] dy_\Re,$$

$$= \sum_{j=0}^{k} \int_{D_i} \frac{1}{\sigma_n} \phi \left( \frac{y_\Re - S_j}{\sigma_n} \right) dy_\Re, \qquad (7.38)$$

where the integral and summation in (7.38) are interchangeable. On the other hand, $P(\hat{x}_\Re = S_i)$ can be evaluated as follows,

$$P(\hat{x}_\Re = S_i) = \sum_{j=0}^{k} P(x_\Re = S_j) \int_{D_i} \frac{1}{\sigma_n} \phi \left( \frac{y_\Re - S_j}{\sigma_n} \right) dy_\Re. \qquad (7.39)$$

It is assumed that all modulation symbols are transmitted with equal probability such that $P(x_\Re = S_j) = 1/(k+1)$, $\forall j$. From the above, (7.39) becomes,

$$P(\hat{x}_\Re = S_i) = \frac{1}{k+1} \sum_{j=0}^{k} \int_{D_i} \frac{1}{\sigma_n} \phi \left( \frac{y_\Re - S_j}{\sigma_n} \right) dy_\Re. \qquad (7.40)$$

From (7.38) and (7.40), it can be seen that $P(\hat{x}_{\Re} = S_i) = C_i/(k+1)$. Thus, using (7.36), (7.38), and (7.40), the expression in (7.35) is reduced to,

$$E\{(y_{\Re} - \hat{x}_{\Re})^2\} = \frac{1}{k+1} \sum_{i=0}^{k} \sum_{j=0}^{k} \int_{D_i} \frac{1}{\sigma_n} (y_{\Re} - S_i)^2 \phi \left( \frac{y_{\Re} - S_j}{\sigma_n} \right) dy_{\Re}, \qquad (7.41)$$

By using $v = y_{\Re} - S_i$,

$$E\{(y_{\Re} - \hat{x}_{\Re})^2\} = \frac{1}{k+1} \sum_{i=0}^{k} \sum_{j=0}^{k} \underbrace{\int_{\tilde{D}_i} \frac{v^2}{\sigma_n} \phi \left( \frac{v - \mu_{ji}}{\sigma_n} \right) dv}_{\mathcal{I}_{ji}} \qquad (7.42)$$

where $\tilde{D}_i = D_i - S_i$ and $\mu_{ji} = 2a(j - i) = S_j - S_i$. To evaluate the integral in (7.42) $\mathcal{I}_{ji}$, we need to consider two cases. The first case is the singly-truncated decision regions (i.e. $i = 0, k$), and the second case is the doubly-truncated decision regions (i.e. $1 \le i \le k - 1$). Due to the symmetry around zero, the values of $\mathcal{I}_{ji}$ are equal for $i = 0$ and $i = k$ (or generally for any $i$ and $k - i$). Thus,

$$\mathcal{I}_{j0} = \mathcal{I}_{jk} = \frac{1}{\sigma_n} \int_{-a}^{\infty} v^2 \phi \left( \frac{v - \mu_{jk}}{\sigma_n} \right) dv$$

$$= z(-a, \mu_{jk}, \sigma_n). \qquad (7.43)$$

For doubly-truncated regions,

$$\mathcal{I}_{ji} = \int_{-a}^{a} v^2 \phi \left( \frac{v - \mu_{ji}}{\sigma_n} \right) dv$$

$$= z(-a, \mu_{ji}, \sigma_n) - z(a, \mu_{ji}, \sigma_n), \quad 1 \le i \le k - 1. \qquad (7.44)$$

Substituting (7.43) and (7.44) into (7.42),

$$E\{(y_{\Re} - \hat{x}_{\Re})^2\} = \frac{1}{k+1} \left( 2 \sum_{j=0}^{k} z(-a, \mu_{jk}, \sigma_n) + \sum_{i=1}^{k-1} \sum_{j=0}^{k} \left[ z(-a, \mu_{ji}, \sigma_n) - z(a, \mu_{ji}, \sigma_n) \right] \right). \qquad (7.45)$$

It is shown in Appendix D that (7.45) reduces to,

$$E\{(y_{\Re} - \hat{x}_{\Re})^2\} = \sigma_n^2 - 8a\sigma_n \sum_{i=1}^{k} \gamma_i \phi \left[ \frac{\beta_i a}{\sigma_n} \right] + 8a^2 \sum_{i=1}^{k} \gamma_i \beta_i Q \left[ \frac{\beta_i a}{\sigma_n} \right], \qquad (7.46)$$

125

where

$$\gamma_i = 1 - \frac{i}{k+1}, \quad \text{and} \quad \beta_i = 2i - 1. \tag{7.47}$$

Combining (7.30), (7.34), and (7.46), and exchanging $\phi$ and $Q$ with the exponential and error functions,

$$E\{|y - \hat{x}|^2\} = \frac{1}{\text{SNR}} - \frac{8a}{\sqrt{\pi \text{SNR}}} \sum_{i=1}^{k} \gamma_i \exp(-\beta_i^2 a^2 \text{SNR}) + 8a^2 \sum_{i=1}^{k} \gamma_i \beta_i \ \text{erfc}\left(\beta_i a \sqrt{\text{SNR}}\right). \tag{7.48}$$

For a normalized QAM system,

$$a = \sqrt{\frac{3}{2(M-1)}}. \tag{7.49}$$

From (7.9), (7.48), and (7.49), the EVM for QAM signals is

$$\text{EVM}_{\text{QAM}} = \left[ \frac{1}{\text{SNR}} - 8\sqrt{\frac{3}{2\pi(M-1)\text{SNR}}} \sum_{i=1}^{\sqrt{M}-1} \gamma_i \exp\left(-\frac{3\beta_i^2 \text{SNR}}{2(M-1)}\right) \right.$$
$$\left. + \frac{12}{(M-1)} \sum_{i=1}^{\sqrt{M}-1} \gamma_i \beta_i \ \text{erfc}\left(\sqrt{\frac{3\beta_i^2 \text{SNR}}{2(M-1)}}\right) \right]^{1/2}, \tag{7.50}$$

where

$$\gamma_i = 1 - \frac{i}{\sqrt{M}}, \quad \text{and} \quad \beta_i = 2i - 1. \tag{7.51}$$

In view of the above results, some remarks are in order. First, similar to the EVM of a BPSK signal in (7.32), the EVM of a QAM signal in (7.50) can be divided into two parts. The first part is 1/SNR, which represents the ideal EVM when no errors are introduced to the symbol detection. The second part, which in QAM case is a sum of exponential and error functions, represents the reduction in measured EVM due to detection error. The second error part is a function of both the modulation order $M$ and the SNR level, and it goes to zero for high values of SNR. Note that as the summation index $i$ in (7.50) increases, the value of the exponential and error functions decreases rapidly. Hence, for high modulation order, an approximation of the EVM value can be obtained by considering only the first few terms of the summations.

126

Second, the expression in (7.46) can be used to evaluate the EVM for QAM systems with odd number of bits per symbol. In this case, the $E\{(y_\Re - \hat{x}_\Re)^2\}$ and $E\{(y_\Im - \hat{x}_\Im)^2\}$ are not equal. Using (7.46), $E\{(y_\Re - \hat{x}_\Re)^2\}$ and $E\{(y_\Im - \hat{x}_\Im)^2\}$ can be evaluated for $k = k_1 - 1$ and $k = k_2 - 1$, where $M = k_1 k_2$, and $k_1$ and $k_2$ represents the number of constellation points on the real and imaginary parts of the signal, respectively. Finally, the EVM can be evaluated by substituting the above values into (7.34) and repeating a similar process to the one in (7.48) and (7.50).

Third, note that the EVM for a normalized PAM signal can be obtained from (7.46) by adding $\sigma_n^2$, setting $k$ to $M - 1$, and $a$ to $\sqrt{3/(M^2 - 1)}$, such that

$$\mathrm{EVM}_{\mathrm{PAM}} = \left[ \frac{1}{\mathrm{SNR}} - 4\sqrt{\frac{3}{\pi(M^2 - 1)\mathrm{SNR}}} \sum_{i=1}^{M-1} \gamma_i \exp\left(-\frac{3\beta_i^2 \mathrm{SNR}}{(M^2 - 1)}\right) \right.$$
$$\left. + \frac{12}{(M^2 - 1)} \sum_{i=1}^{M-1} \gamma_i \beta_i \ \mathrm{erfc}\left(\sqrt{\frac{3\beta_i^2 \mathrm{SNR}}{(M^2 - 1)}}\right) \right]^{1/2}, \quad (7.52)$$

where

$$\gamma_i = 1 - \frac{i}{M}, \quad \text{and} \quad \beta_i = 2i - 1. \tag{7.53}$$

For example, by setting $M = 2$ in (7.52), the EVM for BPSK signals in (7.29) can be obtained.

### 7.5.2   Detection over Rayleigh Fading Channels

For signals detected over Rayleigh fading channels [89],

$$y(n) = \alpha \exp(-\jmath\theta) x(n) + \eta(n), \tag{7.54}$$

where $\alpha$ and $\theta$ are the attenuation and phase shift introduced by the fading channel, and $\alpha$ is a Rayleigh-distributed random variable. Slow fading is assumed such that the channel response is constant over at least one symbol interval. If the channel fading is sufficiently slow, the phase shift $\theta$ can be estimated from the received signal without error. In this case, it can be shown that the instantaneous SNR is chi-square-distributed [89]. To evaluate the average EVM value, we first consider the instantaneous EVM value for a given $\alpha$. In the following analysis, QAM signals are

considered. Thus, from (7.50), the instantaneous EVM is,

$$\text{EVM}_{\text{QAM}}(\alpha) = \left[ \frac{1}{\text{SNR}} - 8\alpha \sqrt{\frac{3}{2\pi(M-1)\text{SNR}}} \sum_{i=1}^{\sqrt{M}-1} \gamma_i \exp\left( -\frac{3\alpha^2\beta_i^2\text{SNR}}{2(M-1)} \right) \right.$$
$$\left. + \frac{12\alpha^2}{(M-1)} \sum_{i=1}^{\sqrt{M}-1} \gamma_i\beta_i \ \text{erfc}\left( \sqrt{\frac{3\alpha^2\beta_i^2\text{SNR}}{2(M-1)}} \right) \right]^{1/2}, \quad (7.55)$$

where $\gamma_i$ and $\beta_i$ are as in (7.51). The PDF of $\alpha$ is,

$$f(\alpha) = 2\alpha\exp(-\alpha^2), \quad \alpha \geq 0. \tag{7.56}$$

The expected value of EVM is evaluated by averaging over $\alpha$,

$$\text{EVM}_{\text{QAM}} = \int_0^\infty \text{EVM}_{\text{QAM}}(\alpha)f(\alpha)\text{d}\alpha. \tag{7.57}$$

The evaluation of the integral in (7.57) is skipped here for brevity. The EVM is found to be,

$$\text{EVM}_{\text{QAM}} = \left[ \frac{1}{\text{SNR}} + \frac{4}{\text{SNR}^2} \sqrt{\frac{3}{2(M-1)}} \sum_{i=1}^{\sqrt{M}-1} \gamma_i \left[ \frac{3\beta_i^2}{2(M-1)} + \frac{1}{\text{SNR}} \right]^{-3/2} \right.$$
$$\left. + \frac{12}{(M-1)} \sum_{i=1}^{\sqrt{M}-1} \gamma_i\beta_i \left( 1 - \sqrt{\frac{3\beta_i^2\text{SNR}}{2(M-1)+3\beta_i^2\text{SNR}}} \left[ 1 + \frac{(M-1)}{2(M-1)+3\beta_i^2\text{SNR}} \right] \right) \right]^{1/2} \tag{7.58}$$

### 7.5.3 Detection with Other Impairments

In the previous section, the effect of Rayleigh fading channels on the measured EVM of received signals was considered. Since it was assumed that the phase shift caused by the channel can be perfectly estimated from the received signal, there was no interference between the real and imaginary parts of the signal. In this section, we consider the case where the multiplicative term, $g(n)$ in (7.2), can have a complex value that is unknown to the receiver. Since $g(n)$ is complex-valued, there will be interference between the real and imaginary parts of the signal. This case can be used to model received signals with impairments such as the IQ imbalance [124] or channel estimation errors [114].

The received signal can be represented using its real and imaginary parts as

$$\begin{bmatrix} y_\Re \\ y_\Im \end{bmatrix} = \begin{bmatrix} g_{11} & g_{12} \\ g_{21} & g_{22} \end{bmatrix} \begin{bmatrix} x_\Re \\ x_\Im \end{bmatrix} + \begin{bmatrix} \mu_\Re \\ \mu_\Im \end{bmatrix}, \tag{7.59}$$

where the index $n$ is dropped to simplify the presentation. In the following, QAM signals are considered. Assume the transmitted signal is as in (7.33). In this case, and for a given value of $\mathbf{g}$, the expected value of the real and imaginary parts of the detected signals are,

$$E\{y_\Re | i, m\} = (2i - k)ag_{11} + (2m - k)ag_{12} \equiv \mu_\Re(i, m), \tag{7.60}$$

$$E\{y_\Im | i, m\} = (2i - k)ag_{21} + (2m - k)ag_{22} \equiv \mu_\Im(i, m). \tag{7.61}$$

Ideally, the signal should be detected such that $(g_{11} = g_{22})$ and $(g_{12} = g_{21} = 0)$. The previous two equalities are lost if the IQ modulator is suffering from gain and phase imbalances, respectively. In this case, there is interference between the real and imaginary parts of $x$ in the detected signal $y$. Since it is assumed that $\mathbf{g}$ is unknown to the receiver, the decision regions are the same as in (7.37).

Following the same analysis presented in Section 7.5.1, similar results to (7.45) are obtained as follow,

$$E\{(y_\Re - \hat{x}_\Re)^2\} = \frac{1}{M} \sum_{i=0}^{k} \sum_{m=0}^{k} \left( 2z(-a, \mu_{imk}^{(R)}, \sigma_n) + \sum_{j=1}^{k-1} \left[ z(-a, \mu_{imj}^{(R)}, \sigma_n) - z(a, \mu_{imj}^{(R)}, \sigma_n) \right] \right), \tag{7.62}$$

$$E\{(y_\Im - \hat{x}_\Im)^2\} = \frac{1}{M} \sum_{i=0}^{k} \sum_{m=0}^{k} \left( 2z(-a, \mu_{imk}^{(I)}, \sigma_n) + \sum_{j=1}^{k-1} \left[ z(-a, \mu_{imj}^{(I)}, \sigma_n) - z(a, \mu_{imj}^{(I)}, \sigma_n) \right] \right), \tag{7.63}$$

where

$$\mu_{imj}^{(R)} = \mu_\Re(i, m) - (2j - k)a, \tag{7.64}$$

$$\mu_{imj}^{(I)} = \mu_\Im(i, m) - (2j - k)a. \tag{7.65}$$

Note that in this case, the symmetry between the real and imaginary components of the detected signal $y$ is lost. Thus, to measure the final EVM value, expectations of both the real and imaginary parts of the signal needs to be considered. The symmetry is restored if $|g_{11}| = |g_{22}|$ and $|g_{12}| = |g_{21}|$. In addition, due to the interference between the I and Q branches of the IQ modulator, the expected

129

value needs to be averaged over all possible values of the Q signal in addition to the I signal. Hence, as compared to (7.45), the expressions in (7.62) and (7.63) contain an extra summation over $m$. Further simplification of (7.62) and (7.63) is not possible since $\mu_{imj}^{(R)}$ and $\mu_{imj}^{(I)}$ have distinctive values for each set of $i$, $m$, and $j$ (unlike $\mu_{ij}$ in (7.45) whose values depend only on the difference $i - j$). Finally, the average EVM can be evaluated as,

$$\text{EVM}_{\text{QAM}}(\mathbf{g}) = \left[E\{(y_\Re - \hat{x}_\Re)^2\} + E\{(y_\Im - \hat{x}_\Im)^2\}\right]^{1/2}.\tag{7.66}$$

While $\mathbf{g}$ is usually considered constant such as in the case of IQ imbalances, in some other cases $\mathbf{g}$ can be modeled as a random process. For example, channel estimation errors can be modeled as a multiplicative random variable with Gaussian distribution [114]. In this case, the EVM expected value can be obtained by averaging over the PDF of $\mathbf{g}$ similar to (7.57).

To examine the validity of the results present in (7.62) and (7.63), we consider the case where the SNR is sufficiently high and $\mathbf{g} \approx \mathbf{I}$ such that the probability of a symbol detection error is zero, where $\mathbf{I}$ is the identity matrix. This is equivalent to assuming that the transmitted sequence $x(n)$ is known to the receiver. In this case,

$$\begin{aligned}
z(-a, \mu_{imk}^{(R)}, \sigma_n) &= \begin{cases} \left[\mu_{kmk}^{(R)}\right]^2 + \sigma_n^2, & \text{for } i = k \\ 0, & \text{otherwise,} \end{cases} \\
z(-a, \mu_{imj}^{(R)}, \sigma_n) - z(a, \mu_{imj}^{(R)}, \sigma_n) &= \begin{cases} \left[\mu_{jmj}^{(R)}\right]^2 + \sigma_n^2, & \text{for } i = j \\ 0, & \text{otherwise,} \end{cases}
\end{aligned}\tag{7.67}$$

Substituting (7.67) in (7.62) and (7.63), and assuming a normalized QAM signal, the EVM is found to be,

$$\text{EVM}_{QAM}(\mathbf{g}) = \sqrt{\frac{1}{\text{SNR}} + 1 + \frac{1}{2}(g_{11}^2 + g_{12}^2 + g_{21}^2 + g_{22}^2) - (g_{11} + g_{22})}.\tag{7.68}$$

It is conventional to assume, without the loss of generality, that the impairments matrix $\mathbf{g}$ is normalized such that $(g_{11}^2 + g_{12}^2 + g_{21}^2 + g_{22}^2 = 2)$. In this case,

$$\text{EVM}_{QAM}(\mathbf{g}) = \sqrt{\frac{1}{\text{SNR}} + 2 - \text{Tr}(\mathbf{g})},\tag{7.69}$$
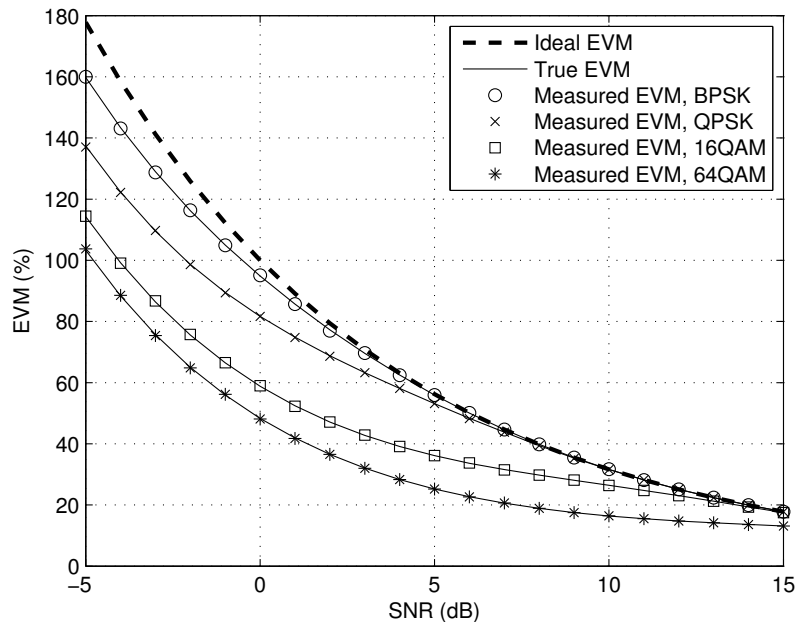
Figure 7.2 Measured versus ideal and true EVM measurements in nondata-aided receivers over AWGN channels.

where $\text{Tr}(\mathbf{g})$ is the trace of matrix $\mathbf{g}$. The expression in (7.69) is identical to (27) in [140] with zero DC offsets, where it is assumed that there are no detection errors.

## 7.6   Simulation Results and Discussion

In this section, the validity of the EVM-SNR relations derived in Section 7.5 is examined using computer simulations. EVM values are measured for BPSK, QPSK, 16QAM and 64QAM modulated signals and are averaged over 100,000 symbols. Over AWGN channels, the EVM measurements are compared with the ideal EVM based on (7.6) and what we define as true EVM based on (7.32), and (7.50). The results are shown in Fig. 7.2. The figure shows that true EVM values align perfectly with measured EVM values. Similar results are obtained over Rayleigh fading channels and are shown in Fig. 7.3, where true EVM in this case is based on (7.58).

Next, signals corrupted with IQ gain and phase imbalances and received over AWGN channels are consider. For a system with gain imbalance $\epsilon_t$ and phase imbalance $\phi_t$, the received signal is

131
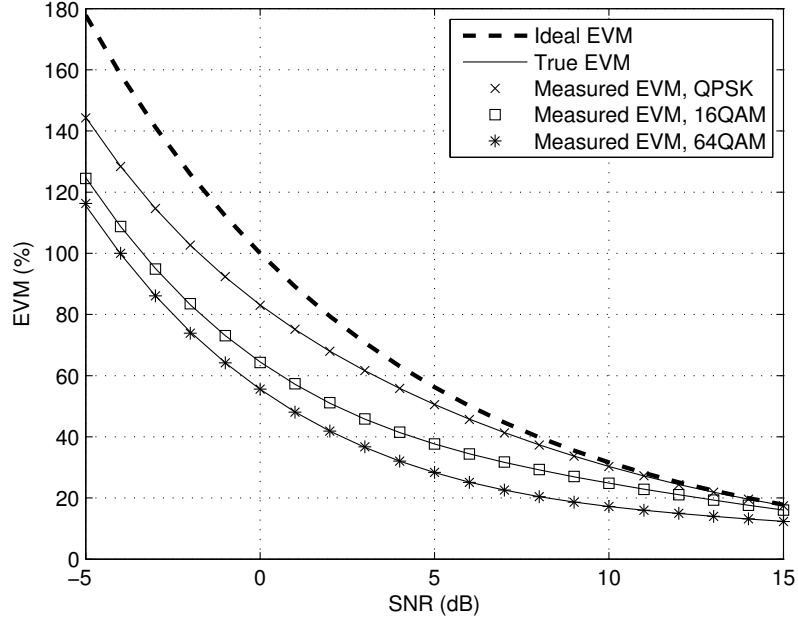
Figure 7.3 Measured versus ideal and true EVM measurements in nondata-aided receivers over Rayleigh fading channels.

modeled as [134, 141],

$$\begin{bmatrix} y_\Re \\ y_\Im \end{bmatrix} = \sqrt{\frac{2}{1 + g_t^2}} \begin{bmatrix} g_t \cos \frac{\phi_t}{2} & \sin \frac{\phi_t}{2} \\ g_t \sin \frac{\phi_t}{2} & \cos \frac{\phi_t}{2} \end{bmatrix} \begin{bmatrix} x_\Re \\ x_\Im \end{bmatrix} + \begin{bmatrix} \mu_\Re \\ \mu_\Im \end{bmatrix}, \tag{7.70}$$

where $g_t = \epsilon_t + 1$ is the ratio between the I and Q gains in the IQ modulator [141]. The gain imbalance in dB is calculated as $20 \log(g_t)$. Fig. 7.4 shows EVM measurements for a 16QAM signal with a phase imbalance of $2°$ and varying gain imbalance. The measured EVM is compared with the theoretical ideal and true EVM based on (7.69) and (7.66), respectively. At SNR $= 45$ dB, ideal and true EVM matches with measured EVM. At SNR $= 10$ dB, detection errors occur and the ideal EVM deviates from the actual measured EVM by around 5% for nondata-aided systems. On the other hand, true EVM matches to measured EVM, as detection error probability were taken into consideration.

The analysis done in Section 7.5 is eventually meant to be used to relate EVM to SNR. EVM is readily available in most measurement devices, as well as a requirement for most wireless standards (e.g. IEEE 802.11a-1999 [6] and IEEE 802.16e-2005 [9]). Reliably estimating the SNR from the mea-
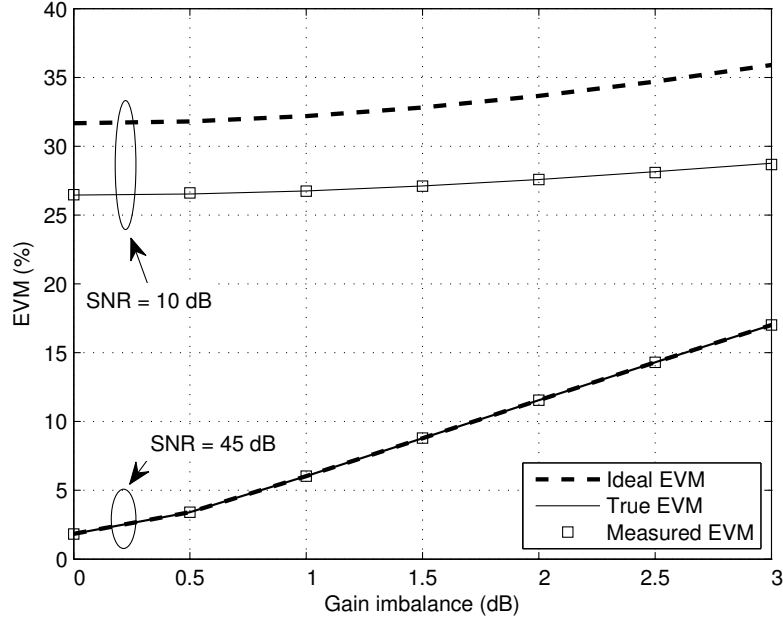
Figure 7.4 Measured versus ideal and true EVM measurements in nondata-aided receivers with IQ impairments and AWGN noise.

sured EVM can reduce the system complexity by eliminating the need for modules that is required to separately estimate the SNR. Usually, the estimated SNR values are quantized with a predefined value. For example, the IEEE 802.16e-2005 standard states that the carrier-to-interference-plus-noise ratio (CINR) should be quantized in $1\,\mathrm{dB}$ increments ranging from a minimum of $-20\,\mathrm{dB}$ to a maximum of $40\,\mathrm{dB}$. In generated simulations, the quantization level is set to $0.1\,\mathrm{dB}$ for more accurate results. Two sets of lookup tables are generated that relates the measured EVM to the SNR based on ideal EVM and true EVM. Both SNR estimators are compared to the maximum likelihood (ML) SNR estimator, where the ML-estimated SNR is computed as [142],

$$\widehat{\mathrm{SNR}}_{\mathrm{ML}} = \frac{\left[\dfrac{1}{N}\displaystyle\sum_{n=1}^{N}\left(y_{\Re}(n)\hat{x}_{\Re}(n) + y_{\Im}(n)\hat{x}_{\Im}(n)\right)\right]^2}{\dfrac{1}{N}\displaystyle\sum_{n=1}^{N}|y(n)|^2 - \left[\dfrac{1}{N}\displaystyle\sum_{n=1}^{N}\left(y_{\Re}(n)\hat{x}_{\Re}(n) + y_{\Im}(n)\hat{x}_{\Im}(n)\right)\right]^2}. \tag{7.71}$$

The effect of number of samples $N$ on the SNR estimation is investigated for QPSK signals. The normalized mean-squared-error (MSE) $\mathcal{E}_{\mathrm{Norm}}$ of the SNR estimations is evaluated for all three methods
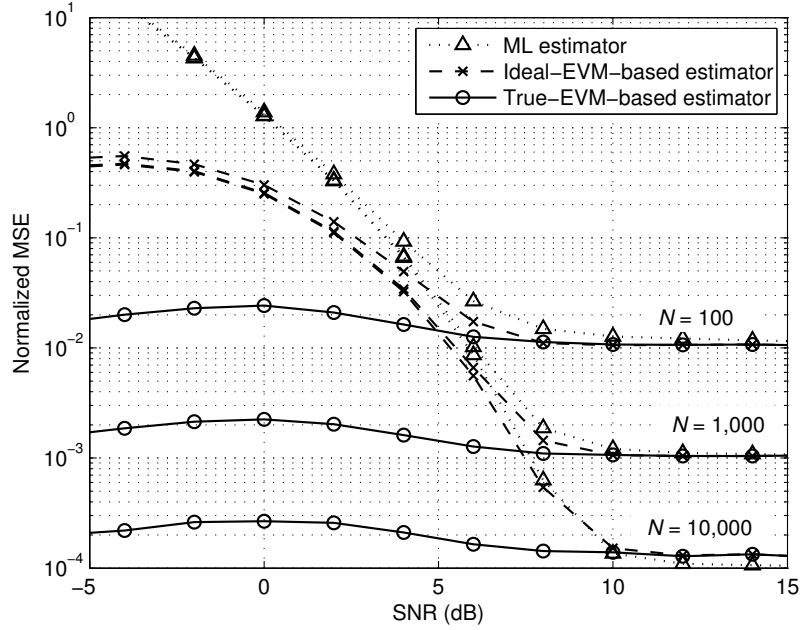
Figure 7.5 Normalized MSE of SNR estimators for different values of $N$.

over AWGN channels and the results are shown in Fig. 7.5, where [142]

$$\mathcal{E}_{\text{Norm}}(\widehat{\text{SNR}}) = \frac{E\left\{\left(\widehat{\text{SNR}} - \text{SNR}\right)^2\right\}}{\text{SNR}^2}. \tag{7.72}$$

In general, it is expected that the performance would improve for larger $N$. Due to detection errors, both ML estimator and ideal-EVM-based estimator perform poorly at low SNR values, independent of $N$. As the SNR increases, the performances show improvement for larger $N$. Note that for sufficiently high SNR values, performances of all estimators are almost equal as there are no detection errors. Considering true-EVM-based estimator, the performance is always better for larger $N$ regardless of the SNR level. In addition, the performance is almost independent of the SNR value.

The performance of the true-EVM-based SNR estimator is further investigated by considering various impairments to received signal. Fig. 7.6 shows the nondata-aided SNR estimator performance for signals corrupted by AWGN, signals received over Rayleigh fading channels, and signals with IQ imbalances (2° phase imbalance and 1 dB gain imbalance). For reference, the performance of ideal-EVM-based SNR estimator is provided under best case scenario where the estimation is done

134
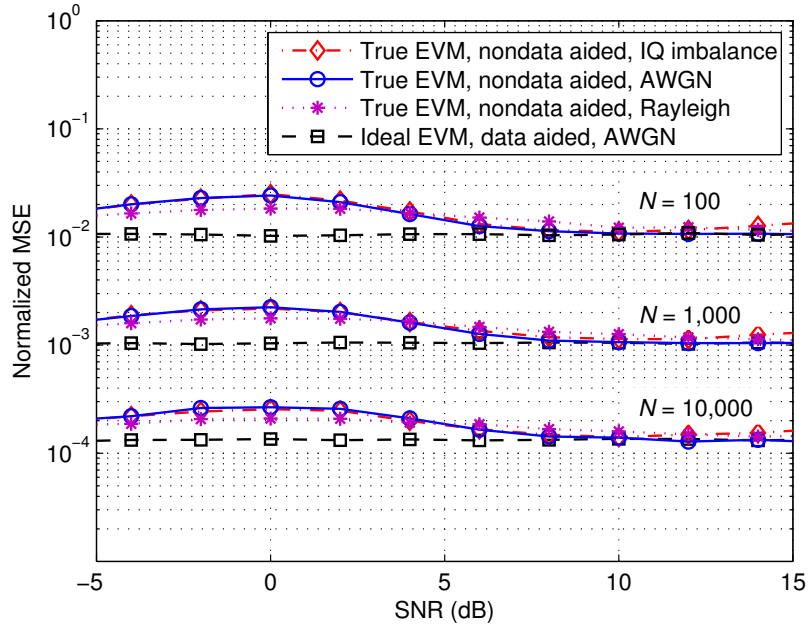
Figure 7.6 Normalized MSE of true-EVM-based SNR estimator under different impairments and for different values of $N$.

over known data sequences (data-aided) and the received signal is only corrupted by AWGN. The figure shows that the performance of the true-EVM-based estimator is consistent under various impairments. The deviation from the best case performance is low and independent of $N$. This shows that even for systems with pilots or preambles available to the receiver, measuring the EVM over data symbols as well as pilots can produce better SNR estimation. This is especially true considering that pilot symbols are usually much less than data symbols in most practical systems.

Note that the performance shown in Fig. 7.6 is obtained under the assumption that impairments to the signal (e.g. $\alpha$ and $\mathbf{g}$) are known. In practical systems, such impairments are estimated either using preambles and pilots, or blindly by using data symbols. The estimation and equalization process is usually not perfect. Thus, the estimation error effect on the system performance is considered. For a signal received over Rayleigh fading channel, the channel estimation output can be represented as,

$$\hat{\alpha} = \alpha + \zeta, \tag{7.73}$$
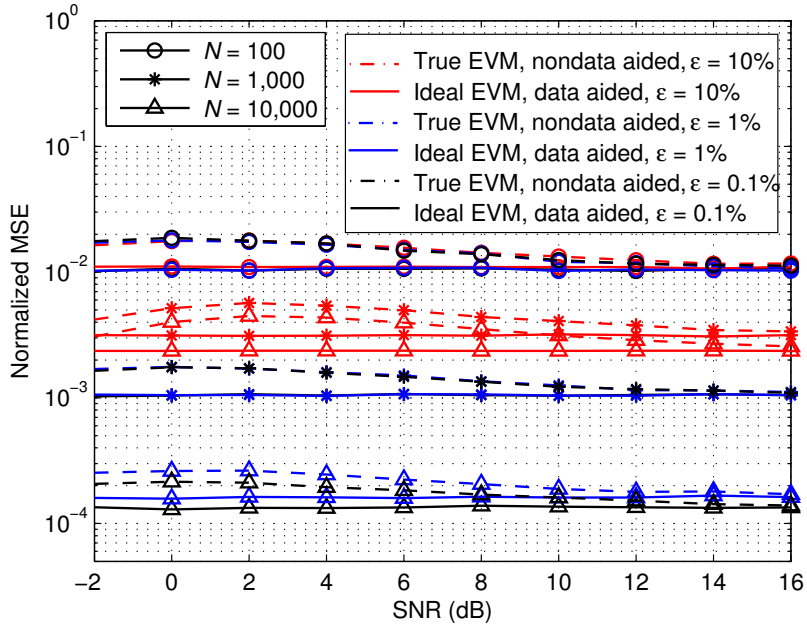
Figure 7.7 Normalized MSE of ideal-EVM data-aided and true-EVM nondata-aided SNR estimators under different channel estimation error levels and for different values of $N$.

where $\zeta$ is the additive estimation error. The channel estimation error $\zeta$ is is modeled as a random variable that has a Gaussian distribution [140] with zero mean (unbiased estimator) and variance $\sigma_{est}^2$. Since the estimator performance is affect by the AWGN in the signal [108], the estimation error variance is considered as a percentage of the noise variance $\sigma_n^2$ such that, $\sigma_{est}^2 = \epsilon \sigma_n^2$. In this sense, one could consider $\epsilon$ to be a measure of the channel estimator quality, where a better estimator would have a lower $\epsilon$. The performance of the ideal EVM data-aided and true EVM nondata-aided SNR estimators is considered in this case under various values of $\epsilon$. The results are shown in Fig. 7.7. The error in SNR estimation can be attributed to both channel estimation errors and the noise averaging (i.e. the number of symbols used for estimation, $N$). At $N = 100$, the MSE due to noise averaging is dominant and the performances of both data-aided and nondata-aided estimators are not affect by the channel estimator quality (or $\epsilon$). As $N$ increases to $1,000$ and $10,000$, the channel estimator quality starts to affect the performance of the SNR estimator. In all cases, it is shown that for the same $N$ and $\epsilon$ the difference between the data-aided and nondata-aided SNR estimators is almost constant. This implies that the gain achieved by using the true-EVM-based SNR estimator is consistent regardless of estimation errors.

136

## 7.7 Conclusion

In this chapter, measured EVM is related to SNR for nondata-aided receivers, called true EVM. True EVM is related to the SNR for QAM and PAM signals. The EVM-SNR relation is evaluated for signals detected over AWGN channels, and Rayleigh fading channels; and for signals with IQ impairments. The derived expressions are verified using computer simulations. The presented results show that when considering nondata-aided receivers, using EVM-SNR relations derived for data-aided receivers (or assuming high SNR) results in poor SNR estimation especially for high modulation orders or low SNR values. On the other hand, using proposed true EVM expressions results in accurate SNR estimation independent of modulation order and SNR value.

# CHAPTER 8

## CONCLUSION AND FUTURE WORK

In this dissertation, we considered the transceiver design for orthogonal frequency division multiplexing (OFDM) and orthogonal frequency division multiple access (OFDMA) advanced systems. In Chapter 2, we introduced OFDM technology and discussed its advantages and disadvantages when applied to future wireless systems. For the remainder of the dissertation, we focused on some of the important challenges that face OFDM-based systems. Practical implementation aspects such as computational complexity, power consumption, bit error rate (BER), and adjacent channel interference (ACI) are considered. Parts of the work presented in this dissertation have been accepted for publication [20–27] and has been recognized by the wireless research community through citations [143–150]. The study we presented in [22] has been the second most accessed document on the IEEE Xplore® [151] for the month of June, 2008. Some of the specific contributions presented in this dissertation are listed below.

## 8.1    Contributions

- Synchronization in OFDMA Uplink Systems

  A novel algorithm for OFDMA initial ranging process based on the IEEE 802.16e-2005 standard is presented in Chapter 3. The proposed algorithm performs multiuser code detection and timing offset estimation for ranging users. It was shown that the proposed algorithm reduces the computational complexity by 80% to 96% depending on the number of users while maintaining the standard deviation of the timing error under 5% of the guard interval. Simulation results showed that the proposed algorithm can perform well with as high as 10 users per ranging channel in a given uplink (UL) frame. Hence, the proposed algorithm can be highly desirable for practical OFDMA-based base stations (BS).

- Spectrum Shaping for OFDM Systems

  We proposed a new method, called adaptive symbol transition (AST), to suppress OFDM sidelobes adaptively and allow the system to shape the transmitted signal spectrum. The proposed AST method extends OFDM symbols and uses the extension to reduce ACI to other users operating in the same band. Simulation results show that AST can achieve a significant gain over conventional sidelobe suppression techniques while maintaining low increase in symbol energy. Moreover, AST does not increase the signal peak-to-average-power ratio (PAPR) and the performance is not sensitive to other system parameters such as the cyclic prefix (CP) size.

- OFDMA Performance under Channel Estimation Errors

  We derived the BER expressions for OFDM signals received over time-varying frequency-selective channels with channel estimation errors. The results were used to obtain the optimum tile dimensions (or optimum pilot insertion rate) in the time-frequency grid. Both analytical and simulated results show that careful choice of the tile dimensions can significantly increase the system throughput.

- OFDMA Channel Estimation with IQ Imbalances

  When considering the UL signal in OFDMA-based zero-IF systems, imperfections of the IQ-modulators causes multiuser interference (MUI). We designed a two-dimensional orthogonal pilot pattern to be used for channel estimation and equalization in this case. Two low complexity methods are proposed to equalize and detect IQ distorted signals using designed pilot pattern. Proposed methods were shown to improve the system performance significantly over conventional detection methods for signals suffering from multiple user IQ distortions.

- EVM-based SNR Estimation in Blind Receivers

  We derived the error vector magnitude (EVM) to signal-to-noise ratio (SNR) relations for signals detected over additive white Gaussian noise (AWGN) channels, and Rayleigh fading channels; and for signals with IQ impairments. The presented results show that when considering blind receivers, using EVM-SNR relations derived for data-aided receivers (or assuming high SNR) results in poor SNR estimation especially for high modulation orders or low SNR values. On the other hand, using proposed true EVM expressions results in accurate SNR estimation independent of modulation order and SNR value.

139

## 8.2 Final Remarks and Future Work

OFDM system offers a number of advantages for high data rate wireless systems, but suffers from some drawbacks. Throughout the dissertation, we tried to address some of the important challenges that face OFDM implementation in practical wireless systems. Meanwhile, there were other research topics that we feel are closely related to our work and can be a possible extension to the studies presented in this dissertation. A discussion of these topics is presented in this section.

- Noncoherent Detection in OFDMA Uplink Systems

  For OFDMA system to maintain orthogonality and reduce multiuser interference (MUI), synchronization between users should be maintained. The approach we proposed in Chapter 3 can be used in primary networks, where the base station (BS) can mandate the transmission time of each user. However, for secondary networks, such as femto cell, users cannot be synchronized prior to transmission. In that case, there is a need for an algorithm to detect received signal under MUI effects through interference detection and cancellation methods. As such, the design and implementation of OFDMA systems in femto cell represents an interesting research topic.

- Low-Complexity Spectrum Shaping for OFDM Systems

  The method we proposed in Chapter 4, as well as most other sidelobe suppression techniques proposed in the literature, suffer from high computational complexity. However, spectrum shaping in cognitive radio (CR) systems needs to be performed online with minimum delay as to take advantage of available spectrum opportunities. Thus, there is a need for an efficient yet low-complexity methods for OFDM spectrum shaping. We are currently working on suboptimal adaptive symbol transition (AST) algorithm that can shape the spectrum of OFDM signals with reduced computational complexity.

- OFDMA Capacity under Various Impairments

  We evaluated the performance of OFDMA systems over wireless selective channels and under channel estimation errors as well as IQ imbalances in Chapters 5 and 6. There are three directions in which this work can be extended. First, the performance of OFDMA systems can be examined under a number of other practical impairments such as timing and frequency offsets or sampling clock errors.

Second, since tiles in the OFDMA uplink belong to multiple users, we assumed the receiver carries out the estimation and equalization on a tile-by-tile basis. A possible improvement to the channel estimation can be attained if the system has the ability to detect and use pilots that belong to the same user but over different tiles. To achieve this goal the system needs to have prior knowledge, to some extend, of the user channel correlation over time and frequency.

Third, the optimum tile dimensions introduced in Chapter 5 were obtained for hard decision receivers using channel capacity and upper bounds on convolutional codes. This work can be extended to obtain the optimum tile dimensions for soft decision receivers. In this case, we need to derive the probability distributions of received signal as function of the wireless selective channel and the channel estimation errors for a given system model.

# REFERENCES

[1] FCC Spectrum Policy Task Force, "FCC report of the spectrum efficiency working group," Federal Communications Commission, Tech. Rep., Nov. 2002.

[2] J. Mitola and G. Q. Maguire Jr., "Cognitive radio: Making software radios more personal," *IEEE Personal Communications*, vol. 6, no. 4, pp. 13–18, Aug. 1999.

[3] J. Mitola, "Cognitive radio," Licentiate Thesis, Dept. of Teleinformatics, Royal Institute of Technology, Sep. 1999.

[4] S. Haykin, "Cognitive radio: brain-empowered wireless communications," *IEEE J. Select. Areas Commun.*, vol. 3, no. 2, pp. 201–220, Feb. 2005.

[5] "Broadband radio access networks (BRAN); HIPERLAN type 2; physical (PHY) layer," ETSI Std. TS 101 475, 2001.

[6] "Supplement to IEEE standard for information technology telecommunications and information exchange between systems - local and metropolitan area networks - specific requirements. part 11: wireless LAN medium access control (MAC) and physical layer (PHY) specifications: high-speed physical layer in the 5 GHz band," IEEE Std. 802.11a-1999, 1999.

[7] "Broadband mobile access communication system (HiSWANa)," ARIB Std. H14.11.27, 2002.

[8] "IEEE standard for local and metropolitan area networks part 16: Air interface for fixed broadband wireless access systems," IEEE Std. 802.16-2004 (Revision of IEEE Std. 802.16-2001), 2004.

[9] "IEEE standard for local and metropolitan area networks part 16: Air interface for fixed and mobile broadband wireless access systems amendment 2: Physical and medium access control layers for combined fixed and mobile operation in licensed bands and corrigendum 1," IEEE Std. 802.16e-2005 and IEEE Std. 802.16-2004/Cor 1-2005 (Amendment and Corrigendum to IEEE Std. 802.16-2004), 2006.

[10] "Asymmetric digital subscriber line (ADSL)," ANSI Std. T1.413, 1995.

[11] "Radio broadcasting systems; digital audio broadcasting (DAB) to mobile, portable and fixed receivers," ETSI Std. EN 300 401, 2001.

[12] "Digital video broadcasting (DVB); framing structure, channel coding and modulation for digital terrestrial television," ETSI Std. EN 300 744, 2001.

[13] "IEEE 802.15 WPAN high rate alternative PHY task group 3a (TG3a)," http://www.ieee802.org/15/pub/TG3a.html.

[14] E. Seidel, "Progress on LTE Advanced - the new 4G standard," White Paper, Nomor Research, Jul. 2008.

[15] http://www.ist-winner.org.

[16] "IEEE 802.22 working group on wireless regional area networks." [Online]. Available: http://www.ieee802.org/22/

[17] A. A. Abidi, "Direct-conversion radio transceivers for digital communications," *IEEE J. Solid-State Circuits*, vol. 30, no. 12, pp. 1399–1410, 1995.

[18] B. Come, R. Ness, S. Donnay, L. Van der Perre, W. Eberle, P. Wambacq, M. Engels, and I. Bolsens, "Impact of front-end non-idealities on bit error rate performance of WLAN-OFDM transceivers," in *Proc. IEEE Radio and Wireless Conf. (RAWCON)*, 2000, pp. 91–94.

[19] R. Liu, Y. Li, H. Chen, and Z. Wang, "EVM estimation by analyzing transmitter imperfections mathematically and graphically," *Springer Analog Integrated Circuits and Signal Processing Journal*, vol. 48, no. 3, pp. 257–262, 2006.

[20] H. A. Mahmoud, T. Yucek, and H. Arslan, *Cognitive Radio, Software Defined Radio, and Adaptive Wireless Systems.* Springer, 2007, ch. OFDM for Cognitive Radio: Merits and Challenges.

[21] ——, "OFDM for cognitive radio: Merits and challenges," *accepted for publication in IEEE Wireless Commun. Mag.*, 2009.

[22] H. A. Mahmoud, H. Arslan, and M. K. Ozdemir, "Initial ranging for WiMAX (802.16e) OFDMA," in *Proc. IEEE Mil. Commun. Conf. (MILCOM)*, 2006.

[23] ——, "An efficient ranging algorithm for WiMAX (802.16e) OFDMA," *Elsevier Comput. Commun. J.*, vol. 32, no. 1, pp. 159–168, Jan. 2009.

[24] H. A. Mahmoud and H. Arslan, "Sidelobe suppression in OFDM-based spectrum sharing systems using adaptive symbol transition," *IEEE Commun. Lett.*, vol. 12, no. 2, pp. 133–135, Feb. 2008.

[25] ——, "Spectrum shaping of OFDM-based cognitive radio signals," in *Proc. IEEE Radio and Wireless Sym. (RWS)*, Jan. 2008.

[26] H. A. Mahmoud, H. Arslan, M. K. Ozdemir, and F. E. Retnasothie, "IQ imbalance correction for OFDMA uplink systems," *accepted for publication in Proc. IEEE Int. Conf. Commun. (ICC)*, Jun. 2009.

[27] H. A. Mahmoud and H. Arslan, "Error vector magnitude to snr conversion for nondata aided receivers," *accepted for publication in IEEE Trans. Wireless Commun.*, 2009.

[28] P. Robertson and S. Kaiser, "The effect of Doppler spreads in OFDM(A) mobile radio systems," in *Proc. IEEE Veh. Technol. Conf. (VTC)*, vol. 1, Sep. 1999, pp. 329–333.

[29] D. T. Harvatin and R. E. Ziemer, "Orthogonal frequency division multiplexing performance in delay and doppler spread channels," in *Proc. IEEE Veh. Technol. Conf. (VTC)*, vol. 3, May 1997.

[30] S. Hara and R. Prasad, "Overview of multicarrier CDMA," *IEEE Commun. Mag.*, vol. 35, no. 12, pp. 126–133, Dec. 1997.

[31] H. Yaghoobi, "Scalable OFDMA physical layer in IEEE 802.16 WirelessMAN," *Intel Technology Journal*, vol. 8, no. 3, pp. 201–212, Aug. 2004.

[32] T. Yucek, "Channel, spectrum and waveform awareness in OFDM-based Cognitive Radio systems," Ph.D. dissertation, University of South Florida, Jul. 2007.

[33] M. Wylie-Green, "Dynamic spectrum sensing by multiband OFDM radio for interference mitigation," in *Proc. IEEE Int. Sym. on New Frontiers in Dynamic Spectr. Access Netw. (DySPAN)*, 2005, pp. 619–625.

[34] T. Weiss, J. Hillenbrand, and F. Jondral, "A diversity approach for the detection of idle spectral resources in spectrum pooling systems," in *Proc. of the 48th Int. Scientific Colloquium*, Ilmenau, Germany, Sep. 2003.

[35] J. Hillenbrand, T. A. Weiss, and F. K. Jondral, "Calculation of detection and false alarm probabilities in spectrum pooling systems," *IEEE Commun. Lett.*, vol. 9, no. 4, pp. 349–351, 2005.

[36] T. Yucek and H. Arslan, "Spectrum characterization for opportunistic cognitive radio systems," in *Proc. IEEE Mil. Commun. Conf. (MILCOM)*, 2006, pp. 1–6.

[37] H. Arslan and T. Yücek, *Adaptation Techniques in Wireless Multimedia Networks*. Nova Science Publishers, 2006, ch. Adaptation of Wireless Mobile Multi-carrier Systems.

[38] T. Keller and L. Hanzo, "Adaptive modulation techniques for duplex OFDM transmission," *IEEE Trans. Veh. Technol.*, vol. 49, no. 5, pp. 1893–1906, Sep. 2000.

[39] C. Y. Wong, R. S. Cheng, K. B. Lataief, and R. D. Murch, "Multiuser OFDM with adaptive subcarrier, bit, and power allocation," *IEEE J. Sel. Areas Commun.*, vol. 17, no. 10, pp. 1747–1758, Oct. 1999.

[40] S. W. Lei and V. K. N. Lau, "Adaptive interleaving for OFDM in TDD systems," *IEE Proc. Commun.*, vol. 148, no. 2, pp. 77–80, 2001.

[41] A. Dowler, A. Doufexi, and A. Nix, "Performance evaluation of channel estimation techniques for a mobile fourth generation wide area OFDM system," in *Proc. IEEE Veh. Technol. Conf. (VTC)*, vol. 4, 2002.

[42] S. Haykin and M. Moher, *Modern Wireless Communications*. New York, NY: Prentice-Hall, 2004.

[43] Y. Li and N. Sollenberger, "Interference suppression in OFDM systems using adaptive antenna arrays," in *Proc. IEEE Global Telecommun. Conf. (GLOBECOM)*, vol. 1, Nov. 1998, pp. 213–218.

[44] Institute of Electrical and Electronics Engineers, "IEEE standard computer dictionary: A compilation of IEEE standard computer glossaries," New York, NY, 1990.

[45] SDR Forum, "Software Defined Radio Technology for Public Safety," SDR Forum, Apr. 14, 2006, approved Document SDRF–06–A–0001–V0.00.

[46] "IEEE standard for information technology- telecommunications and information exchange between systems- local and metropolitan area networks- specific requirements part 11: wireless LAN medium access control (MAC) and physical layer (PHY) specifications," IEEE Std. 802.11g-2003 (Amendment to IEEE Std. 802.11, 1999 Edn. (Reaff 2003) as amended by IEEE Stds 802.11a-1999, 802.11b-1999, 802.11b-1999/Cor 1-2001, and 802.11d-2001), 2003.

[47] A. Batra, J. Balakrishnan, G. Aiello, J. Foerster, and A. Dabak, "Design of a multiband OFDM system for realistic UWB channel environments," *IEEE Trans. Microw. Theory Tech.*, vol. 52, no. 9, pp. 2123–2138, 2004.

[48] V. S. Somayazulu, J. R. Foerster, and S. Roy, "Design challenges for very high data rate UWB systems," in *Proc. IEEE Asilomar Conf. on Signals, Systems and Computers*, 2002, pp. 717–721.

[49] D. M. W. Leenaerts, "Transceiver design for multiband OFDM UWB," *EURASIP J. on Wireless Commun. and Netw.*, vol. 2006, no. 2, pp. 25–25, 2006.

[50] H. Zheng and H. C. Luong, "A 1.5 V 3.1 GHz8 GHz CMOS synthesizer for 9-band MB-OFDM UWB transceivers," *IEEE J. Solid-State Circuits*, vol. 42, no. 6, pp. 1250–1260, Jun. 2007.

[51] B. Razavi, T. Aytur, C. Lam, F.-R. Yang, R.-H. Yan, H.-C. Kang, C.-C. Hsu, and C.-C. Lee, "Multiband UWB transceivers," in *Proc. IEEE Custom Integr. Circuits Conf. (CICC)*, Sep. 2005, pp. 141–148.

[52] J. Lee and D. Chiu, "A 7-band 3–8 GHz frequency synthesizer with 1 ns band-switching time in 0.18 m CMOS technology," in *Proc. IEEE Custom Integr. Circuits Conf. (CICC)*, 2005, pp. 204–205.

[53] A. Ismail and A. Abidi, "A 3.1 to 8.2 GHz direct conversion receiver for MB-OFDM UWB communications," in *Proc. IEEE Int. Solid State Circuits Conf. (ISSCC)*, vol. 1, Feb. 2005, pp. 208–593.

[54] R. Rajbanshi, A. M. Wyglinski, , and G. J. Minden, "An efficient implementation of NC-OFDM transceivers for cognitive radios," in *Proc. IEEE Int. Conf. on Cognitive Radio Oriented Wireless Netw. and Commun. (CROWNCOM)*, Jun. 2006.

[55] H. Celebi and H. Arslan, "Cognitive positioning systems," *IEEE Trans. Wireless Commun.*, vol. 6, no. 12, pp. 4475–4483, 2007.

[56] ——, "Utilization of location information in cognitive wireless networks," *IEEE Wireless Commun. Mag.*, vol. 14, no. 4, pp. 6–13, 2007.

[57] H. Celebi, "Location awareness in Cognitive Radio networks," Ph.D. dissertation, University of South Florida, Aug. 2008.

[58] D. E. Breen Jr, "Characterization of multi-carrier locator performance," Master's thesis, Worcester Polytechnic Institute, May 2004.

[59] A. M. Wyglinski, "Effects of bit allocation on non-contiguous multicarrier-based cognitive radio transceivers," in *Proc. IEEE Veh. Technol. Conf. (VTC)*, Sep. 2006.

[60] T. Weiss and F. K. Jondral, "Spectrum pooling: an innovative strategy for the enhancement of spectrum efficiency," *IEEE Commun. Mag.*, vol. 42, no. 3, pp. 8–14, Mar. 2004.

[61] T. Weiss, A. Krohn, F. Capar, I. Martoyo, and F. Jondral, "Synchronization algorithms and preamble concepts for spectrum pooling systems," in *IST Mobile and Wireless Telecommun. Summit*, Jun. 2003.

[62] C. Muschallik, "Improving an OFDM reception using an adaptive Nyquist windowing," *IEEE Trans. Consum. Electron.*, vol. 42, no. 3, pp. 259–269, Aug. 1996.

[63] S. H. Muller-Weinfurtner, "Optimum Nyquist windowing in OFDM receivers," *IEEE Trans. Commun.*, vol. 49, no. 3, pp. 417–420, Mar. 2001.

[64] T. Weiss, J. Hillenbrand, A. Krohn, and F. K. Jondral, "Mutual interference in OFDM-based spectrum pooling systems," in *Proc. IEEE Veh. Technol. Conf. (VTC)*, vol. 4, May 2004, pp. 1873–1877.

[65] H. Yamaguchi, "Active interference cancellation technique for MB-OFDM cognitive radio," in *Proc. IEEE European Microwave Conf.*, vol. 2, Oct. 2004, pp. 1105–1108.

[66] S. Brandes, I. Cosovic, and M. Schnell, "Sidelobe suppression in OFDM systems by insertion of cancellation carriers," in *Proc. IEEE Veh. Technol. Conf. (VTC)*, vol. 1, Sep. 2005, pp. 152–156.

[67] ——, "Reduction of out-of-band radiation in OFDM systems by insertion of cancellation carriers," *IEEE Commun. Lett.*, vol. 10, no. 6, pp. 420–422, Jun. 2006.

[68] S. Pagadarai, R. Rajbanshi, A. M. Wyglinski, and G. J. Minden, "Sidelobe suppression for OFDM-based cognitive radios using constellation expansion," in *Proc. IEEE Wireless Commun. and Netw. Conf. (WCNC)*, Apr. 2008, pp. 888–893.

[69] "IEEE standard for local and metropolitan area networks — part 16: Air interface for fixed broadband wireless access systems— amendment 2: Medium access control modifications and additional physical layer specifications for 2-11 GHz," IEEE Std. 802.16a-2003 (Amendment to IEEE Std. 802.16-2001), 2003.

[70] T. S. Rappaport, *Smart Antennas: Adaptive Arrays, Algorithms, and Wireless Position Location.* IEEE, 1998.

[71] O. Hoshuyama, A. Sugiyama, and A. Hirano, "A robust adaptive beamformer for microphone arrays with a blocking matrix using constrained adaptive filters," *IEEE Trans. Signal Process.*, vol. 47, no. 10, pp. 2677–2684, 1999.

[72] S. Brandes, I. Cosovic, and M. Schnell, "Reduction of out-of-band radiation in OFDM based overlay systems," in *Proc. IEEE Int. Sym. on New Frontiers in Dynamic Spectr. Access Netw. (DySPAN)*, Nov. 2005, pp. 662–665.

[73] I. Cosovic, S. Brandes, and M. Schnell, "A technique for sidelobe suppression in OFDM systems," in *Proc. IEEE Global Telecommun. Conf. (GLOBECOM)*, vol. 1, Nov. 2005, pp. 204–208.

[74] ——, "Subcarrier weighting: a method for sidelobe suppression in OFDM systems," *IEEE Commun. Lett.*, vol. 10, no. 6, pp. 444–446, Jun. 2006.

[75] I. Cosovic and T. Mazzoni, "Suppression of sidelobes in OFDM systems by multiple-choice sequences," *European Trans. Telecommun.*, vol. 17, no. 6, pp. 623–630, 2006.

[76] G. Dong, H. Chen, M. Yang, and J. Dai, "Dynamic frequency selection (DFS) in IEEE802.16e OFDM system working at unlicensed bands," in *Proc. IEEE Int. Conf. on Adv. Commun. Tech. (ICACT)*, vol. 2, Feb. 2007.

[77] T. C. H. Alen, A. S. Madhukumar, and F. Chin, "Capacity enhancement of a multi-user OFDM system using dynamic frequency allocation," *IEEE Trans. Broadcast.*, vol. 49, no. 4, pp. 344–353, Dec. 2003.

[78] "Supplement to IEEE standard for information technology- telecommunications and information exchange between systems- local and metropolitan area networks- specific requirements-part II: Wireless LAN medium access control (MAC) and physical layer (PHY) specifications: Higher-speed physical layer extension in the 2.4 GHz band," IEEE Std. 802.11b-1999, 2000.

[79] http://www.wi-fi.org.

[80] T. M. Schmidl and D. C. Cox, "Robust frequency and timing synchronization for OFDM," *IEEE Trans. Commun.*, vol. 45, no. 12, pp. 1613–1621, Dec. 1997.

[81] J. J. van de Beek, P. O. Borjesson, M.-L. Boucheret, D. Landstrom, J. Arenas, P. Odling, C. Ostberg, M. Wahlqvist, and S. K. Wilson, "A time and frequency synchronization scheme for multiuser OFDM," *IEEE J. Select. Areas Commun.*, vol. 17, no. 11, pp. 1900–1914, Nov. 1999.

[82] M. Morelli, "Timing and frequency synchronization for the uplink of an OFDMA system," *IEEE Trans. Commun.*, vol. 52, no. 2, pp. 296–306, Feb. 2004.

[83] X. Fu and H. Minn, "Initial uplink synchronization and power control (ranging process) for OFDMA systems," in *Proc. IEEE Global Telecommun. Conf. (GLOBECOM)*, vol. 6, Nov. 29-Dec. 3, 2004, pp. 3999–4003.

[84] J. Krinock, M. Singh, M. Paff, V. Tien, A. Lonkar, L. Fung, and C.-C. Lee, "Comments on OFDMA ranging scheme described in IEEE 802.16ab-01/01r1," IEEE 802.16abc-01/24, Aug. 2001.

[85] J. J. van de Beek, M. Sandell, and P. O. Borjesson, "ML estimation of time and frequency offset in OFDM systems," *IEEE Trans. Signal Process.*, vol. 45, no. 7, pp. 1800–1805, 1997.

[86] I. L. standards committee, "Air interface for fixed broadband wireless access systems," July 2001.

[87] D. H. Lee, "OFDMA uplink ranging for IEEE 802.16e using modified generalized chirp-like polyphase sequences," in *Proc. IEEE and IFIP Int. Conf. in Central Asia on Internet*, Sep. 2005.

[88] H. Minn and X. Fu, "A new ranging method for OFDMA systems," in *Proc. IEEE Global Telecommun. Conf. (GLOBECOM)*, vol. 3, Nov. 28- Dec. 2, 2005.

[89] J. G. Proakis, *Digital Communications*, 4th ed. McGraw-Hill, 2001.

[90] WiMAX Forum, "WiMAX system evaluation methodology," Sep. 2007.

[91] Recommendation ITU-R M.1225, "Guidelines for evaluation of radio transmission technologies for IMT-2000," *Int. Telecommun. Union (ITU)*, 1997.

[92] D. Cabric, S. M. Mishra, and R. W. Brodersen, "Implementation issues in spectrum sensing for cognitive radios," in *Proc. IEEE Asilomar Conf. on Signals, Systems and Computers*, vol. 1, Nov. 2004, pp. 772–776.

[93] J. Heiskala and J. Terry, *OFDM Wireless LANs: A Theoretical and Practical Guide*. Sams publishing, 2002, ch. 2.

[94] W. Gander, "Least squares with a quadratic constraint," *Numerische Mathematik*, vol. 36, no. 3, pp. 291–307, 1980.

[95] J. Bonnet and G. Auer, "Chunk-based channel estimation for uplink OFDM," in *Proc. IEEE Veh. Technol. Conf. (VTC)*, vol. 4, May 2006, pp. 1555–1559.

[96] Y. Ma and R. Tafazolli, "Channel estimation for OFDMA uplink: a hybrid of linear and BEM interpolation approach," *IEEE Trans. Signal Process.*, vol. 55, no. 4, pp. 1568–1573, Apr. 2007.

[97] H. Liu, Y. Ma, and R. Tafazolli, "Optimum pilot placement for chunk-based OFDMA uplink: Single chunk scenario," in *Proc. IEEE Veh. Technol. Conf. (VTC)*, Oct. 2007, pp. 2194–2198.

[98] ——, "Optimum pilot placement for chunk-based OFDMA uplink: Time direction scenario," in *Proc. IEEE Veh. Technol. Conf. (VTC)*, May 2008, pp. 2547–2551.

[99] P. Hoeher, S. Kaiser, and P. Robertson, "Two-dimensional pilot-symbol-aided channel estimation by Wiener filtering," *Proc. IEEE Int. Conf. on Acoust., Speech, and Signal Process. (ICASSP)*, vol. 3, pp. 1845–1848, Apr. 1997.

[100] P. Tan and N. C. Beaulieu, "Effect of channel estimation error on bit error probability in OFDM systems over rayleigh and ricean fading channels," *IEEE Trans. Commun.*, vol. 56, no. 4, pp. 675–685, Apr. 2008.

[101] Y. Li, L. J. Cimini, and N. R. Sollenberger, "Robust channel estimation for OFDM systems with rapid dispersive fading channels," *IEEE Trans. Commun.*, vol. 46, no. 7, pp. 902–915, Jul. 1998.

[102] W. C. Jakes, *Microwave mobile communications*. Wiley, New York, 1974.

[103] Y.-S. Choi, P. J. Voltz, and F. A. Cassara, "On channel estimation and detection for multi-carrier signals in fast and selective rayleigh fading channels," *IEEE Trans. Commun.*, vol. 49, no. 8, pp. 1375–1387, Aug. 2001.

[104] M. Russell and G. L. Stuber, "Interchannel interference analysis of OFDM in a mobile environment," in *Proc. IEEE Veh. Technol. Conf. (VTC)*, vol. 2, Jul. 1995, pp. 820–824.

[105] Y. Li and L. J. Cimini, "Bounds on the interchannel interference of OFDM in time-varying impairments," *IEEE Trans. Commun.*, vol. 49, no. 3, pp. 401–404, Mar. 2001.

[106] X. Tang, M.-S. Alouini, and A. J. Goldsmith, "Effect of channel estimation error on M-QAM BER performance in Rayleigh fading," *IEEE Trans. Commun.*, vol. 47, no. 12, pp. 1856–1864, Dec. 1999.

[107] I. Gaspard, "Impact of the channel estimation onto the BER-performance of PSAM-OFDM systems in mobile radio channels," in *Proc. IEEE Veh. Technol. Conf. (VTC)*, vol. 1, May 2001, pp. 673–677.

[108] H. Cheon and D. Hong, "Effect of channel estimation error in OFDM-based WLAN," *IEEE Commun. Lett.*, vol. 6, no. 5, pp. 190–192, 2002.

[109] M.-X. Chang and Y. T. Su, "Performance analysis of equalized OFDM systems in Rayleigh fading," *IEEE Trans. Wireless Commun.*, vol. 1, no. 4, pp. 721–732, Oct. 2002.

[110] J. Chen, Y. Tang, S. Li, and Y. Li, "Effect of channel estimation error onto the BER performance of PSAM-OFDM in Rayleigh fading," in *Proc. IEEE Veh. Technol. Conf. (VTC)*, vol. 4, Oct. 2003, pp. 2444–2448.

[111] L. Cao and N. C. Beaulieu, "Exact error-rate analysis of diversity 16-QAM with channel estimation error," *IEEE Trans. Commun.*, vol. 52, no. 6, pp. 1019–1029, Jun. 2004.

[112] M. Al-Gharabally and P. Das, "On the performance of OFDM systems in time varying channels with channel estimation error," *Proc. IEEE Int. Conf. Commun. (ICC)*, vol. 11, pp. 5180–5185, Jun. 2006.

[113] P. O. Borjesson and C.-E. W. Sundberg, "Simple approximations of the error function $Q(x)$ for communications applications," *IEEE Trans. Commun.*, vol. 27, no. 3, pp. 639–643, Mar. 1979.

[114] M. M. Wang, W. Xiao, and T. Brown, "Soft decision metric generation for QAM with channel estimation error," *IEEE Trans. Commun.*, vol. 50, no. 7, pp. 1058–1061, 2002.

[115] W. Xiao, "Optimal detection of M-QAM signal with channel estimation error," *Proc. IEEE Int. Conf. Commun. (ICC)*, vol. 5, pp. 3251–3255, May 2003.

[116] C. E. Shannon, "A mathematical theory of communication," *Bell Syst. Tech. J.*, vol. 27, no. 3, pp. 379–423, Jul. 1948.

[117] K. Larsen, "Short convolutional codes with maximal free distance for rates 1/2, 1/3, and 1/4," *IEEE Trans. Inf. Theory*, vol. 19, no. 3, pp. 371–372, May 1973.

[118] P. Frenger, P. Orten, and T. Ottosson, "Convolutional codes with optimum distance spectrum," *IEEE Commun. Lett.*, vol. 3, no. 11, pp. 317–319, Nov. 1999.

[119] A. R. Wright and P. A. Naylor, "I/Q mismatch compensation in zero-IF OFDM receivers with application to DAB," in *Proc. IEEE Int. Conf. on Acoust., Speech, and Signal Process. (ICASSP)*, vol. 2, 2003.

[120] A. Tarighat and A. H. Sayed, "On the baseband compensation of IQ imbalances in OFDM systems," in *Proc. IEEE Int. Conf. on Acoust., Speech, and Signal Process. (ICASSP)*, vol. 4, 2004.

[121] J. Tubbax, B. Come, L. Van der Perre, L. Deneire, S. Donnay, and M. Engels, "Compensation of IQ imbalance in OFDM systems," in *Proc. IEEE Int. Conf. Commun. (ICC)*, vol. 5, 2003.

[122] H. Shafiee and S. Fouladifard, "Calibration of IQ imbalance in OFDM transceivers," in *Proc. IEEE Int. Conf. Commun. (ICC)*, vol. 3, 2003.

[123] J. Lin and E. Tsui, "Joint adaptive transmitter/receiver IQ imbalance correction for OFDM systems," in *Proc. IEEE Int. Sym. on Pers., Indoor and Mobile Radio Commun. (PIMRC)*, vol. 2, 2004.

[124] A. Tarighat and A. H. Sayed, "OFDM systems with both transmitter and receiver IQ imbalances," in *Proc. IEEE Workshop on Signal Process. Adv. in Wireless Commun. (SPAWC)*, 2005, pp. 735–739.

[125] T. C. W. Schenk, P. F. M. Smulders, and E. R. Fledderus, "Estimation and compensation of Tx and Rx IQ imbalance in OFDM-based MIMO systems," in *Proc. IEEE Radio and Wireless Sym. (RWS)*, 2006, pp. 215–218.

[126] M. Valkama, Y. Zou, and M. Renfors, "On I/Q imbalance effects in MIMO space-time coded transmission systems," in *Proc. IEEE Radio and Wireless Sym. (RWS)*, 2006, pp. 223–226.

[127] Y. Jin, J. Kwon, Y. Lee, D. Lee, and J. Ahn, "Obtained diversity gain in OFDM systems under the influence of IQ imbalance," *IEICE Trans. on Commun.*, vol. 91, no. 3, p. 814, 2008.

[128] L. Giugno, V. Lottici, and M. Luise, "Low-complexity gain and phase I/Q mismatch compensation using orthogonal pilot sequences," in *European Signal Process. Conf. (EUSIPCO)*, Sep. 2006.

[129] R. Chrabieh and S. Soliman, "IQ imbalance mitigation via unbiased training sequences," in *Proc. IEEE Global Telecommun. Conf. (GLOBECOM)*, Nov. 2007, pp. 4280–4285.

[130] A. Haider and A. Chatterjee, "Low-cost alternate EVM test for wireless receiver systems," in *Proc. IEEE VLSI Test Sym.*, May 2005, pp. 255–260.

[131] R. Hassun, M. Flaherty, R. Matreci, and M. Taylor, "Effective evaluation of link quality using error vector magnitude techniques," in *Proc. IEEE Wireless Commun. Conf.*, Aug. 1997, pp. 89–94.

[132] T. Nakagawa and K. Araki, "Effect of phase noise on RF communication signals," in *Proc. IEEE Veh. Technol. Conf. (VTC)*, vol. 2, Sep. 2000.

[133] M. Helfenstein, E. Baykal, K. Muller, A. Lampe, P. Semicond, and S. Zurich, "Error vector magnitude (EVM) measurements for GSM/EDGE applications revised under production conditions," in *Proc. IEEE Int. Sym. on Circuits and Syst. (ISCAS)*, May 2005, pp. 5003–5006.

[134] A. Georgiadis, "Gain, phase imbalance, and phase noise effects on error vector magnitude," *IEEE Trans. Veh. Technol.*, vol. 53, no. 2, pp. 443–449, 2004.

[135] K. M. Gharaibeh, K. G. Gard, and M. B. Steer, "Accurate Estimation of Digital Communication System Metrics – SNR, EVM and $\rho$ in a Nonlinear Amplifier Environment," *IEEE Trans. Commun.*, pp. 734–739, Sep. 2005.

[136] R. A. Shafik, M. S. Rahman, A. R. Islam, and N. S. Ashraf, "On the Error Vector Magnitude as a Performance Metric and Comparative Analysis," *International Conference on Emerging Technologies (ICET)*, pp. 27–31, 2006.

[137] S. Forestier, P. Bouysse, R. Quere, A. Mallet, J. M. Nebus, and L. Lapierre, "Joint Optimization of the Power-Added Efficiency and the Error-Vector Measurement of 20-GHz pHEMT Amplifier Through a New Dynamic Bias-Control Method," *IEEE Trans. Microw. Theory Tech.*, vol. 52, no. 4, pp. 1132–1141, 2004.

[138] F. L. Lin and H. R. Chuang, "EVM and BER Simulation of an NADC-TDMA Radiophone Influenced by the Operator's Body in Urban Mobile Environments," *Wireless Personal Communications*, vol. 17, no. 1, pp. 135–147, 2001.

[139] N. L. Johnson and S. Kotz, *Distributions in statistics: Continuous univariate distributions.* John Wiley & Sons, 1970, vol. 1.

[140] M. Al-Gharabally and P. Das, "On the performance of OFDM systems in time varying channels with channel estimation error," in *Proc. IEEE Int. Conf. Commun. (ICC)*, vol. 11, Jun. 2006, pp. 5180–5185.

[141] J. K. Cavers and M. W. Liao, "Adaptive compensation for imbalance and offset losses in direct conversion transceivers," *IEEE Trans. Veh. Technol.*, vol. 42, no. 4, pp. 581–588, Nov. 1993.

[142] D. R. Pauluzzi and N. C. Beaulieu, "A comparison of SNR estimation techniques for the AWGN channel," *IEEE Trans. Commun.*, vol. 48, no. 10, pp. 1681–1691, Oct 2000.

[143] S. Soundararajan and P. Agrawal, "A scheduling algorithm for IEEE 802.16 and IEEE 802.11 hybrid networks," in *Proc. IEEE Int. Conf. Broadband Commun., Netw. and Sys. (BROAD-NETS)*, 2007, pp. 320–322.

[144] D. H. Lee and H. Morikawa, "Non-synchronized random access process of single carrier FDMA system," in *Technical report of IEICE Radio Commun. Sys. (RCS)*, vol. 107, no. 147, 2007, pp. 137–142.

[145] ——, "Analysis on random access process of single carrier FDMA system," in *Proc. ICST Int. Conf. on Wireless Internet (WICON)*, 2007, pp. 1–9.

[146] J. Zeng and H. Minn, "A novel OFDMA ranging method exploiting multiuser diversity," in *Proc. IEEE Global Telecommun. Conf. (GLOBECOM)*, Nov. 2007, pp. 1498–1502.

[147] ——, "Diversity exploiting MIMO-OFDMA ranging," in *Proc. IEEE Int. Conf. Information, Commun. and Signal Process. (ICICS)*, Dec. 2007, pp. 1–5.

[148] ——, "An investigation into initial ranging method for mobile OFDMA systems," in *Proc. IEEE Sarnoff Symposium*, Apr. 2008, pp. 1–5.

[149] L. Sanguinetti, M. Morelli, and H. V. Poor, "An ESPRIT-based approach for initial ranging in OFDMA systems," in *Proc. IEEE Workshop on Signal Process. Adv. in Wireless Commun. (SPAWC)*, Jul. 2008.

[150] G. Bansal, M. J. Hossain, and V. K. Bhargava, "Optimal and suboptimal power allocation schemes for OFDM-based cognitive radio systems," *IEEE Trans. Wireless Commun.*, vol. 7, no. 11, pp. 4710–4718, Nov. 2008.

[151] http://ieeexplore.ieee.org.

**APPENDICES**

**Appendix A**

From (3.7), the expected value of $\mathcal{E}_g$ is,

$$E\left[\mathcal{E}_g\right] = E\left[L + \sum_{n=0}^{L-1} W_{\Re}^2(m) + \sum_{n=0}^{L-1} W_{\Im}^2(m) + 2\sum_{n=0}^{L-1} c_p^{(k)}(m)\cos\left[\phi_m(\tau_k)\right]W_{\Re}(m)\right.$$

$$\left. + 2\sum_{n=0}^{L-1} c_p^{(k)}(m)\sin\left[\phi_m(\tau_k)\right]W_{\Im}(m)\right]. \quad \text{(A.1)}$$

Note that,

$$E\left[c_p^{(k)}(m)\right] = 0, \quad \text{(A.2)}$$

and,

$$E\left[W_{\Re}(m)\right] = E\left[W_{\Im}(m)\right] = 0. \quad \text{(A.3)}$$

Since $m$ values are randomly chosen between 0 and $N_t - 1$, $\phi_m(\tau_k)$ can be approximated as a uniformly-distributed random variable between $\pi$ and $-\pi$. Thus,

$$E\left[\cos\left[\phi_m(\tau_k)\right]\right] = E\left[\sin\left[\phi_m(\tau_k)\right]\right] = 0. \quad \text{(A.4)}$$

Therefore the expected value of the last two terms in (A.1) goes to zero for large values of $L$. Then,

$$E\left[\mathcal{E}_g\right] = L + E\left[\sum_{n=0}^{L-1} W_{\Re}^2(m)\right] + E\left[\sum_{n=0}^{L-1} W_{\Im}^2(m)\right]$$

$$= L + LN_0. \quad \text{(A.5)}$$

Next, we calculate $E\left[\mathcal{E}_g^2\right]$ from (3.7). Note that,

$$E\left[\left(\sum_{n=0}^{L-1} W_{\Re}^2(m)\right)^2\right] = \frac{1}{2}LN_0^2 + \frac{1}{4}L^2N_0^2, \quad \text{(A.6)}$$

153

**Appendix A (Continued)**

$$E\left[\left(2\sum_{n=0}^{L-1}c_p^{(k)}(m)\cos\left[\phi_m(\tau_k)\right]W_\Re(m)\right)^2\right]=LN_0, \tag{A.7}$$

$$E\left[\left(\sum_{n=0}^{L-1}W_\Re^2(m)\right)\left(\sum_{n=0}^{L-1}W_\Im^2(m)\right)\right]=\frac{1}{2}L^2N_0^2. \tag{A.8}$$

Then,

$$E\left[\mathcal{E}_g^2\right]=L^2+LN_0^2+L^2N_0^2+2LN_0+2L^2N_0. \tag{A.9}$$

**Appendix B**

From (3.10),

$$
\begin{aligned}
\mathcal{E}_r(u) = & \sum_{n=0}^{L-1}\left\{\sum_{k=0}^{K-1} c_p^{(k)}(m) \cos\left[\phi_m(\tau_k - u)\right]\right\}^2 + \sum_{n=0}^{L-1}\hat{W}_\Re^2(m) \\
& + \sum_{n=0}^{L-1}\left[2\hat{W}_\Re(m)\cdot\sum_{k=0}^{K-1} c_p^{(k)}(m)\cos\left[\phi_m(\tau_k - u)\right]\right] \\
= & \sum_{n=0}^{L-1}\sum_{k=0}^{K-1}\cos^2\left[\phi_m(\tau_k - u)\right] \\
& + \sum_{n=0}^{L-1}\sum_{k=0}^{K-1}\sum_{\substack{v=0 \\ v\neq k}}^{K-1}\left\{c_p^{(k)}(m)c_p^{(v)}(m)\cos\left[\phi_m(\tau_k - u)\right]\cos\left[\phi_m(\tau_v - u)\right]\right\} \\
& + \sum_{n=0}^{L-1}\hat{W}_\Re^2(m) + \sum_{n=0}^{L-1}\left\{2\hat{W}_\Re(m)\cos\left[\phi_m(u)\right]\sum_{k=0}^{K-1} c_p^{(k)}(m)\cos\left[\phi_m(\tau_k - u)\right]\right\}. \quad \text{(B.1)}
\end{aligned}
$$

The expected value of the second and last terms in (B.1) is zero. Therefore,

$$
\begin{aligned}
E\left[\mathcal{E}_r(u)\right] = & E\left[\sum_{n=0}^{L-1}\sum_{k=0}^{K-1}\cos^2\left[\phi_m(\tau_k - u)\right]\right] + \\
& E\left[\sum_{n=0}^{L-1}\hat{W}_\Re^2(m)\right]. \quad \text{(B.2)}
\end{aligned}
$$

$$
E\left[\mathcal{E}_r(u)\right] = \begin{cases} \frac{1}{2}LK + \frac{1}{2}L + \frac{1}{2}LN_0 & \text{, for } u = \tau_k \text{ for} \\ & \text{only one value of } k. \\ \frac{1}{2}LK + \frac{1}{2}LN_0 & \text{, for } u \neq \tau_k \text{ for} \\ & \text{all values of } k. \end{cases} \quad \text{(B.3)}
$$

The assumption that $u = \tau_k$ for only one value of $k$ implies that in the same symbol and for a give timing offset $u$, only one code exist.

**Appendix C**

The probability density function (PDF) of a random variable $V$ that has a doubly-truncated normal distribution is [139],

$$f(v) = \frac{1}{\sigma} \frac{\phi\left(\dfrac{v-\mu}{\sigma}\right)}{\Phi\left(\dfrac{B-\mu}{\sigma}\right) - \Phi\left(\dfrac{A-\mu}{\sigma}\right)}, \quad A \leq V \leq B, \tag{C.1}$$

where $\mu$ and $\sigma^2$ are the mean and variance of the untruncated random variable, respectively, and $\Phi(v) = 1 - Q(v)$ is the cumulative distribution function (CDF) of the standard normal distribution. The mean $\mu_v$, and variance $\sigma_v^2$ of $V$ are [139],

$$\mu_v = \mu + \frac{\phi\left(\dfrac{A-\mu}{\sigma}\right) - \phi\left(\dfrac{B-\mu}{\sigma}\right)}{\Phi\left(\dfrac{B-\mu}{\sigma}\right) - \Phi\left(\dfrac{A-\mu}{\sigma}\right)}\sigma, \tag{C.2}$$

and,

$$\sigma_v^2 = \sigma^2 + \frac{\left(\dfrac{A-\mu}{\sigma}\right)\phi\left(\dfrac{A-\mu}{\sigma}\right) - \left(\dfrac{B-\mu}{\sigma}\right)\phi\left(\dfrac{B-\mu}{\sigma}\right)}{\Phi\left(\dfrac{B-\mu}{\sigma}\right) - \Phi\left(\dfrac{A-\mu}{\sigma}\right)}\sigma^2$$
$$- \left[\frac{\phi\left(\dfrac{A-\mu}{\sigma}\right) - \phi\left(\dfrac{B-\mu}{\sigma}\right)}{\Phi\left(\dfrac{B-\mu}{\sigma}\right) - \Phi\left(\dfrac{A-\mu}{\sigma}\right)}\right]^2 \sigma^2. \tag{C.3}$$

For a random variable that has lower-truncated normal distribution, $B \to \infty$. In this case, $\phi(\infty) = 0$ and $\Phi(\infty) = 1$. Since $\sigma_v^2 = E\{V^2\} - \mu_v^2$, then, using (C.2) and (C.3), it can be shown that if $V$ has lower-truncated normal distribution,

$$E\{V^2\} = \sigma_v^2 + \mu_v^2$$
$$= \sigma(A + \mu)\frac{\phi\left(\dfrac{A-\mu}{\sigma}\right)}{Q\left(\dfrac{A-\mu}{\sigma}\right)} + \mu^2 + \sigma^2. \tag{C.4}$$

**Appendix C (Continued)**

Note that from (C.1) and as $B \to \infty$,

$$E\{V^2\} = \frac{1}{\sigma Q\left(\frac{A-\mu}{\sigma}\right)} \int_A^\infty v^2 \phi\left(\frac{v-\mu}{\sigma}\right) dv. \tag{C.5}$$

We define a new function $z(A, \mu, \sigma)$, where

$$z(A, \mu, \sigma) = \frac{1}{\sigma} \int_A^\infty v^2 \phi\left(\frac{v-\mu}{\sigma}\right) dv. \tag{C.6}$$

From (C.5), the solution to (C.6) is,

$$z(A, \mu, \sigma) = E\{V^2\} Q\left(\frac{A-\mu}{\sigma}\right)$$

$$= \sigma(A + \mu)\phi\left(\frac{A-\mu}{\sigma}\right) + (\mu^2 + \sigma^2)Q\left(\frac{A-\mu}{\sigma}\right) \tag{C.7}$$

**Appendix D**

From (C.7), and since $\phi(v) = \phi(-v)$ and $Q(v) + Q(-v) = 1$, the following properties of the $z$-function can be inferred,

$$z(A, \mu, \sigma) + z(-A, -\mu, \sigma) = \mu^2 + \sigma^2, \tag{D.1}$$

and from (D.1),

$$z(-A, \mu, \sigma) - z(A, \mu, \sigma) = z(-A, -\mu, \sigma) - z(A, -\mu, \sigma). \tag{D.2}$$

From (7.45), in the first summation, $\mu_{jk}$ can be substituted with $-\mu_i$, for $i, j = 0, \ldots, k$, where $\mu_i = 2ai$. In the second summation, the double summation can be reduced to one summation by substituting $\mu_{ji}$, for $i = 1, \ldots, k-1$ and $j = 0, \ldots, k$ with $\mu_i$, for $i = -k+1, \ldots, k-1$. The expression in (7.45) can then be rewritten as,

$$
\begin{aligned}
E\{(y_\Re - \hat{x}_\Re)^2\} =& \frac{1}{k+1}\left(2\sum_{i=0}^{k} z(-a, -\mu_i, \sigma_n) + \sum_{i=-k+1}^{-1}(k+i)\Big[z(-a, -\mu_i, \sigma_n) - z(a, -\mu_i, \sigma_n)\Big]\right.\\
&+(k-1)\Big[z(-a, \mu_0, \sigma_n) - z(a, \mu_0, \sigma_n)\Big] + \sum_{i=1}^{k-1}(k-i)\Big[z(-a, \mu_i, \sigma_n) - z(a, \mu_i, \sigma_n)\Big]\right)\\
=& \frac{1}{k+1}\left((k-1)\Big[z(-a, \mu_0, \sigma_n) - z(a, \mu_0, \sigma_n)\Big] + 2\sum_{i=0}^{k} z(-a, -\mu_i, \sigma_n)\right.\\
&\left.+2\sum_{i=1}^{k-1}(k-i)\Big[z(-a, \mu_i, \sigma_n) - z(a, \mu_i, \sigma_n)\Big]\right).
\end{aligned}\tag{D.3}
$$

By using the property in (D.2) on the last summation in (D.3),

$$
\begin{aligned}
E\{(y_\Re - \hat{x}_\Re)^2\} =& \frac{1}{k+1}\left((k-1)\Big[z(-a, \mu_0, \sigma_n) - z(a, \mu_0, \sigma_n)\Big] + 2\sum_{i=0}^{k} z(-a, -\mu_i, \sigma_n)\right.\\
&\left.+2\sum_{i=1}^{k-1}(k-i)\Big[z(-a, -\mu_i, \sigma_n) - z(a, -\mu_i, \sigma_n)\Big]\right).
\end{aligned}\tag{D.4}
$$

**Appendix D (Continued)**

After some manipulation, we have,

$$E\{(y_\Re - \hat{x}_\Re)^2\} = \frac{1}{k+1}\bigg((k+1)\Big[z(-a,\mu_0,\sigma_n) + z(a,\mu_0,\sigma_n)\Big]$$

$$+ 2\sum_{i=0}^{k-1}(k-i)\Big[z(-a,-\mu_{i+1},\sigma_n) - z(a,-\mu_i,\sigma_n)\Big]\bigg). \quad \text{(D.5)}$$

Using (D.1) and (C.7), and after some more manipulation,

$$E\{(y_\Re - \hat{x}_\Re)^2\} = \sigma_n^2 - 8a\sigma_n \sum_{i=1}^{k}\gamma_i\phi\left[\frac{\beta_i a}{\sigma_n}\right] + 8a^2\sum_{i=1}^{k}\gamma_i\beta_i Q\left[\frac{\beta_i a}{\sigma_n}\right], \quad \text{(D.6)}$$

where

$$\gamma_i = 1 - \frac{i}{k+1}, \quad \text{and} \quad \beta_i = 2i - 1. \quad \text{(D.7)}$$

**ABOUT THE AUTHOR**

Hisham Abdelaziz Mahmoud received the B.S. (with highest honors) degree in electrical engineering from Cairo University at Fayoum, Fayoum, Egypt, in 2002, and the M.S. degree in electrical engineering from Cairo University, Cairo, Egypt, in 2005. He is currently pursuing his Ph.D. degree at the Electrical Engineering Department, University of South Florida, Tampa, FL. His research interests include wireless systems, OFDM-based systems, synchronization, channel estimation, spectrum sensing and shaping for cognitive radio, and channel coding.